5-4-2021

Characterizing Novel Filovirus Proteins and 3-Deazaneplanocin A Derivatives as Antivirals against Non-Segmented Negative Sense RNA Viruses

Joyce Sweeney Gibbons
Georgia State University

CHARACTERIZING NOVEL FILOVIRUS PROTEINS AND 3-DEAZANEPLANOCIN A DERIVATIVES AS ANTIVIRALS AGAINST NON-SEGMENTED NEGATIVE SENSE RNA VIRUSES

by

JOYCE SWEENEY GIBBONS

Under the Direction of Christopher F. Basler, PhD

ABSTRACT

Filoviruses belong to a family of RNA viruses that includes deadly emerging zoonotic pathogens such as Ebola and Marburg viruses. A concern of public health is whether recently discovered filoviruses have the potential to infect humans and cause disease. Filoviruses encode proteins that suppress innate immune signaling and this is postulated as a contributing determinant of virulence in animals. Měnglà virus (MLAV), a recently discovered bat filovirus, can infect human cells using a vesicular stomatitis virus (VSV)-MLAV GP pseudotype system. In Chapter 2, we characterize MLAV's VP35, VP40 and VP24 proteins on their ability to regulate both human and bat type I IFN responses. Our assessment also includes MARV and EBOV protein homologs for points of comparison.

Analogous to its filovirus equivalents, MLAV VP35 and VP40 proteins inhibited type I IFN responses. MLAV VP40 suppressed the IFNβ production pathway, and this is independent of its inhibition on the type I IFN signaling pathway. MLAV VP24 did not behave like either EBOV VP24, an inhibitor of type I IFN, or MARV VP24, an activator of the antioxidant response pathway.

Another critical concern is the lack of approved pan-filovirus therapeutics. Broad-spectrum nucleoside analogs have demonstrated antiviral activity against filoviruses. 3-deazaneplanocin (DzNep) and its brominated derivates (CL123, CL4033 and CL4053) are adenosine analogs and exhibit inhibition of non-segmented negative sense (NNS) RNA viruses. The antiviral effect is through inhibition of the enzyme, S-adenosylhomocysteine hydrolase (SAHase), resulting in obstruction of viral methyltransferase activity and consequently impaired translation of viral mRNA. The D-like-CL4033 and L-like-CL4053 exert antiviral activity against NNS RNA viruses, however the L-isomer, CL4053, has approximately a 1000 fold higher 50 percent inhibitory concentration (IC50) relative to the D-isomer, CL4033, suggesting an alternative antiviral mechanism. In chapter 3 we have elucidated, using VSV as a model NNS RNA virus, mechanisms of how DzNep, CL123, CL4033 and CL4053 exert their antiviral activity in cell culture. Our data indicates that DzNep, CL123 and CL4033 inhibit VSV by preventing viral mRNA cap methylation. A virus selected for CL123-resistance demonstrates cross-resistance against all derivatives, suggesting L-like-CL4053 may function through a similar mechanism of inhibition as the D-like-CL4033.

INDEX WORDS: Filoviruses, Innate immune antagonism, Interferon, Deazaneplanocin derivatives, Non-segmented negative sense RNA viruses, Vesicular Stomatitis Virus

CHARACTERIZING NOVEL FILOVIRUS PROTEINS AND 3-DEAZANEPLANOCIN A DERIVATIVES AS ANTIVIRALS AGAINST NON-SEGMENTED NEGATIVE SENSE RNA VIRUSES

by

JOYCE SWEENEY GIBBONS

A Dissertation Submitted in Partial Fulfillment of the Requirements for the Degree of

Doctor of Philosophy

in the College of Arts and Sciences

Georgia State University

2021

CHARACTERIZING NOVEL FILOVIRUS PROTEINS AND 3-DEAZANEPLANOCIN A DERIVATIVES AS ANTIVIRALS AGAINST NON-SEGMENTED NEGATIVE SENSE RNA VIRUSES

by

JOYCE SWEENEY GIBBONS

Committee Chair: Christopher Basler

Committee: Margo Brinton

Donald Hamelberg

Ming Luo

Electronic Version Approved:

Office of Graduate Studies

College of Arts and Sciences

Georgia State University

May 2021

DEDICATION

This dissertation is dedicated to my parents, Donald and Catherine Sweeney, and my husband, Christopher Gibbons.

To my parents - you are the most amazing and supportive parents. Thank you for encouraging my curiosity, for allowing me to play in your chemistry and physics labs, for reading the newspaper and books to me, for letting me build forts, tree-houses, and bridges in the most ridiculous places and for always believing that I could achieve anything I set my mind to. I am forever grateful. You pushed me to achieve the highest possible academic and personal success. You never once doubted my abilities, even when I failed multiple times. Thank you. I love you guys.

To my husband, Christopher Gibbons. I would not have finished this journey had you not been in my life, thank you. Thank you for unconditionally loving me, for standing by me and thank you for just being you. You have taught me how to love unconditionally and to be a kinder, and more forgiving person, thank you. You are my heart, my soul, and my everything. I am eternally grateful for your unconditional love, friendship, support, and patience. Cobestie spouses for life. I love you, more. Honk, honk.

.

ACKNOWLEDGEMENTS

To my Ph.D. mentor, Christopher Basler, thank you for providing me with a rigorous and solid tool kit on how to effectively do science. Your training has been invaluable, and I could not have asked for a better scientific mind to guide me. Thank you for your patience, your encouragement, and your dedication in helping me get started on my science journey.

To my dissertation committee - Margo Brinton, Donald Hamelberg, and Ming Luo - thank you for your guidance and valuable scientific contribution to the beginning of my scientific career. In particular, Donald Hamelberg, thank you for listening to me, encouraging me to stick with the program and to ignore the white-noise. Your guidance was most valuable and uplifting.

To the Basler Lab members, thank you for years of support, friendship, encouragement and stimulating science conversations. In particular, Caroline Williams, aka Love Bug, your love and friendship are very precious to me. Thank you for being a wonderful and supportive friend. Love Bugs for life.

To my siblings, Nicola McCarthy, Brefne Sweeney, Shane Sweeney and Danielle Bingham, thank you for supporting, encouraging, and loving me. I am fortunate to have siblings who care and love me the way you do. I love you guys.

TABLE OF CONTENTS

LIST OF TABLES

LIST OF FIGURES

LIST OF ABBREVIATIONS

3-Deazaneplanocin (DzNep)
Antioxidant response element (ARE)
Base pairs (bp)
Bombali *ebolavirus* (BOMV)
Bundibugyo *ebolavirus* (BDBV)
Complementary deoxyribonucleic acid (cDNA)
Cyclic GMP-AMP (cGAS)
Democratic Republic of Congo (DRC)
Deoxyribonucleic acid (DNA)
Double-strand ribonucleic acid (dsRNA)
Ebola virus disease (EVD)
Glycoprotein (GP)
Huángjiāo *thamnovirus* (HUJV)
Inclusion bodies (IBs)
Interferon (IFN)
Interferon alpha/beta receptor 1 (IFNAR1)
Interferon alpha/beta receptor 2 (IFNAR2)
Interferon beta (IFNβ)
Interferon inhibitory domain (IID)
Interferon regulatory factor (IRF)
Interferon stimulated gene factor 3 (ISGF3)
Interferon stimulated genes (ISGs)
Janus kinase 1 (Jak1)
Karyopherin alpha (KPNA)
Kelch-like ECH-associated protein 1 (Keap1)
Kilobases (kb)
Kilodaltons (kDa)
Large protein (L protein)
Leader (le)
Lloviu virus (LLOV)
Marburg virus (MARV)
Marburg virus disease (MVD)
Měnglà virus (MLAV)
Messenger ribonucleic acid (mRNA)
Methyltransferase domain (MTD)
Newcastle disease virus (NDV)
Nicotinamide adenine dinucleotide (NAD+)
Nipah virus (NiV)
Non-human primates (NHPs)
Non-segmented negative sense (NNS)
Nuclear factor erythroid 2-related factor 2 (Nrf2)
Nucleocapsid (NC)
Nucleoprotein (NP)

Open reading frame (ORF)
Pairwise sequence comparison (PASC)
Promoter element 1 (PE1)
Promoter element 2 (PE2)
Protein kinase, interferon-inducible double stranded RNA dependent activator (PACT)
Ravn virus (RAVV)
Respiratory syncytial virus (RSV)
Reston *ebolavirus* (RESTV)
Reverse transcription-quantitative polymerase chain reaction (RT-qPCR)
Ribonucleic acid (RNA)
Ribonucleoprotein (RNP)
RNA-dependent RNA polymerase (RdRp)
Sendai Virus (SeV)
Signal transducer and activator of transcription 1 (STAT1)
Signal transducer and activator of transcription 2 (STAT2)
Single-strand ribonucleic acid (ssRNA)
small soluble GP (ssGP)
soluble GP (sGP)
Stimulator of IFN genes (STING)
Sudan *ebolavirus* (SUDV)
Tai Forest *ebolavirus* (TAFV)
Trailer (tr)
Transcription start signal (TSS)
Tyrosine kinase 2 (Tyk2)
United Kingdom (UK)
United States of America (USA)
Universal Interferon (UIFN)
Untranslated regions (UTRs)
Vesicular Stomatitis Virus (VSV)
Viral protein 24 (VP24)
Viral protein 30 (VP30)
Viral protein 35 (VP35)
Viral protein 40 (VP40)
Xīlang *striavirus* (XILV)
Zaire *ebolavirus* (EBOV)

1 INTRODUCTION

1.1 Filoviruses

1.1.1 Taxonomic classification

Of the order *Mononegavirales*, the *Filoviridae* family contains six phylogenetically related genera (*Table 1.1*) [1, 2]. Genome nucleotide sequences can diverge between 55-58% to be considered part of a genus, and 23-26% divergence can occur at the species level [3]. Of the six genera, *Ebolavirus* contains the most species, Bombali *ebolavirus* (BOMV), Bundibugyo *ebolavirus* (BDBV), Reston *ebolavirus* (RESTV), Sudan *ebolavirus* (SUDV), Tai Forest *ebolavirus* (TAFV), and Zaire *ebolavirus* (EBOV) [2]. *Marburgvirus* contains one species, *Marburg marburgvirus*; however, there are two distinct lineages, Marburg virus (MARV) and Ravn virus (RAVV), with approximately 20% genetic divergence in their genome sequences [2, 4, 5]. The remaining virus species were discovered within the last decade, with viral RNA and not infectious virus being isolated [6-10]. *Cuevavirus* contains one virus species, Lloviu virus (LLOV) [9, 10]. LLOV RNA was isolated from Schreiber's bats that had died in Cueva del Lloviu, Spain [10]. Recently, novel fish filoviruses were found in China, resulting in the creation of two more genera, *Striavirus*, containing the species Xīlang *striavirus* (XILV) and *Thamnovirus* containing the Huángjiāo *thamnovirus* (HUJV) species [8]. The latest proposed addition to the *Filoviridae* family is the *Dianlovirus* genus, which contains one species, Měnglà virus (MLAV) [6]. The near complete MLAV RNA genome was isolated from the liver of a *Rousettus* bat in China [6].

Table 1.1.1 Taxonomy of the Filoviridae family

Order	Family	Genus	Species
Mononegavirales	*Filoviridae*	*Cuevavirus*	Lloviu virus (LLOV)
		Dianlovirus	Měnglà virus (MLAV)
		Ebolavirus	Bombali *ebolavirus* (BOMV)
			Bundibugyo *ebolavirus* (BDBV)
			Reston *ebolavirus* (RESTV)
			Sudan *ebolavirus* (SUDV)
			Tai Forest *ebolavirus* (TAFV)
			Zaire *ebolavirus* (EBOV)
		Marburgvirus	*Marburg marburgvirus*
			- Marburg virus (MARV)
			- Ravn virus (RAVV)
		Striavirus	Xīlang *striavirus* (XILV)
		Thamnovirus	Huángjiāo *thamnovirus* (HUJV)

1.1.2 History of outbreaks

The first documented filovirus outbreak occurred in 1967 in laboratory workers in Marburg and Frankfurt, Germany, and Belgrade, Serbia (*Table 1.2.1*) [5, 11, 12]. After ruling out all other known infectious pathogens with the capacity to cause hemorrhagic fever, it was determined that a new virus had been discovered, MARV [11, 12]. Ironically, the MARV-infected laboratory workers were isolating tissue from imported Ugandan African green monkeys (*Chlorocebus tantalus*) for use in poliomyelitis vaccine production

[12]. Over the next fifty years, sporadic outbreaks of MARV and RAVV infections occurred predominantly within sub-Saharan African countries (*Table 1.2.1*) [5, 13]. The largest outbreaks of *Marburgviruses* occurred in the Democratic Republic of the Congo (DRC) (1998-2000) and Angola (2004-2005) with both outbreaks having high case fatality rates of 83 and 90%, respectively [4, 14]. Several cases were reported outside of African countries; however, both the United States of America (USA) and Netherlands' cases originated due to an infection in Uganda [15, 16], and the isolated Russian case occurred due to a laboratory infection [17].

Table 1.2.1 Chronological cases and outbreaks of Marburgviruses

Year	Country	Species	Reported cases	Deaths	% Fatality
1967	Germany and Serbia[1]	MARV	32	7	22%
1975	South Africa	MARV	3	1	33%
1980	Kenya	MARV	2	1	50%
1987	Kenya	RAVN	1	1	100%
1990	Russia[2]	MARV	1	1	100%
1998-2000	DRC	MARV/RAVV	154	128	83%
2004-2005	Angola	MARV	252	227	90%
2007	Uganda	MARV/RAVV	4	1	25%
2008	USA[3]	MARV	1	0	0%
2008	Netherlands[3]	MARV	1	1	50%
2012	Uganda	MARV	15	4	27%
2014	Uganda	MARV	1	1	100%
2017	Uganda	MARV	3	3	100%

Table adapted from [13] and https://www.cdc.gov/vhf/marburg/outbreaks/chronology.html#eleven.
[1] MARV infected African green monkeys imported from Uganda; [2] Laboratory infection; [3] Travelers returning from a cave in Maramagambo forest, Uganda.

In 1976, two outbreaks of a "Marburg-Like Virus Disease" occurred in southern Sudan and the DRC (*Table 1.3.2*) [18-22]. Based on an antigenic comparison, it was determined that this new infectious agent was distinct from MARV. In fact, each outbreak was caused by two different species of *Ebolavirus*, EBOV and SUDV [18, 19, 21, 22].

EBOV is the most commonly occurring species, and most outbreaks have occurred in countries within the equatorial belt of Africa [13, 23]. Since the first documented case in 1976, the DRC has had 12 outbreaks constituting greater than a third of the total outbreaks [13]. In 2018, a mere week after the ninth DRC outbreak was declared over, the North Kivu province of northeastern DRC experienced the second deadliest EBOV outbreak with 3,470 reported cases and a 66% fatality rate [13]. The deadliest EBOV outbreak occurred over a period of two years, 2014-2016, with an estimated 28,652 suspected and reported cases and an approximately 40% case fatality rate [13]. The magnitude of this outbreak was enormous and also unusual in that the most affected countries of Liberia, Sierra Leone, and Guinea are all located on the western coast of Africa. The 2014 outbreak also exported cases to Nigeria, Mali, the USA, Senegal, the United Kingdom (UK), Spain, and Italy [13]. In February 2021, two new outbreaks of EBOV were announced. In Guinea, as of mid-March, there have been 18 confirmed cases and 9 deaths. Based on sequencing of the virus genome, it is believed that this outbreak is the result of a dormant virus infection from an individual previously infected in the 2014-2016 EBOV outbreak [24, 25]. In the DRC, as of early March, 11 confirmed cases and 4 deaths have been reported. Similar to the ongoing Guinea outbreak, it is thought that the DRC outbreak was originated by a persistently infected individual from the 2018-2020 DRC outbreaks [26, 27].

Table 1.3.2 Chronological cases and outbreaks of Ebolaviruses

Year	Country	Species	Reported cases	Deaths	% Fatality
1976	Sudan	SUDV	284	151	53%
1976	DRC	EBOV	318	280	88%
1976	England[1]	EBOV	1	0	0%
1977	DRC	EBOV	1	1	100%
1979	Sudan	SUDV	34	22	65%
1989	Philippines & USA[2]	RESTV	7	0	0%
1992	Italy[3]	RESTV	0	0	0%
1994	Gabon	EBOV	51	31	61%
1994	Cote d'Ivoire	TAFV	1	0	0%
1995	DRC	EBOV	315	254	81%
1996	Gabon	EBOV	31	21	68%
1996	Gabon	EBOV	60	45	75%
1996	South Africa	EBOV	2	1	50%
1996	Philippines & USA[3]	RESTV	0	0	0%
1996	Russia[1]	EBOV	1	1	100%
2000	Uganda	SUDV	425	224	53%
2001	Gabon	EBOV	65	53	81%
2001	Republic of the Congo	EBOV	59	44	75%
2003	Republic of the Congo	EBOV	143	128	89%
2003	Republic of the Congo	EBOV	35	29	83%
2004	Sudan	SUDV	17	7	41%
2004	Russia[1]	EBOV	1	1	100%
2005	Republic of the Congo	EBOV	12	10	83%
2007	DRC	EBOV	264	187	71%
2007	Uganda	BDBV	131	42	32%
2008	Philippines[2, 4]	RESTV	6	0	0%
2008	DRC	EBOV	32	15	47%
2011	Uganda	SUDV	1	1	100%
2012	Uganda	SUDV	11	4	36%
2012	DRC	BDBV	38	13	34%
2012	Uganda	SUDV	6	3	50%
2014	Various countries[5]	EBOV	28,652	11,325	40%
2014	DRC	EBOV	69	49	71%
2017	DRC	EBOV	8	4	50%
2018	DRC	EBOV	54	33	61%
2018	DRC, Uganda	EBOV	3,470	2,287	66%
2020	DRC	EBOV	130	55	42%
2021	Guinea[6]	EBOV	18	9	50%
2021	DRC[6]	EBOV	11	4	36%

Table adapted from [13] and https://www.cdc.gov/vhf/ebola/outbreaks/history/chronology.html#thirtyfour.
[1] Laboratory infection; [2] Asymptomatic; [3] RESTV contaminated monkeys [4] RESTV contaminated pigs
[5]Guinea, Liberia, Sierra Leone, Italy, Mali, Nigeria, Senegal, Spain, UK, USA [6]Ongoing outbreaks

1.1.3 Natural reservoirs

Filoviruses are zoonotic viruses, and it is of significant public interest to identify the natural reservoir. The natural reservoir is critical for the virus's environmental maintenance, and presumably, the reservoir species would not succumb to the virus infection and would be capable of virus transmission [28]. Since filoviruses are endemic to African countries, substantial field studies to determine the natural reservoir have been conducted across several African countries, including the DRC [29], Gabon [30-33], Ghana [34, 35], Guinea [36], Kenya [37], Republic of the Congo [32, 33], Sierra Leone [38], Uganda [39-41], South Africa [42], and Zambia [43, 44].

Bats became a suspected filovirus reservoir for several reasons. Following the 1995 EBOV outbreak in Kikwit, DRC, a study was undertaken to determine if plant and animal life native to Kikwit were susceptible to EBOV infection [45]. Of the 24 plant species, and the 19 animal species, only three different species of bats, Angola-free tailed bat (*Tadarida condylura*), Little free-tailed bat (*Tadarida pumila*), and Wahlberg's epauletted fruit bat (*Epomophorus wahlbergi*) were capable of being infected, producing virus, and did not appear to show any overt signs of illness [45]. EBOV RNA was found to be present in the bats' lungs and feces suggesting a potential for virus transmission [45].

In 2007, ten different bat species collected at various Gabon sites were tested for MARV RNA and IgG antibodies. Only one bat species, Egyptian rousette (*Rousettus aegyptiacus*), a fruit bat typical to many African countries, tested positive for both [31]. Since several outbreaks of MARV are associated with humans entering caves, [14-16, 46, 47] animal species inhabiting caves were of particular interest. In Goroumbwa Mine

(Durba, DRC), 20.5% of the sampled Egyptian rousette fruit bats tested positive for MARV antibodies [29]. Definitive evidence of the Egyptian rousette bat as the bonafide MARV natural reservoir was provided in 2009 when the infectious virus was isolated from five Egyptian rousette bats native to Kitaka Cave (Uganda). Multiple distinct MARV strains were found circulating in the bats, which is consistent with the long-term maintenance of the virus within the species [41]. In 2012, live MARV virus was again isolated from seven Egyptian rousette bats native to Python Cave (Uganda) [40]. MARV RNA was also present in organs (kidneys, colon, lungs, and reproductive tissues) that could potentiate virus dissemination. Increased number of bats with virus infections were observed in older juvenile bats during bi-annual birthing times and these increased number of bat infections coincided with 54/65 or 83% of MARV outbreaks in humans [40]. Recently, infectious MARV was isolated from four Egyptian rousette bats in caves located in Sierra Leone [38]. To date, no west African countries have reported MARV outbreaks; however, this study highlighted the geographic distribution of MARV-infected bats.

The natural reservoir for *Ebolavirus* has yet to be identified [48]. Based on survey studies of infectable species and the presence of *Ebolavirus* antibodies and RNA [30, 32-36, 44, 45, 49-54], a species, or multiple species, of bat is the likely natural reservoir. The latest addition to the *Ebolavirus* genus, BOMV, was discovered in molossid bats (*Chaerephon pumilus* and *Mops condylurus*) [55]. LLOV RNA, the sole species of the genus *Cuevavirus*, was found in Schreiber's bats (*Miniopterus schreibersii*) [9, 10]. MLAV RNA as well as RNA from unclassified filoviruses were isolated from *Rousettus* and *Eonycteris* genera [6, 56]. Interestingly, HUJV and XILV RNA were found in Actinopterygii

(ray-finned fish) [8]; however, whether these species are natural versus accidental hosts remains to be determined.

1.1.4 Structure and composition

Filoviruses are pleomorphic, enveloped structures with a virion diameter of ~80 nm and an average length of ~1000 nm (**Figure 1**) [57-65]. EBOV particles can be of three different types: single genome, multi-genome and empty [64]. Particles containing as many as 22 genome copies have been identified, and this genome polyploidy may allow for greater infectivity rates [64, 66, 67]. MARV and EBOV genomes contain a similar number of nucleotides, 19.1 kilobases (kb) and 18.9 kb, respectively [68, 69].

The helical nucleocapsid (NC), ~50 nm in diameter, constitutes the core of the host-derived, lipid envelope and consists of the non-segmented, negative sense (NNS) RNA genome, encapsidated with the nucleoprotein (NP) and four viral structural proteins, viral protein (VP) 24, VP35, VP30 and the RNA-dependent RNA polymerase (RdRp) Large (L) protein [59, 60, 62, 64, 70, 71]. VP24 and VP35 form bridges across the NP coated RNA and help stabilize and condense the NC [59, 64, 70, 72]. The VP30 and L protein are not required for NC assembly but are required for infectivity [61, 62, 64, 73, 74]. The major matrix protein, VP40, decorates the inner-most part of the virion lipid membrane and is indispensable for assembly and release of the virus particle from the host cell [59, 60, 62, 64, 75-78]. The final component of the virion is a class I transmembrane glycoprotein ($GP_{1,2}$). Homotrimers of $GP_{1,2}$ are embedded within and protrude out of the exterior portion of the virion lipid membrane and ultimately will be used to bind to and enter into a target host cell [79-83].

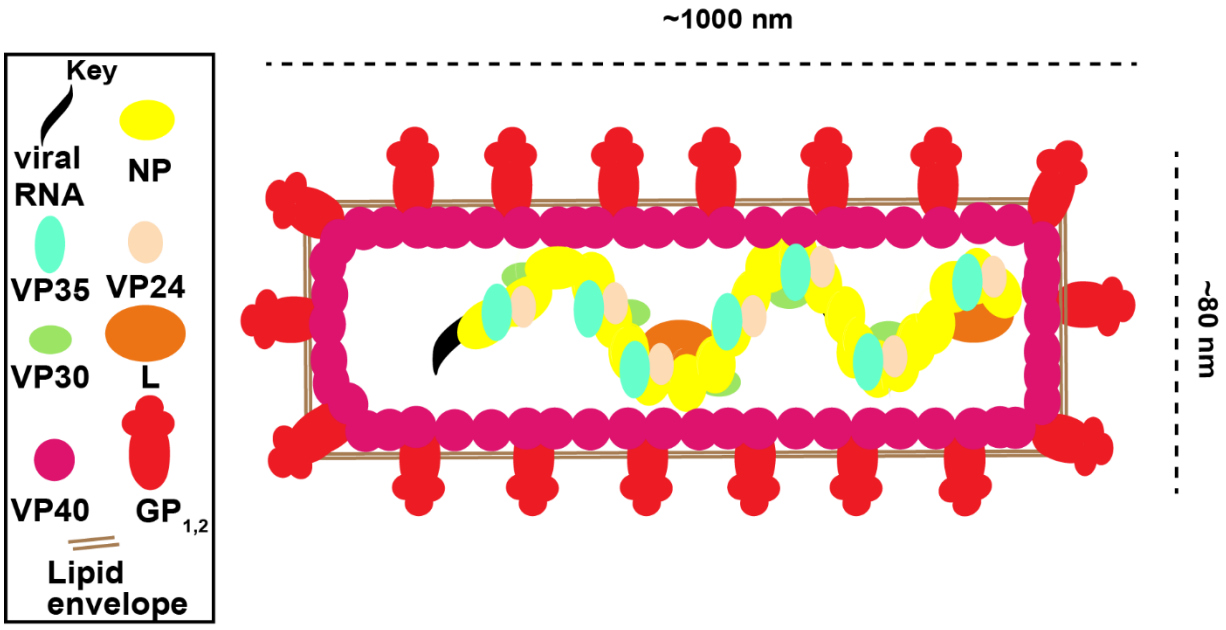

Figure 1 Structure and protein composition of the virion.
Cartoon representation of the virion structure along with ~length and diameter of the virion. Structural proteins associated with the virion are indicated and color coded as per the key.

1.1.5 Genome organization and proteins products

1.1.5.1 Genome organization

Filovirus genomes encode seven genes, which, depending on the genus, generate seven to nine proteins (**Figure 2**) [84-91]. The genome is organized as follows, 3'-Leader-NP-VP35-VP40-GP-VP30-VP24-L-Trailer-5' [85, 86]. The leader (le) and trailer (tr) sequences are contained within the untranslated regions (UTRs) of the genomic RNA. These UTRs flank the 3' and 5' open reading frames (ORFs) and contain essential sequences and RNA structures for initiation and termination of viral transcription and replication (**Figure 2**) [85, 86, 89, 90, 92-96]. The 3' UTR contains the bipartite replication promoter, promoter element 1 (PE1), and promoter element 2 (PE2), and is separated by

a spacer region that includes the transcription start signal (TSS) [92, 93, 97]. PE1 is predicted to exist as a stable RNA hairpin loop [85, 92, 93, 98]. Immediately downstream of PE1 is the spacer region, the length of which must be a multiple of six ("hexamer phasing") to allow for replication and transcription [92, 93, 96, 97, 99]. For EBOV and MARV, the PE1 is similarly organized and sized, ranging from 48-55 nucleotides, followed by a varying sized spacer and PE2 regions (**Figure 2**) [85, 92, 93, 98]. Recently, a LLOV chimeric minigenome (MG) system, was found to be replication competent with the EBOV le and tr sequences but not with the MARV le sequence suggesting that LLOV contains a promoter organization similar to that of EBOV [100] .

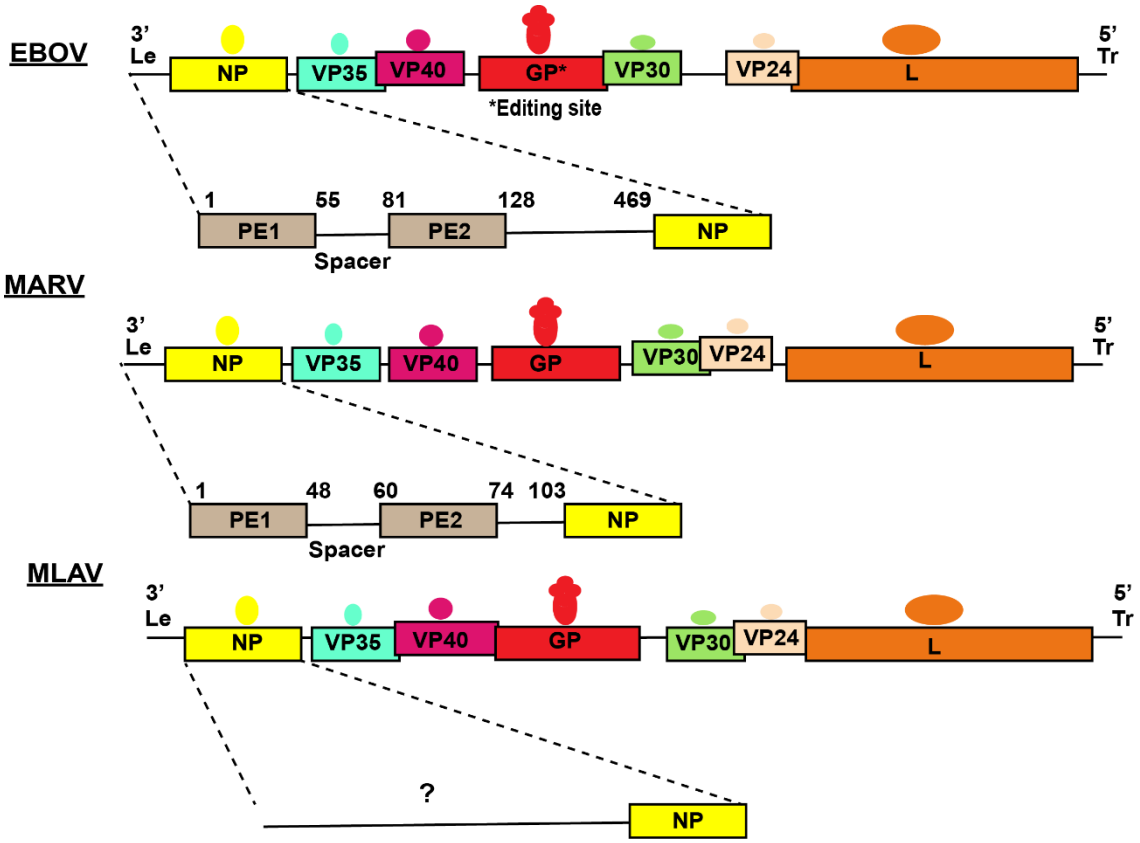

Figure 2 Genome organization with bipartite promoters.

Cartoon representation of EBOV, MARV and MLAV genome organization showing gene order, overlapping genes and protein products. The nucleotide locations of EBOV and MARV promoter element sequences are given in detail. The MLAV promoter region is currently unknown. PE promoter element; Le leader; Tr trailer Promoter figures modified from [92, 93].

The details of the MLAV promoter are currently unknown; presumably, it is similar to other characterized filoviruses given that chimeric MLAV MG replicons containing either MARV or EBOV le and tr sequences had the ability to replicate *in vitro* [6].

The individual filovirus genes are bordered by highly conserved gene start and end sequences, followed by an intergenic region (IR) or a downstream gene overlap (**Figure 2**) [85, 86, 98, 101, 102]. A gene overlap occurs when the stop signal of an upstream gene overlaps with the start signal sequence of the adjacent downstream gene. MARV contains one gene overlap at the VP30-VP24 junction, whereas EBOV contains three: VP35-VP40, GP-VP30, and VP24-L [85, 86]. Interestingly, MLAV appears to be a combination of both EBOV and MARV patterns with four gene overlaps occurring at VP35-VP40 (similar to EBOV), VP40-GP (unique to MLAV), VP30-VP24 (similar to MARV) and VP24-L (similar to EBOV) [6]. LLOV appears to be unique among the filoviruses in that six ORFs are present with VP24 and L being fused together [10].

The GP gene of EBOV and LLOV undergoes an unusual transcription editing mechanism and produces three unique mRNA transcripts, soluble GP (sGP), immature $GP_{1,2}$, and small soluble GP (ssGP) [103-105]. The transcriptional editing event occurs when the RdRp encounters a string of seven uridines on the genomic viral RNA (vRNA). The polymerase can stutter or slip on this sequence which results in the insertion or deletion of nucleotides in the mRNA products. Insertion of an additional adenosine (8 adenosines) produces the immature $GP_{1,2}$ mRNA and either insertion of two adenosines or deletion of one adenosine (6 or 9 adenosines) produces the ssGP mRNA. Synthesis of the unedited, full length gene (7 adenosines) produces the small GP (sGP) [103-105].

1.1.5.2 Protein products

Translation and cleavage of filovirus proteins produces seven proteins for MARV and MLAV and ten for EBOV (*Table 1.4.1*) [84-91]. Five of the proteins, NP, VP35, VP24, VP30 and L are components of the mature nucleocapsid [59, 60, 64] with NP, VP35 and VP24 being necessary and sufficient for NC transport to the host membrane [106]. Four of these proteins, NP, VP35, VP30 and L make up the ribonucleoprotein (RNP) complex that is required for EBOV transcription and replication [94]. The MARV RNP complex comprises the same set of proteins but VP30 appears to be expendable in a MG system [95, 107]. VP40 and VP24 are the major and minor matrix proteins, respectively [108], and $GP_{1,2}$ is responsible for cell entry [109]. The major roles of the viral proteins are given in *Table 1.4.1*.

NP is the major protein involved in the generation of the NC and is also required for virus transcription, replication, and assembly [59-62, 64, 73, 75, 76, 91, 94, 95, 110-117]. The NP can also independently generate perinuclear localized inclusion bodies (IBs) which are the sites of filovirus replication [118-121]. Additionally, the C-terminal domain of NP is implicated in helping with virus assembly and budding [75, 76, 110, 118].

The VP30 phosphoprotein is a novel protein among NNS RNA viruses [85, 86, 88] and recently, several VP30 crystal structures have provided detailed insight into both the structure and roles of VP30 in binding NP and modulating both transcription and replication [122-126].

VP35 is analogous to the P proteins of other NNS RNA viruses and in addition to its role in the maturation of the NC, is a required co-factor of the L protein. VP35 is believed to function as a bridge between the NP-RNA and L during transcription and

replication [59, 60, 64, 73, 91, 94, 95, 115, 117]. Similar to NP, VP35 is found localized within IBs [118, 119]. Antagonism of the innate immune pathway, in particular, inhibition of type I interferon (IFN) production, is a well characterized function of VP35, and this functionality will be discussed in more detail below [127, 128].

Named for its large size, the L protein contains all the obligatory enzymatic motifs and binding sites for polymerization, capping, methylation, and polyadenylation of nascent RNA [94, 95, 115, 129-132]. There is only one partial crystal structure of the SUDV methyltransferase domain (MTD) currently available [133]. Much of what we know about the filovirus L protein comes from our studies of RdRp proteins of other NNS RNA viruses [131-137]. In particular, cryo-EM structures of full length L vesicular stomatitis virus (VSV) and more recently rabies virus L, has given detailed insight into the L domain organization [131, 135]. Filovirus L proteins presumably share a similar organization and functionality [138, 139]; however, further work needs to be done to confirm this. Based on the structure of the VSV L and sequence comparisons, several shared motifs exist within the L proteins of NNS RNA viruses [131, 140]. The RdRp domain contains the classic fingers-palm-thumb polymerase architecture and a conserved GDNQ catalytic motif, which is responsible for polymerization. The capping domain contains the conserved HR residues, which aid in the addition of the 5' guanosine cap to the viral mRNA. The third enzymatic domain resides within the MTD and this contains the conserved motif for SAM binding (GxGxG) and methyl-transfer catalysis (K-D-K-E) [131, 133, 140, 141]. The domain and structural organization for VSV L is given in detail in **Figure 9** and **Figure 22**.

VP40 forms multimeric lattices beneath the host plasma membrane and is the primary protein involved in assembly and budding of the virion [59, 60, 75-77, 142-146]. Both MARV and MLAV VP40 are potent inhibitors of the interferon signaling pathway [127, 128] and these roles will be discussed in detail below. VP24 is the minor matrix protein and also, in addition to VP30, appears to be a unique protein among the NNS RNA viruses [59, 60, 64]. Curiously, the VP24s of the filoviruses have evolved quite different strategies for hijacking cellular pathways. MARV VP24 can activate the antioxidant response pathway whereas EBOV and LLOV antagonize the type I IFN signaling pathway [127, 128]. These functionalities will be discussed more in detail below.

The filoviruses have only one glycoprotein, $GP_{1,2}$, that is required for virus binding and fusion with cellular membranes [79, 109, 147-150]. It also functions as a major antigenic determinant with the most virus epitopes being reported for $GP_{1,2}$ [151, 152]. EBOV infected cells can also secrete sGP which is believed to function as a decoy for antibodies targeting the $GP_{1,2}$ [153]. Cleavage of the sGP C-terminus produces the Δ-peptide, which functions as a viroporin [154]. The roles of ssGP are currently undetermined [103].

Table 1.4.1 Protein functions

Protein	~Molecular Weight (kDa)[1]	Function
NP	90-110	Major component in NC formation; RNP component; essential for replication and transcription
VP35	35	NC & RNP component; essential for replication and transcription; IFN antagonist; inhibits DC maturation
VP30	27-30	NC & RNP component; transcriptional activator (EBOV)
L	250	NC & RNP component; essential for replication and transcription; polymerizes, caps, methylates and polyadenylates nascent viral RNA
VP40	35-40	Major matrix protein; NC assembly and egress; IFN antagonist (MARV and MLAV)
VP24	24-25	NC component; condenses nucleocapsid; minor matrix protein; egress; IFN antagonist (EBOV and LLOV)
GP	150	Binds and fuses receptor for cell entry; major antigenic protein; cytotoxic factor
sGP	50	Decoy antigen; curtails cytotoxic effects of GP; potential virulence factor
Δ-peptide	5	Unknown roles; potential viroporin
ssGP	50	Unknown

Table modified from [117][1] Based on reducing conditions of gel migration; Data sourced from [91, 103, 108, 109, 115, 127].

1.1.6 Life cycle: entry, transcription, replication, and egress

The life cycle of a filovirus begins when its $GP_{1,2}$ binds and fuses with the host endosomal lipid membrane [79, 109, 147-150] (**Figure 3**). Filoviruses have a broad cellular tropism. Antigen-presenting cells, in particular monocyte-derived macrophages and dendritic cells, are hypothesized to be the preferential target cells [155-160]. The extracellular receptor that $GP_{1,2}$ binds with to gain entry is currently unknown. However, the α-folate receptor and C-type lectins are implicated in contributing to entry [161-165]. The virus enters through the host-mediated pathway of macropinocytosis [166] and fusion of the viral and endosomal membranes occurs with the aid of the interaction between the endosomal cholesterol receptor, Niemann-Pick type C1 (NPC1) and $GP_{1,2}$ [150, 167]. Upon fusion, the NC is released into the cytoplasm. All transcription and replication events occur within the cytoplasm [168]. The RNP complex initiates primary transcription with the polymerase entering a single site at the 3' end of the genomic RNA [169, 170]. The polymerase recognizes and binds conserved sequences found within the bipartite promoter region and scans downstream to begin transcription of viral mRNA [130, 168]. Transcription proceeds via the start-stop mechanism with the polymerase recognizing conserved gene start sequences and end sequences flanking each of the genes [95, 98, 130, 168]. Similar to other NNS RNA viruses, filoviruses produce mRNAs in a gradient with genes closer in proximity to the 3' bipartite promoter producing more mRNA than genes more distant from the 3' bipartite promoter (**Figure 3**) [171] [130]. All viral mRNAs are 5' guanosine capped and methylated. Methylation occurs on the seven position of the 5' guanosine cap, as well as at the first and second nucleotide on the 2' hydroxyl of the ribose ring. Viral mRNAs are also polyadenylated at the 3' end of the viral transcript. [130-

132, 172]. The host translational machinery is hijacked for the synthesis of viral proteins and this allows the production of more genomic and antigenomic viral RNA. How the polymerase switches between transcription and replication is regulated is not entirely understood for NNS RNA viruses; however, the molar concentration of the nucleocapsid protein may be a driving factor [130]. When this switch does occur, the polymerase will ignore all gene start and stop signals and replicate the entire full length antigenome (5'-3'). From this, full length genomic RNA (3'-5') can be produced [130, 168]. Replication of filoviruses occurs within NP-derived IBs and all components of the NC (NP, VP35, VP30, VP24 and L) are also localized here [118-121]. Recently, it was postulated that a two-stage interaction with both the N and C terminal domains of NP and VP40 may function as a switching mechanism between viral replication and NC assembly [110]. Ultimately, VP40 association with both the NC and the host membrane will allow for assembly and budding of new virions [59, 60, 75-77, 142-146]. To aid in assembly and release, the late domain motifs of VP40 interact with host proteins such as Tsg101 and Nedd4 [75, 146, 173-176]. The final step in the virus life cycle occurs when the virus buds from the host cell from filopodia-like protrusions [65]. $GP_{1,2}$, which has been transported to the cell surface membrane [103], also helps in the virus egress by counteracting the effects of the host restriction factor, type II transmembrane glycoprotein, tetherin [177-179].

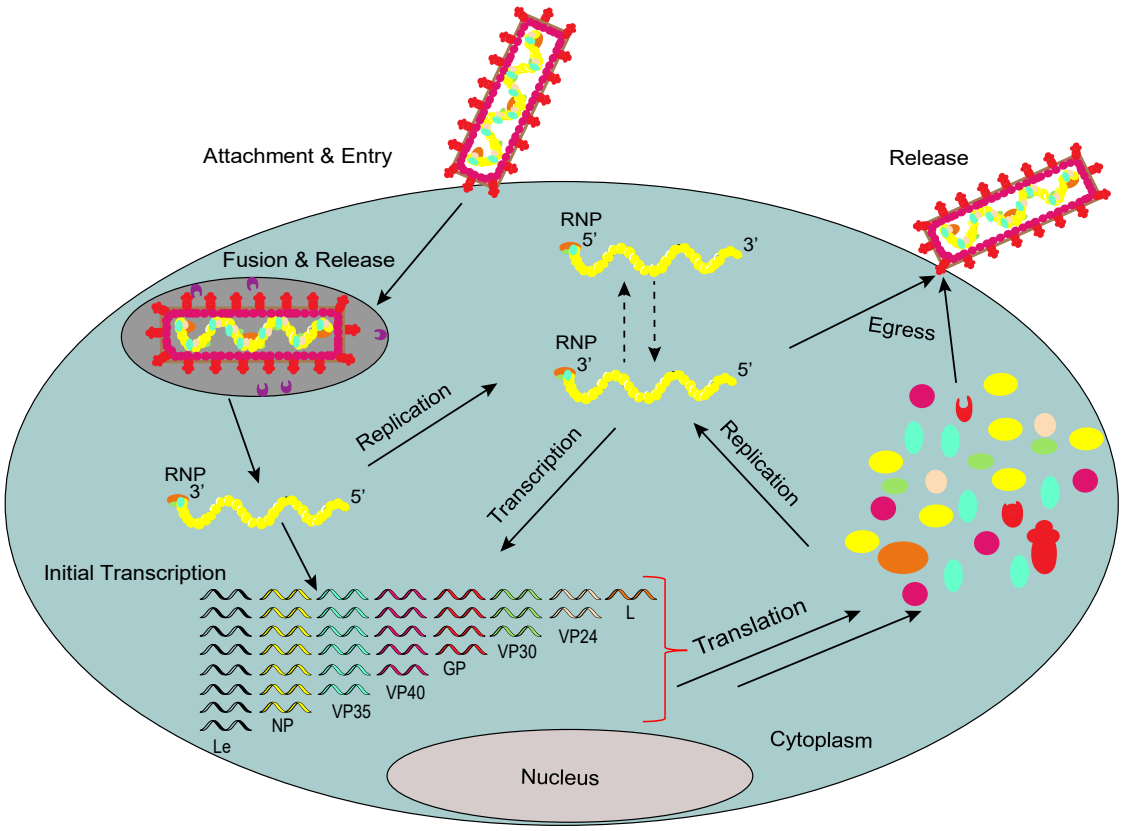

Figure 3 EBOV life cycle.
Cartoon representation of the proposed life cycle of EBOV from initial attachment, entry, genome transcription and replication to budding and egress. RNP ribonucleoprotein.

1.1.7 Broad-spectrum nucleoside analog inhibitors

At the end of 2019, the FDA approved Ervebo, a VSV-based recombinant vector vaccine pseudotyped with the EBOV GP [180]. Ervebo has proved effective at inhibiting EBOV spread when delivered in a ring vaccination method; however, it is important to note that this vaccine is effective only against EBOV and no other filovirus species [181, 182]. At the end of 2020, two more antibody-based therapeutics (Inmazeb and Ebanga) against EBOV were FDA approved [183, 184]. Currently, there are no FDA-approved pan-filovirus inhibitors. Nucleoside analogs demonstrating potential as pan-filovirus inhibitors are described below [185, 186].

1.1.7.1 BCX4430, GS-5734 and T-705 antiviral activities

Nucleoside analogs are attractive candidates for inhibiting NNS RNA viruses, and the presumed target of inhibition is the viral RdRp domain within the L protein [185-189]. Nucleoside derivatives utilize one of three mechanisms for direct RdRp inhibition: 1) non-obligate chain termination, 2) obligate chain termination and 3) mis-sense incorporation [190]. BCX4430 (Galidesivir), a non-obligate chain terminator, has shown both *in vitro* and *in vivo* efficacy against both EBOV and MARV species (**Figure 4**) [191, 192]. More importantly, BCX4430 protected 100% of non-human primates (NHPs) against a lethal dose of MARV when administered twice daily starting at 48 hours-post-infection [191]. GS-5734 (Veklury or Remdesivir), a non-obligate chain terminator, has demonstrated broad-spectrum antiviral activity against a myriad of viruses and was most recently recognized by the FDA as an approved treatment of SARS-CoV-2 (**Figure 4**) [193-198]. Previously, Remdesivir, due to its *in vitro* and *in vivo* activity against EBOV [197], was also re-purposed for EBOV treatment during the 2014-2016 West African EBOV outbreak and the 2018-2020 DRC outbreak [199-201]. Treatment with Remdesivir during the 2018-2020 DRC outbreak was halted mid-trial due to inferior inhibition as compared to treatment with Inmazeb and Ebanga [199]. Finally, T-705 (Avigan or Favipiravir) is postulated to function via a mis-sense antiviral mechanism and has shown potent activity against NNS RNA viruses as well multiple influenza virus strains (**Figure 4**) [202-207].T-705 is currently approved and stockpiled in Japan for treatment of influenza infections [208]. In 2014, utilizing a type I IFN receptor (IFNAR) knockout A129 mouse model, T-705 (administered post virus infection, 2 times daily at 150 mg/kg) was found to offer full protection from a lethal aerosolized dose of EBOV strain E718 [202]. A similar study,

using EBOV infected IFNAR knockout mice, found that T-705 (twice daily at 300 mg/kg) rendered complete protection relative to vehicle treated mice when administered six days post infection [207]. Unfortunately, results of T-705's efficacy at inhibiting EBOV in non-human primates, cynomolgus macaques (*Macaca fascicularis*), were disappointing with all animals succumbing to EBOV infection, even when different dosing regimens were employed [209]. However, the T-705-treated and EBOV-infected monkeys did show reduced viral loads and a longer time of survival. Also, in MARV-infected animals treated with intravenous doses of T-705, 83% survival was observed [209]. T-705 was also employed during the 2014-2016 EBOV outbreak. However, the effectiveness in EBOV-infected humans was confounding due to the design of the trials and potential dosing issues. As was seen in the NHP studies, T-705 did reduce viral RNA levels and extended the survival times to death [210-215].

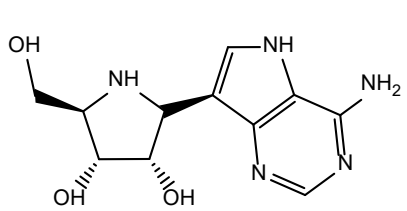

BCX 4430

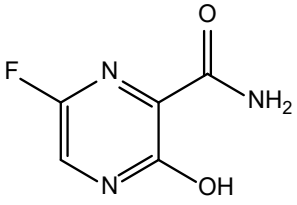

T-705

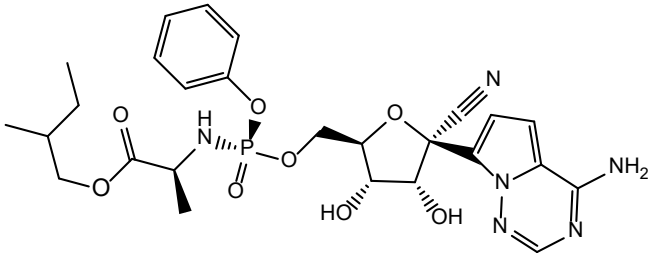

GS-5734

Figure 4 Structures of nucleoside analogs with *in vitro* and *in vivo* activity against EBOV and MARV.

Chemical structures of the nucleoside analogs, BCX-4430, T-705 and GS-5734.

1.1.7.2 S-Adenosylhomocysteine hydrolase inhibitors

Rational structural modifications to the different nucleoside moieties (the nitrogenous nucleobase and the ribose sugar) can be conducted to facilitate the synthesis of nucleoside analogs with targeted specificities for cellular proteins [186, 189, 216]. The removal of the ribose ring oxygen and its replacement with carbon, produced the adenosine analog, Aristeromycin (**Figure 5**) [217]. Synthesis of Aristeromycin ultimately lead to the generation of the carbocyclic nucleoside analog series, some of which exhibited very potent antiviral activities against both DNA and RNA viruses [189, 218]. Dehydration across the 4',6' bond of the cyclopentyl ring gave rise to Neplanocin A [219-222], which had previously been isolated from the sponge *Ampullariella regularis* and was known to exert antimicrobial activity (**Figure 5**) [223, 224]. The cellular toxicity associated with Neplanocin A was removed when 3-deazaneplanocin (DzNep) was synthesized [225]. DzNep differs from its parent compound, Neplanocin A, in that that the nitrogen at the 3 position in the nucleobase is replaced with a carbon (**Figure 5**) [225]. DzNep is of particular interest within the filovirus field and was demonstrated to potently inhibit EBOV replication in cell culture [226]. More importantly, a single dose (2 mg/kg at the time of infection or one hour post infection) of DzNep completely protected BALB/c mice that were infected with mouse-adapted EBOV at 300 times the 50% lethal dose (LD50) [227]. Curiously, only the DzNep-treated and infected mice were observed to produce massive amounts of IFN alpha, the reason for which has not been resolved [227]. Unfortunately, for reasons unknown, when DzNep was transitioned into the NHP model, the compound was not effective at protecting NHPs from EBOV infection.

Brominated derivatives of DzNep (CL123, CL4033 and CL4053) have been developed to explore their potential for anti-filovirus activity (**Figure 5**) [228, 229]. In chapter 3 of this dissertation, we assess the mechanisms of antiviral activity of these DzNep congeners using VSV as a model NNS RNA virus.

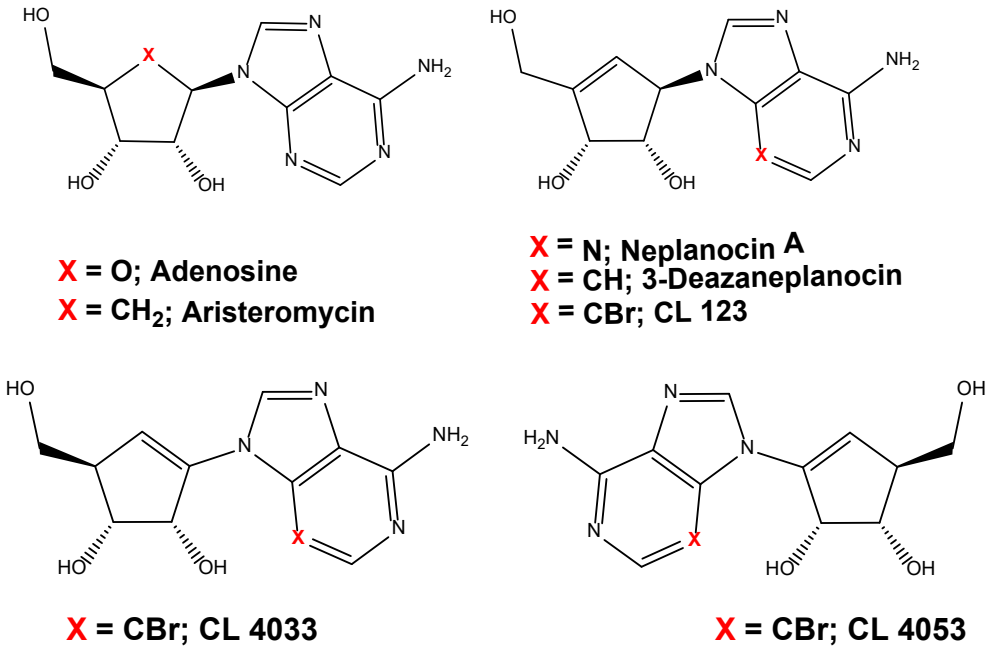

Figure 5 Structure of adenosine and SAHase inhibitors.
*Chemical structures of adenosine and SAHase inhibitors where **X** represents the point of modification within the structure. The atom (s) of **X** are given below each structure.*

The known cellular target of inhibition for the described carbocyclic adenosine analogs is S-adenosylhomocysteine hydrolase (SAHase, E.C.3.3.1.1) [218]. SAHase hydrolyzes S-adenosylhomocysteine (SAH) into homocysteine and adenosine with the chemical equilibrium lying in favor of SAH synthesis. Removal of homocysteine and adenosine shifts the equilibrium in the hydrolysis direction [230]. In the absence of SAH breakdown, increased intracellular levels of SAH are observed [231, 232]. SAH can potently inhibit S-adenosylmethionine (SAM)-dependent methyltransferases [225, 231-

256]. For viruses that encode SAM-dependent methyltransferases, inhibition of SAHase could inhibit the viral methyltransferase. Indeed, the antiviral activities of SAHase inhibitors against distinct species of viruses has been well demonstrated [218, 226-229, 257-297]. Additionally, there is a strong correlation between antiviral activity and SAHase inhibition [218]. The proposed mechanism of inhibition of neplanocin analogs (SAHase inhibitors) is given in **Figure 6.**

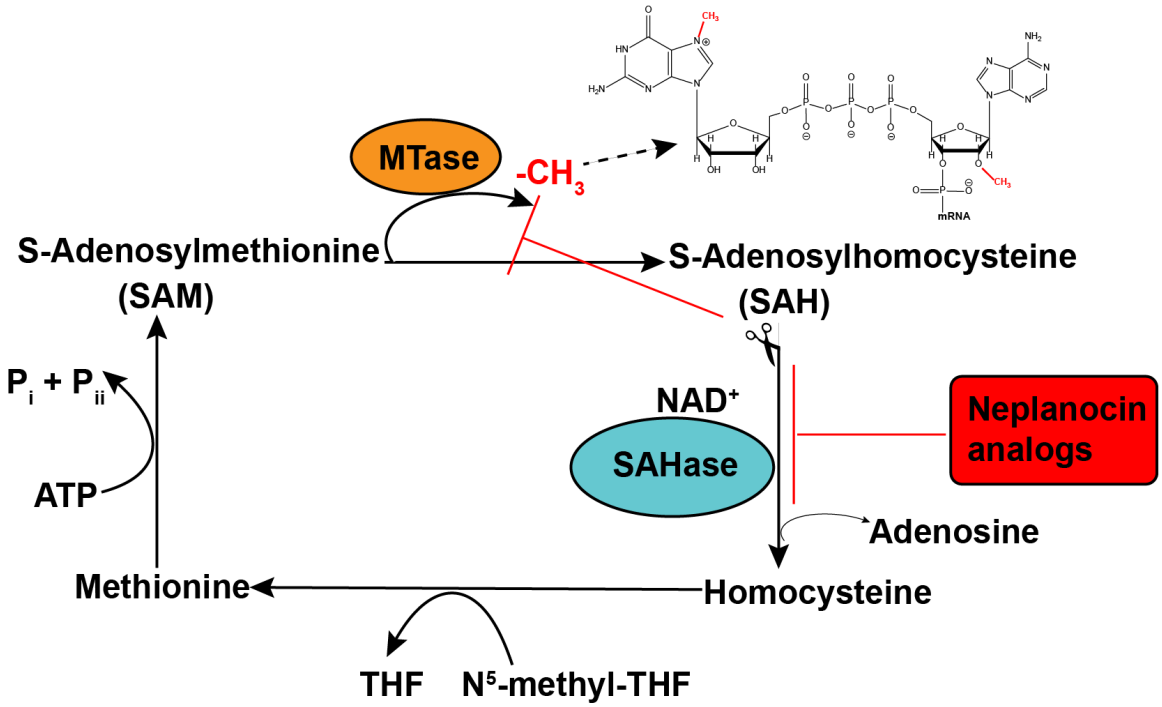

Figure 6 Proposed mechanism of antiviral inhibition by neplanocin analogs. *Cartoon representation of how neplanocin analogs are hypothesized to exert their antiviral activity. The structure of the viral methylated caps is given adjacent to the orange colored MTase. The neplanocin analogs (SAHase inhibitors, red box) are indicated at the point of their inhibition (SAHase hydrolysis). SAHase S-adenosylhomocysteine hydrolase; NAD+ nicotinamide adenine dinucleotide; THF tetrahydrofolate; ATP adenosine triphosphate; MTase methyltransferase; SAM S-Adenosylmethionine and SAH S-Adenosylhomocysteine. Schematic modified from [270].*

1.2 Host signaling pathways and Filovirus interactions

1.2.1 Type I IFN pathway

The type I IFN pathway is an ancient defense system that vertebrates have evolved and maintained to combat microbial infections [298-300] . The pathway consists of two major branches, the production of type I IFN and the subsequent signaling induced by the type I IFN production. To date, there are eight distinct type I IFN proteins that have been identified within mammals. The most well characterized are IFN-α and IFN-β (referred to as IFN α/β in the below) [299, 301]. To induce the production of IFN α/β, animal cells utilize the germ-line encoded pathogen recognition receptor (PRR) proteins. Currently, there are five different classes of PRRs: 1) toll-like receptors (TLRs), 2) nucleotide-binding oligomerization domain-like receptors (NLRs), 3) C-type lectin receptors (CLRs), 4) retinoic acid-inducible gene I (RIG-I)-like receptors (RLRs), and 5) DNA sensors (cyclic GMP-AMP, cGAS, and stimulator of IFN genes, STING). These PRRs function as sentinel sensors both intracellularly and extracellularly to detect and signal the presence of foreign pathogens. The PRR recognition of these foreign pathogens comes with the ability to be able to differentiate between “self” and “non-self” molecular motifs. Examples of “non-self” motifs or pathogen-associated molecular patterns (PAMPs) include the lipopolysaccharide (LPS) found in gram-negative bacteria (TLRs), sugars present in bacteria cell walls (CLRs), cytosolic DNA (cGAS), or virus nucleic acids (RLRs, TLRs and NLRs). Upon detection and discrimination of the PAMP by the PRR, a signaling cascade within the cell will stimulate activation of multiple proteins. This culminates in cytoplasmic transcription factors (interferon regulatory factor (IRF) 3 and IRF7) localizing to the nucleus to bind and turn on the IFN α/β promoter for

the production of IFN α/β genes [302-309]. Secretion of IFN α/β cytokines from the cell allows binding to their receptor (IFNAR) in either an autocrine or a paracrine fashion. This binding event stimulates the activation of the type I IFN signaling pathway. IFN α/β binding of IFNAR causes it to dimerize and activate intracellular, IFNAR-associated kinases, Janus kinase 1 (Jak1) and tyrosine kinase 2 (Tyk2) [310]. The activation of Jak1 and Tyk2 by transphosphorylation provides a docking site for the subsequent recruitment and phosphorylation of signal transducer and activator of transcription (STAT) proteins. Heterodimers of phosphorylated STAT1 and STAT2, together with IRF9 form the interferon-stimulated gene factor (ISGF) 3 complex and localize to the nucleus with the help of a nuclear transporting protein, karyopherinα (KPNA). Interaction of the ISGF3 complex with a conserved DNA sequence, interferon-stimulated response elements (ISREs), stimulates the production of hundreds of interferon-stimulated genes (ISGs) [311-317]. These ISGs will render an antiviral cellular milieu [316, 317].

For NNS RNA viruses, the contribution of RLRs to detection of their RNA and production of IFN α/β has been well documented [128, 302, 304]. The RLR family consists of three nucleic acid sensors: 1) RIG-I, 2) melanoma differentiation association gene 5 (MDA5), and 3) laboratory of genetics and physiology 2 (LGP2). RIG-I preferentially detects 5’ triphosphates (5’ppp) of short (~10-300 base pairs (bp)) double-strand (ds) RNAs and single-strand (ss) RNAs. MDA5 recognizes longer dsRNAs. The most recent addition to the group, LGP2, is thought to play more of a regulatory role for RIG-I and MDA5. The helicase domain of RIG-I recognizes the PAMPs found on NNS RNA virus RNAs (5’ppp) and activation of the pathway occurs through its tandem caspase and activation recruitment domains (CARD). Activated RIG-I then travels to the mitochondria

where it interacts with the mitochondrial antiviral-signaling (MAVS) protein to form a signalosome platform. This platform recruits cellular kinases TANK binding kinase 1 (TBK1) and inhibitor of nuclear factor kappa-B kinase subunit epsilon (IKKε) that will phosphorylate the latent transcription factor IRF3. Phosphorylation and dimerization of IRF3 results in movement to the nucleus where IFN α/β genes will be turned on (**Figure 7**) [302, 318].

1.2.2 Filovirus antagonism of the type I IFN pathway

1.2.2.1 Filovirus antagonism of the type I IFN pathway and virulence

For filoviruses, inhibition of the type I IFN pathway has been well characterized [127, 128, 319]. Suppression of interferon responses is one of the factors that is believed to contribute to the virulence of EBOV and MARV in animals. Immunocompetent mice are not susceptible to either MARV or EBOV infection; however, immunodeficient mice (IFNAR knockout and severe combined immunodeficiency (SCID)) mice can be lethally infected with EBOV, MARV or RAVV [320-322]. Additionally, serially passaging of RAVV in immunocompetent mice (using SCID-RAVV as the initial source of virus) was demonstrated to evolve virus that could cause a lethal infection in the immunocompetent mice. Sequencing the mouse-adapted RAVV genome revealed amino acid substitutions in several of the viral proteins, of which, seven non-synonymous amino acid changes were in the matrix VP40 protein [322, 323]. Later, it was demonstrated that the non-mouse-adapted MARV and RAVV VP40 proteins were incapable of inhibiting mouse type I IFN responses. However, two of the seven non-synonymous RAVV VP40 amino acid changes that developed during the mouse adaptation process, V57A and T165A, were

adequate to inhibit mouse type I IFN responses. These data suggest VP40 as a potential candidate for host adaptation and virulence [324].

1.2.2.2 Filovirus antagonism of the type I IFN pathway

Three viral proteins, VP35, MARV and MLAV VP40 and EBOV and LLOV VP24 can potently suppress type I IFN responses and ISG production. Interestingly, the three viral proteins antagonize the signaling pathway through very distinct mechanisms (**Figure 7**) [128, 319].

In 1999, EBOV infection was found to inhibit interferon responses [325]. Shortly thereafter, EBOV VP35 was characterized as an inhibitor of the type I IFN pathway that could inhibit both dsRNA and Sendai virus-induced activation of an IFN-β promoter construct [326]. Since then, VP35 has been shown to inhibit at multiple points in the RIG-I pathway and to impair activation of IFN-inducible ISGs [327-340]. Basic residues within the VP35 IFN inhibitory domain (IID), located within the C-terminal region, bind dsRNA and VP35 mediated inhibition of RIG-I signaling, strongly correlates with this dsRNA binding capacity [327-331, 334-336, 338, 341, 342]. In addition to sequestering dsRNA, VP35 can disrupt the interaction between protein kinase, interferon-inducible double stranded RNA dependent activator (PACT) and RIG-I [339, 343]. PACT aids in the activation of RIG-I signaling [344]. Cellular kinases TBK1 and IKKε functions are also modulated by VP35, where VP35 is thought to function as a decoy substrate for these kinases and is phosphorylated instead of IRF3 [345, 346]. Antagonism of VP35 at these different points in the RIG-I pathway resulted in inhibition of phosphorylation of IRF3 and subsequently diminished IFN-β responses [128, 339, 346]. Additionally, MARV, MLAV

and EBOV VP35 can inhibit phosphorylation of the IFN-inducible ISG, protein kinase R (PKR), although the mechanism of how this occurs is not fully understood [339, 340, 347].

As mentioned above, during type I IFN signaling, phosphorylated STAT1 utilizes the NPI-1 KPNAs to translocate to the nucleus [313, 314]. The EBOV VP24 minor matrix protein can also bind to the members of the NPI-1 family of KPNAs (KPNA1, KPNA5 and KPNA6). It is known that the type I IFN signaling mechanism of inhibition by EBOV VP24 is driven by VP24's disruption of the phosphorylated-STAT1-KPNA interaction [348-350]. Presumably, LLOV's VP24, which is also capable of inhibiting the type I IFN response, inhibits through a similar mechanism as EBOV VP24 [351].

MARV and MLAV VP40 can also prevent type I IFN signaling. Both MARV and MLAV VP40 can potently inhibit the phosphorylation of STAT1 that occurs during type I IFN signaling. Universal-IFN treatment and overexpression of Jak1 can induce phosphorylation of STAT1 and both MARV and MLAV VP40 inhibit phosphorylation of STAT1, regardless of either stimulation [128, 324, 339, 352, 353]. To date, we have not been able to fully elucidate how MARV and MLAV VP40 proteins are capable of this inhibition.

In chapter 2 of this dissertation, we describe the regulation of both human and bat innate immune responses by MLAV VP35, VP40 and VP24 proteins.

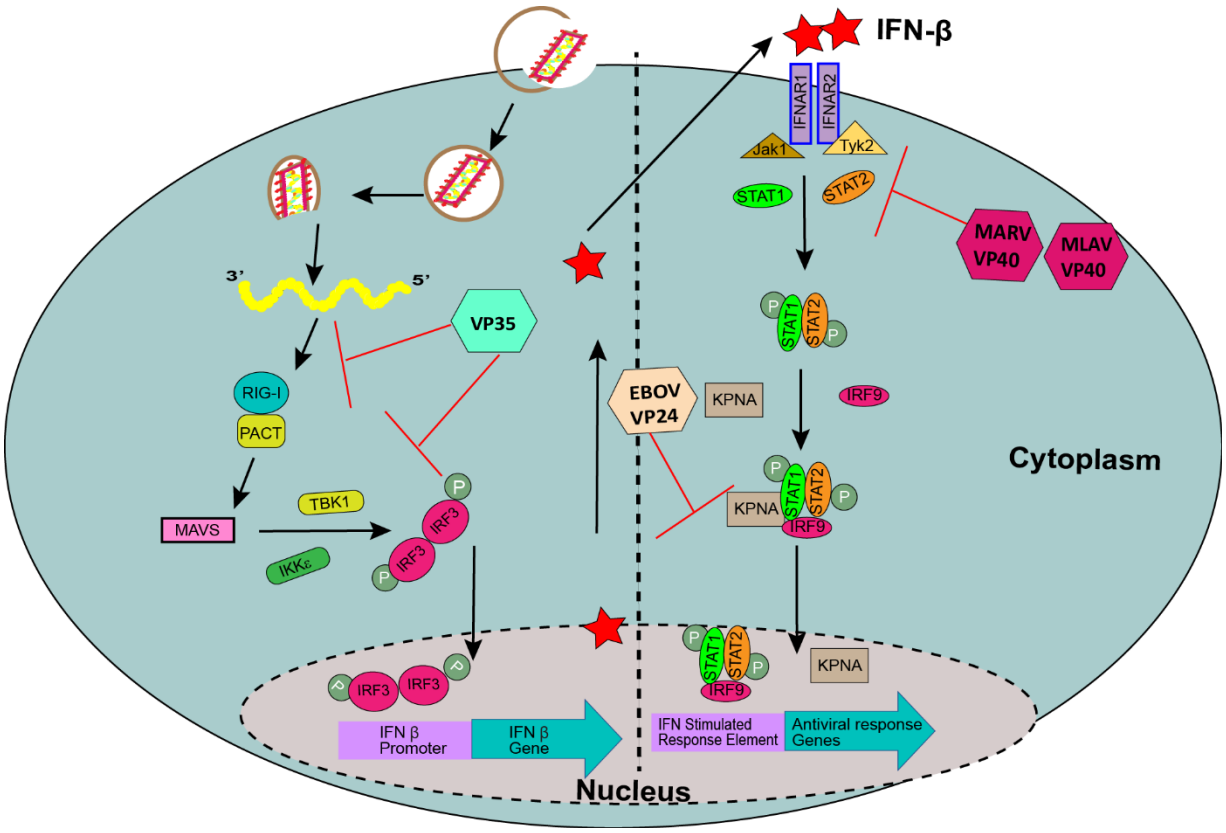

Figure 7 Type I IFN pathway inhibition by filovirus VP35, VP40 and VP24.
Cartoon representation of the cellular events leading to the production of IFNβ. Points of inhibition by filovirus viral proteins are also noted. RIG-I retinoic acid-inducible gene I; PACT protein kinase, interferon-inducible double stranded RNA dependent activator; MAVS mitochondrial antiviral signaling protein; TBK1 TANK binding kinase 1; IKKε inhibitor of nuclear factor kappa-B kinase subunit epsilon; IRF3/9 interferon regulatory factor 3/9; IFN interferon; IFNAR1/2 interferon alpha/beta receptor 1/2; Jak1 janus kinase 1; Tyk2 tyrosine kinase 2; STAT1/2 signal transducer and activator of transcription 1/2; KPNA karyopherin alpha.

1.2.3 MARV VP24 activation of the ARE pathway

MARV VP24 does not inhibit IFN activities but rather activates a cytoprotective response in both infection and transfection-based experiments [354, 355]. Under basal conditions, the transcription factor nuclear factor erythroid 2-related factor 2 (Nrf-2) is held in the cytoplasm by an interaction with Kelch-like ECH-associated protein 1 (Keap1). This

interaction allows Nrf2 to be tagged for proteasomal degradation, thereby preventing its nuclear accumulation. If cellular stress occurs (reactive oxygen species, UV damage, etc.), this Keap1-Nrf2 interaction is disrupted and Nrf2 translocates to the nucleus to bind with an antioxidant response element (ARE) DNA sequence. Nrf2 can translocate into the nucleus due to the presence of a nuclear localization signal in its C-terminus [356]. Nrf2 binding with the ARE stimulates the production of antioxidant genes and will render a cytoprotective state [357, 358]. MARV VP24, specifically the K-loop residues, can disrupt the Nrf2-Keap1 interaction. This disruption inhibits Keap1 mediated degradation of Nrf2, allowing Nrf2 to shuttle to the nucleus and consequently turn on ARE genes. It is postulated that MARV uses this cytoprotective state as a means to assist its replication cycle [339, 354, 355].

In Chapter 2 of this dissertation, we further confirm the importance of the MARV VP24 K-loop residues for interaction with both human and bat Keap1. We also determine that MLAV VP24 appears to be functionally distinct from its EBOV and MARV VP24 counterparts.

1.3 VSV: A prototype NNS RNA virus

1.3.1 VSV genome and L protein organization

Vesicular Stomatitis Virus (VSV) belongs to the *Rhabdoviridae* family and often serves as the prototype virus for NNS RNA viruses. VSV has provided seminal research for NNS RNA viruses on genome organization, modes of transcription and replication as well as mechanisms of capping, methylation, and polyadenylation of viral mRNA [130].

The genome gene organization is 3’-Le-N-P-M-G-L-Tr-5’ (**Figure 8**) The transcriptase complex, which contains the nucleoprotein (N) encapsidated viral genome

(N-vRNA), the L protein and the phosphoprotein (P) [359-361], initiates primary transcription at the 3' end of the N-vRNA. L polymerizes the nascent mRNA transcript while P serves as a cofactor [359, 362-366].

During transcription, L adds a 5' guanosine cap and also methylates and polyadenylates all viral mRNA transcripts [172, 367-374]. The functional diversity of the L protein can be attributed to its organization into five highly interconnected domains - RdRp, capping, connector, MTD, and the C-terminal domain (**Figure 9 and Figure 22**). As described above, three of these domains, RdRp, capping and MTD, possess enzymatic activity. The other two domains, connector, and C-terminal are thought to have a structural role [131, 132, 375].

Since work with Ebola and Marburg viruses requires a biosafety level four (BSL-4) lab, we decided to utilize VSV as a surrogate virus. In Chapter 3 of this dissertation, we utilize VSV as a model NNS RNA virus to investigate the anti-VSV mechanisms of DzNep and its 3-brominated derivatives.

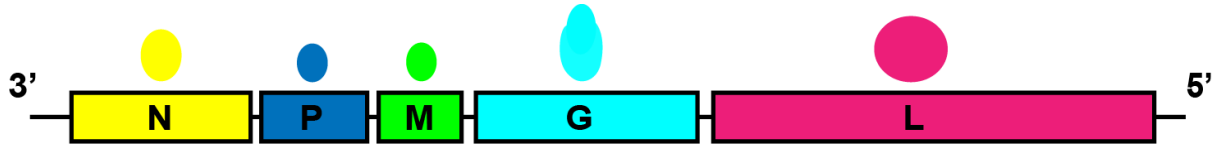

Figure 8 VSV genome organization.
Cartoon representation of VSV's genome organization. N nucleoprotein (yellow); P phosphoprotein (blue); M matrix protein (green); G glycoprotein (cyan); L large protein (pink).

Figure 9 VSV L protein domain organization.
Cartoon representation of VSV's L domain organization. RdRp RNA-dependent RNA polymerase domain (cyan); Cap Capping domain (green); CD connector domain (yellow); MT methyltransferase domain (orange); CTD C-terminal domain (red); N, N-terminal; C, C-terminal. Adapted from [131].

2 IMPACT OF MĚNGLÀ VIRUS PROTEINS ON HUMAN AND BAT INNATE IMMUNE PATHWAYS

2.1 Author figure contributions

The below outlines the figure contribution of each author.

Joyce Sweeney Gibbons - Figure 10 A-D, Figure 12 A-C, Figure 15 A-C, Figure 16 A-C, Figure 17 A-D, and Figure 18 A, B and D.

Caroline G. Williams - Figure 10 E, Figure 11, Figure 13 A-F, and Figure 18 C and E

Timothy Keiffer - Figure 14 A-B.

2.2 Abstract

Měnglà virus (MLAV), identified in *Rousettus* bats, is a phylogenetically distinct member of the family *Filoviridae*. Because the filoviruses Ebola virus (EBOV) and Marburg virus (MARV) modulate host innate immunity, MLAV VP35, VP40 and VP24 proteins were compared with their EBOV and MARV homologs for innate immune pathway modulation. In human and *Rousettus* cells, MLAV VP35 behaved like EBOV and MARV VP35s, inhibiting virus-induced activation of the interferon (IFN)-β promoter and IRF3 phosphorylation. MLAV VP35 also interacted with PACT, a host protein engaged by EBOV VP35 to inhibit RIG-I signaling. MLAV VP35 also inhibits PKR activation. MLAV VP40 was demonstrated to inhibit type I IFN induced gene expression in human and bat cells. It blocked STAT1 tyrosine phosphorylation induced either by type I IFN or over-expressed Jak1, paralleling MARV VP40. MLAV VP40 also inhibited virus-induced IFNβ promoter activation, a property shared by MARV VP40 and EBOV VP24. A Jak kinase

inhibitor did not recapitulate this inhibition in the absence of viral proteins. Therefore, inhibition of Jak-STAT signaling is insufficient to explain inhibition of IFNβ promoter activation. MLAV VP24 did not inhibit IFN-induced gene expression or bind karyopherin α proteins, properties of EBOV VP24. MLAV VP24 differed from MARV VP24 in that it failed to interact with Keap1 or activate an antioxidant response element reporter gene, due to the absence of a Keap1-binding motif. These functional observations support a closer relationship of MLAV to MARV than to EBOV but also are consistent with MLAV belonging to a distinct genus.

2.3 Importance

EBOV and MARV, members of the family *Filoviridae*, are highly pathogenic zoonotic viruses that cause severe disease in humans. Both viruses use several mechanisms to modulate the host innate immune response, and these likely contribute to severity of disease. Here, we demonstrate that MLAV, a filovirus newly discovered in a bat, suppresses antiviral type I interferon responses in both human and bat cells. Inhibitory activities are possessed by MLAV VP35 and VP40, which parallels how MARV blocks IFN responses. However, whereas MARV activates cellular antioxidant responses through an interaction between its VP24 protein and host protein Keap1, MLAV VP24 lacks a Keap1 binding motif and fails to activate this cytoprotective response. These data indicate that MLAV possesses immune suppressing functions that could facilitate human infection. They also support the placement of MLAV in a different genus than either EBOV or MARV.

2.4 Introduction

Měnglà virus (MLAV) was discovered when its genomic RNA was identified in the liver of a bat of the *Rousettus* genus that had been collected in Měnglà County, Yunnan Province, China [6]. To date, only RNA sequence is available and viable MLAV has not yet been isolated. MLAV has been proposed to represent a new genus, *Dianlovirus,* within the family *Filoviridae*. The filovirus family includes three additional genera, *Ebolavirus*, *Marburgvirus* and *Cuevavirus,* that contain viral species isolated from or identified in mammals [1]. Placement of MLAV in a distinct genus was based on its comparatively low sequence identity to other filoviruses, phylogenetic and pairwise sequence comparison (PASC) analyses [6]. It was also noted to have, compared to other filoviruses, unique gene overlaps and a unique transcription start signal [6]. MLAV displays some features more reminiscent of *Marburgvirus* members than *Ebolavirus* members. Specifically, MLAV RNA was identified in tissue from a *Rousettus* bat, the same genus of bat which serves as a MARV reservoir in Africa [48]. In addition, the MLAV Large (L) protein exhibits closer phylogenetic relatedness to *Marburgvirus* L than to the L of other filoviruses, and in contrast to *Ebolavirus* and *Cuevavirus* members, MLAV can express its glycoprotein (GP) without the need for editing of the GP mRNA [128].

Filoviruses are noteworthy because of their capacity to cause severe human disease [128]. Some members of the *Ebolavirus* and *Marburgvirus* genera are zoonotic pathogens that have caused repeated outbreaks with substantial lethality in humans [376]. The largest such outbreak on record was caused by *Zaire ebolavirus* (EBOV) and occurred in West Africa between 2013 and 2016. This resulted in upwards of 28,000 infections, more than 11,000 deaths, and the export of infected cases to the United States

and Europe [377]. EBOV is also the cause of the second largest filovirus outbreak, which was first recognized in August 2018 and has continued well into 2019 [378].The largest outbreak of MARV occurred in Angola between 2004-2005 and had a reported case fatality rate of 88 percent [376].

Likely contributing to the virulence of filoviruses are viral encoded proteins that target host cell innate immune signaling pathways [128]. Filovirus VP35 proteins suppress interferon (IFN)-α/β responses that play critical roles in innate antiviral immunity [379]. VP35 impairment of IFN-α/β production occurs by inhibition of RIG-I-like receptor (RLR) signaling through several mechanisms, including VP35 binding to RLR activating dsRNAs and the interaction of VP35 with PACT, a host protein that facilitates RIG-I activation [331, 335, 336, 342, 343, 380-386]. VP35s also inhibit the phosphorylation and activation of the IFN-induced kinase PKR [340, 387-389]. EBOV VP24, but not MARV VP24, interacts with the NPI-1 subfamily of karyopherin alpha (KPNA) (also known as importin alpha) nuclear transport proteins, which includes KPNA1, KPNA5 and KPNA6 [349, 350]. The NPI-1 subfamily also mediates nuclear import of STAT1 following its activation by IFN [313, 349, 390]. The interaction of EBOV VP24 with KPNA competes with tyrosine phosphorylated STAT1 (pY-STAT1), blocking pY-STAT1 nuclear import and suppressing expression of IFN stimulated genes (ISGs), a response that mediates the antiviral effects of IFN [348-350, 391]. MARV VP40 protein has been demonstrated to suppress IFN-induced signaling and ISG expression, while EBOV VP40 has no known role in IFN antagonism [392]. Activation of the Jak family of kinases associated with IFN receptors is inhibited by MARV VP40, blocking phosphorylation and activation of the downstream STAT proteins, including STAT1 [392-394]. EBOV VP24 and MARV VP40 have also been described to

modestly inhibit IFN-α/β production, although the mechanism(s) are not defined [353, 395]. While MARV VP24 does not appear to block IFN responses, it has been demonstrated to interact with Kelch-like ECH-associated protein 1 (Keap1). Under homeostatic conditions, Keap1, a cellular substrate adaptor protein of the Cullin3/Rbx1 ubiquitin E3 ligase complex, targets the transcription factor Nuclear factor erythroid 2-related factor 2 (Nrf2) for polyubiquitination and proteasomal degradation [354, 355, 396]. MARV VP24 disrupts the Keap1-Nrf2 interaction, leading to Nrf2-induced expression of genes possessing antioxidant response elements (ARE) [354, 355, 396]. This activity induces a cytoprotective state that may prolong the life of MARV infected cells. MARV VP24 also relieves Keap1 repression of the NF-κB pathway [397].

Given the link between EBOV and MARV innate immune suppressors and virulence, and the unknown potential of MLAV to cause human disease, this study sought to determine whether MLAV possesses effective suppressors of innate immunity. Given the differences in innate immune evasion mechanisms between EBOV and MARV, it was also of interest to determine whether MLAV innate immune evasion mechanisms more closely resemble EBOV or MARV. The data demonstrate that MLAV VP35 functions as an IFN antagonist by mechanisms that mirror those of EBOV and MARV VP35. MLAV VP40 is demonstrated to act as a suppressor of IFN-induced signaling, whereas MLAV VP24 does not, mirroring the inhibitory functions of MARV. Both MLAV VP35 and VP40 effectively suppressed IFN responses in human and *Rousettus* cells. Interestingly, MLAV VP24 does not detectably interact with Keap1 or activate ARE gene expression due to the absence of Keap1-binding sequences found in MARV VP24. Cumulatively, the data demonstrate the presence of IFN evasion functions in MLAV that are effective in human

cells, suggesting the virus may have the capacity to cause human disease. The similarities in VP40 immune evasion functions are consistent with a closer genetic relationship of MLAV to MARV than EBOV, but the differences in VP24 function are consistent with MLAV occupying a distinct genus within the filovirus family.

2.5 Materials and Methods

2.5.1 Cells and viruses

HEK293T cells were maintained in Dulbecco's Modified Eagle Medium (DMEM), supplemented with 10% fetal bovine serum (FBS) and cultured at 37°C and 5% CO_2. RO6E cells, immortalized fetal cells from *Rousettus aegyptiacus*, were obtained from BEI Resources and maintained in DMEM F12 and supplemented with 5% FBS. Sendai Virus Cantell (SeV) was grown in 10-day-old embryonating chicken eggs for forty-eight hours at 37°C.

2.5.2 Plasmids

MLAV NP, VP35, VP40, VP30 and VP24 coding sequences (based on accession number KX371887) were synthesized by Genscript. The synthesized open reading frames were cloned into a pCAGGS expression vector with a FLAG-tag at the N-terminus of each coding sequence. EBOV and MARV viral proteins, GFP-STAT1, HA-Jak1, HA-PACT, HA-KPNA5, HA-Keap1 and IRF3 expression plasmids were previously described [343, 350, 355, 380, 393]. VP24 K-loop chimeras were made using overlapping PCR. MARV VP24 residues 202-RRIDIEPCCGETVLSESV-219 were inserted into MLAV VP24 between residues 202 and 219 (MLAV $VP24_{MARV\ 202\text{-}219}$) and the corresponding MLAV residues 202- RAINASGRENESVVQNPI- 219 were inserted into MARV VP24 at the same position (MARV $VP24_{MLAV\ 202\text{-}219}$).

2.5.3 Cytokines

Universal type I IFN (UIFN) (PBL) was used at 1000 U/mL in DMEM supplemented with 0.3% FBS for 30 minutes at 37°C, unless otherwise stated.

2.5.4 IRF3 Phosphorylation assay

HEK293T cells ($1x10^6$) were transfected using Lipofectamine 2000® (Life Technologies)**.** The amount of transfected IRF3 was 100 ng per well. Twenty-four hours post transfection, cells were mock-treated, UIFN-treated or SeV-infected, depending on the assay. Subsequently, cells were lysed in NP40 buffer (50mM Tris-HCl [pH 8.0], 280mM NaCl, 0.5% NP-40) supplemented with cOmplete™ protease inhibitor cocktail (Roche) and PhosSTOP (Roche). Lysates were incubated for ten minutes on ice and clarified for ten minutes at 21,100 x g at 4°C. Phosphorylation status of the proteins was determined by western blot.

2.5.5 IFNβ and ISG54 promoter-reporter gene assays

HEK293T cells ($5x10^4$) and RO6E cells ($2x10^5$) were co-transfected using Lipofectamine 2000® with 25 ng of an IFNβ promoter-firefly luciferase reporter plasmid or an interferon stimulated gene 54 (ISG54) promoter-firefly luciferase reporter plasmid, 25 ng of a constitutively expressing *Renilla* luciferase plasmid (pRL-TK, Promega) and the indicated viral protein expression plasmids – HEK293T cells: 62.5, 6.25, and 0.625 ng for VP35 and VP40 and 25, 2.5, and 0.25 ng for VP24; RO6E cells: 250, 25, and 2.5 ng for EBOV and MARV proteins and 125, 12.5, and 1.25 ng for MLAV proteins. Twenty-four hours post transfection cells were mock-treated, SeV-infected (150 hemagglutinin activity units (HAU)) or UIFN-treated (1000 U/mL). Eighteen hours post-infection or treatment, cells were lysed and analyzed for luciferase activity using a Dual Luciferase® Reporter

Assay System (Promega) per the manufacturer's protocol. Firefly luciferase activity was normalized to *Renilla* luciferase activity. Assays were performed in triplicate; error bars indicate the standard error of the mean (SEM) for the triplicate. Viral protein expression was confirmed by western blot.

2.5.6 IFNβ reporter gene assay in the presence of a Jak1/Jak2 inhibitor

HEK293T cells ($5x10^4$) were co-transfected using Lipofectamine 2000® with 25 ng of an IFNβ promoter firefly luciferase reporter plasmid, 25 ng of pRL-TK *Renilla* luciferase reporter plasmid and 62.5, 6.25, and 0.625 ng of the indicated viral protein expression plasmids. Twenty-four hours post-transfection, cells were pre-treated for one hour with 5 μM of Ruxolitinib (SelleckChem), a Jak1/Jak2 inhibitor, and then mock- or SeV- infected in the presence of the inhibitor [398]. Eighteen hours post-infection or treatment, cells were lysed and assayed using a dual luciferase assay and analyzed as above. To verify inhibition of Jak1/Jak2 by Ruxolitinib, cells were transfected with 25 ng of an ISG54 promoter-firefly luciferase reporter plasmid and 25 ng of pRL-TK reporter plasmid. Twenty-four hours post-transfection, cells were pre-treated for one hour with 5 μM of Ruxolitinib and then mock- or UIFN-treated for eighteen hours in the presence of the inhibitor and assayed for luciferase activity as above.

2.5.7 Measurements of endogenous gene expression

HEK293T cells ($5x10^4$) were transfected with 125 ng of empty vector or viral expression plasmids using Lipofectamine 2000®**.** Twenty-four hours post-transfection, cells were either mock-treated, SeV-infected, or UIFN treated (1000U/mL). At fourteen-hours post-treatment or infection, total cellular RNA was extracted using RNeasy® Mini Kit (Qiagen), as per the manufacturer's protocol. SuperScript™ IV (Thermo Fisher

Scientific) was used to generate oligo dT cDNA which served as the template for quantitative PCR (qPCR). qPCR was performed using PerfeCTa® SYBR Green FastMix® (VWR Scientific) along with gene specific primers for human β-actin, IFNβ and ISG54.

2.5.8 ARE reporter assay

HEK293T cells ($5x10^4$) were co-transfected using Lipofectamine 2000® with an antioxidant response element (ARE) reporter gene, pGL4.37 [luc2P/ARE/Hygro] (Promega) (30 ng) and a pRL-TK reporter plasmid (25 ng) along with either empty vector or 62.5, 6.25, and 0.625 ng of EBOV, MARV, MLAV VP24 or chimeric MARV and MLAV expression plasmids. Eighteen hours post-transfection, luciferase activity was assessed and analyzed as above.

2.5.9 Co-immunoprecipitation assays

HEK293T cells were co-transfected using Lipofectamine 2000® with plasmids for FLAG-tagged MLAV proteins, HA-tagged host proteins, and pCAGGS empty vector. Twenty-four hours post-transfection cells were rinsed with PBS and lysed in NP40 buffer supplemented with cOmplete™ protease inhibitor cocktail (Roche). Lysates were clarified by centrifugation and incubated with anti-FLAG M2 (Sigma-Aldrich) or anti-HA (Thermo Fisher) magnetic beads for two hours at 4°C. Beads were washed five times in NP40 buffer and precipitated proteins were eluted by boiling with SDS sample loading buffer or elution with 3X FLAG peptide (Sigma-Aldrich). Whole cell lysates and immunoprecipitated samples were analyzed by western blot.

2.5.10 Western blot analysis

Blots were probed with anti-FLAG (Sigma-Aldrich), anti-β-tubulin (Sigma-Aldrich), anti-HA (Sigma-Aldrich), anti-phospho-IRF3 (S396) (Cell Signaling), anti-IRF3 (Santa Cruz), anti-phospho-STAT1 (Y701) (BD Transduction Laboratories), anti-STAT1 (BD Transduction Laboratories), anti-phospho-PKR (T446) (Abcam), or anti-PKR (Cell Signaling) antibodies, as indicated. Antibodies were diluted in Tris-buffered saline with 0.1% Tween-20 (TBS-T) with 5% milk or, when detecting phospho-proteins, 5% bovine serum albumin.

2.5.11 VP40 Budding Assay

10 µg of EBOV, MARV and MLAV VP40 expression plasmids were transfected into either HEK293T ($3x10^6$) or RO6E ($2x10^6$) cells using Lipofectamine 2000® (Life Technologies). Media was harvested 48 hours post-transfection, briefly clarified by centrifugation, and layered over a 20% sucrose cushion in NTE buffer (10 mM NaCl, 10 mM Tris [pH 7.5], 1 mM EDTA [pH 8.0]). The samples were then subjected to ultracentrifugation in a Beckman SW41 rotor at 222,200 x g for 2 hours at 10°C; media was aspirated after ultracentrifugation and virus-like particles (VLPs) were solubilized in NTE buffer at 4°C overnight. Cellular lysates were generated by washing transfected cells with PBS and lysing cells in NP40 buffer containing cOmplete™ protease inhibitor cocktail (Roche). To detect the presence of VP40, 5% of cell lysates and 10% of VLPs were analyzed by western blotting. To confirm that VP40s from isolated VLPs had a membrane that can protect internal components from protease digestion, 10% of VLPs were incubated in NTE buffer with 500 ng/µl of trypsin solution (Corning), either in the absence

or presence of 0.5% Triton X-100 (Sigma), at 37°C for 1 hour prior to western blot analysis.

2.5.12 Statistics

Statistical significance was determined by one-way ANOVA followed with Tukey multiple comparison as compared to the indicated control; **p < 0.0001, * p < 0.001 (GraphPad PRISM8).

2.6 Results

2.6.1 MLAV VP35 blocks virus-induced IFNβ promoter activation in both human and bat cells.

As a measure of the capacity of MLAV VP35, VP40 and VP24 to modulate type I IFN production, the human cell line HEK293T or the *Rousettus* bat cell line RO6E were assessed by reporter gene assay for their effect on Sendai virus (SeV)-induced IFNβ promoter activation. Either empty vector or FLAG-tagged expression plasmids for the VP35, VP40 and VP24 proteins of EBOV, MARV and MLAV were co-transfected with an IFNβ promoter firefly luciferase reporter and a constitutively expressing *Renilla* luciferase plasmid. Twenty-four hours post-transfection, cells were either mock-infected or infected for an additional 18 hours with SeV, a potent activator of the IFNβ promoter [399]. As expected, SeV infection activated the IFNβ promoter in the absence of viral protein expression. EBOV and MARV VP35 impaired IFNβ reporter activation in a dose-dependent manner in both cell lines, with EBOV exhibiting greater potency as previously shown (**Figure 10A and 10B**) [381, 386]. Similarly, MLAV VP35 dramatically diminished IFNβ promoter activity in a dose dependent manner (**Figure 10A and 10B**).

Expression of EBOV VP24, Lloviu virus (LLOV) VP24 or MARV VP40 has also been reported to impair IFNβ and, in the case of EBOV VP24, IFNλ production [351, 353, 395]. In the present study, in HEK293T cells, modest inhibition of IFNβ promoter activation was evident for EBOV VP24, EBOV VP40, and MARV VP40. MLAV VP40 exhibited potent dose-dependent inhibition of IFNβ promoter activation (**Figure 10A**). Weak, but statistically significant inhibition of IFNβ reporter gene expression was detected for MARV VP24 and MLAV VP24, however, the biological significance of this minimal inhibition is uncertain. In RO6E cells, MLAV VP40 inhibition of IFNβ promoter activation was also detected but only at the highest concentration of transfected plasmid (**Figure 10B**).

To evaluate whether or not the inhibition of the IFNβ reporter also correlates with inhibition of endogenous IFNβ gene expression, qRT-PCR assays were performed. MLAV VP35 and VP40 showed significant inhibition of IFNβ transcripts consistent with the results of the reporter assays. Expression of MLAV VP24 had no effect on IFNβ copy numbers, which may suggest that the minor inhibition observed in the luminescence assay is not biologically relevant (**Figure 10C**).

EBOV and MARV VP35 inhibition of RLR signaling pathways results in inhibition of the phosphorylation and activation of transcription factor interferon regulatory factor 3 (IRF3) [330, 380, 400]. In order to determine whether MLAV VP35 can inhibit activation of IRF3, HEK293T cells were co-transfected with either empty vector or an IRF3 expression plasmid and plasmids that express FLAG-tagged EBOV, MARV, and MLAV VP35 (**Figure 10D**). Twenty-four hours post-transfection, cells were either mock- or SeV-infected to induce IRF3 phosphorylation. Over-expression of IRF3 substantially increased

detection of the phosphorylated form. As previously reported, EBOV VP35 potently inhibited IRF3 phosphorylation. MARV VP35 also inhibited IRF3 phosphorylation, although less efficiently, consistent with less robust inhibition of RIG-I signaling as compared to EBOV VP35 [381, 386]. MLAV VP35 inhibited IRF3 phosphorylation comparable to EBOV VP35 (**Figure 10D**).

EBOV and MARV VP35 interact with host protein PACT, and this interaction contributes to VP35 inhibition of RIG-I signaling [340, 343]. To determine if MLAV VP35 might suppress IFN production through a similar mechanism, the PACT-VP35 interactions were evaluated by co-immunoprecipitation assay (**Figure 10E**). FLAG-tagged EBOV, MARV, and MLAV VP35 or empty vector expression plasmids were co-transfected with HA-tagged PACT in HEK293T cells. A VP35 dsRNA binding mutant ($VP35_{KRA}$) that has previously been shown to lack the ability to interact with PACT was included as a negative control [343]. All three wildtype VP35 proteins were demonstrated to interact with PACT, with MLAV VP35 interacting comparably to EBOV VP35 (**Figure 10E**). Together, these data suggest that MLAV VP35 employs mechanisms similar to EBOV and MARV VP35 for inhibition of RIG-I dependent activation of type I IFN responses and that the potency of inhibition is similar to EBOV VP35.

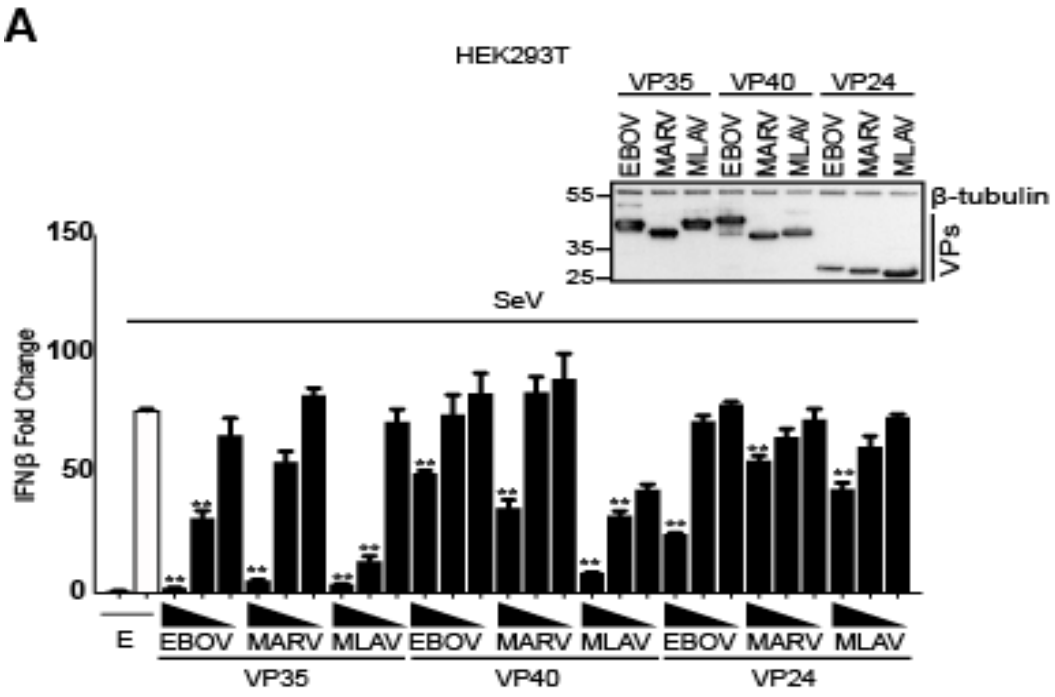
A
HEK293T
VP35
VP40
VP24
EBOV
MARV
MLAV
55
35
25
β-tubulin
VPs
SeV
IFNβ Fold Change
150
100
50
0
E
EBOV
MARV
MLAV
VP35
VP40
VP24

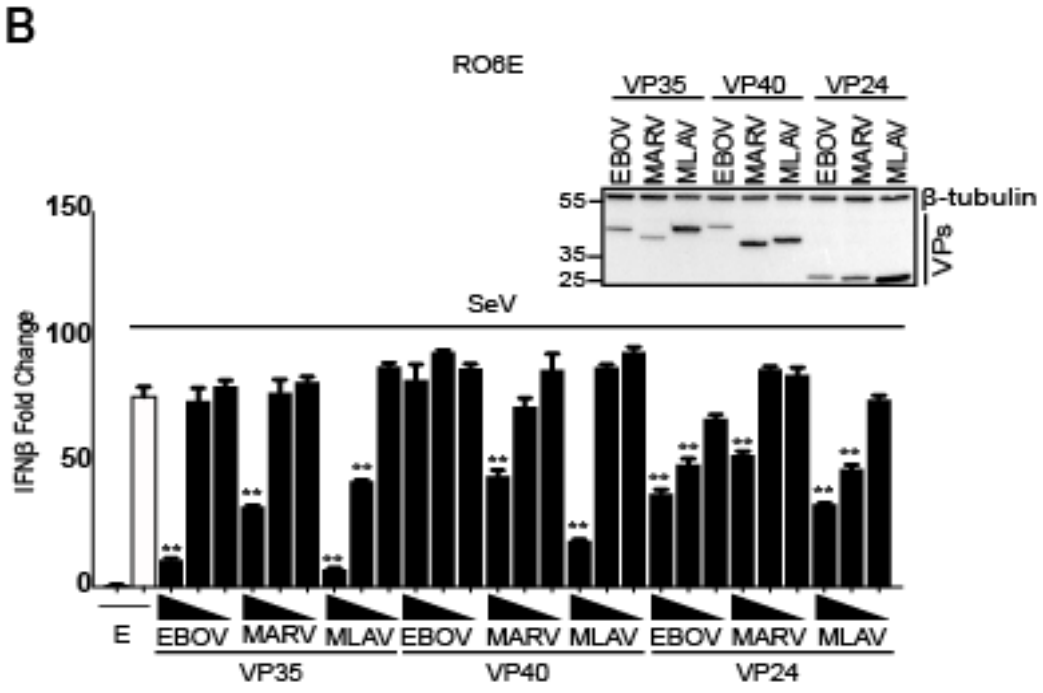
B
RO6E
VP35
VP40
VP24
EBOV
MARV
MLAV
55
35
25
β-tubulin
VPs
SeV
IFNβ Fold Change
150
100
50
0
E
EBOV
MARV
MLAV
VP35
VP40
VP24

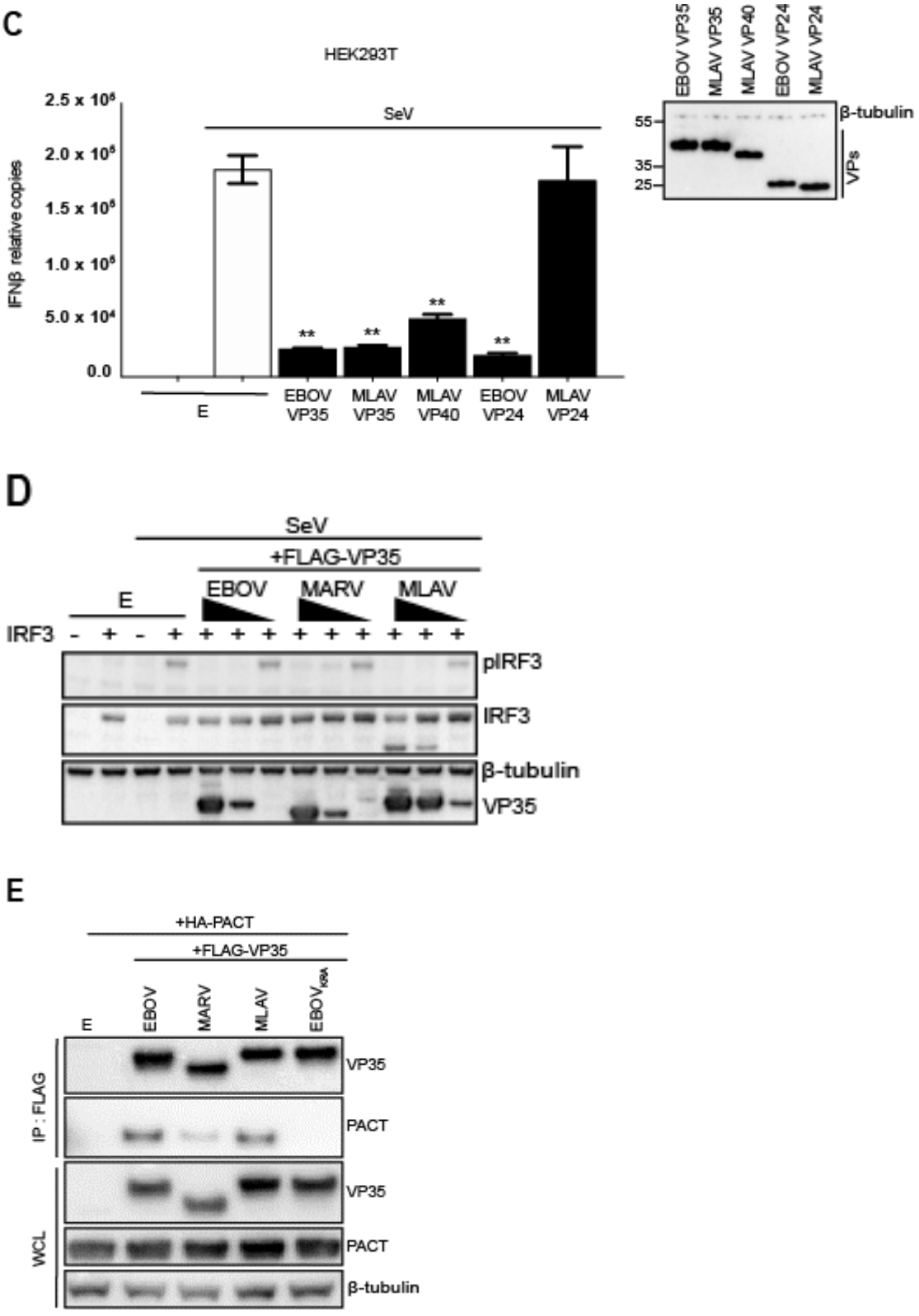

Figure 10 MLAV VP35 blocks virus-induced IFNβ promoter activation in both human and bat cells.

(A) *HEK293T cells were transfected with an IFNβ promoter firefly luciferase reporter plasmid, a constitutively-expressed Renilla luciferase reporter plasmid and either empty vector (E) or the specified FLAG-tagged viral proteins. The amounts of VP35 and VP40 plasmids were 62.5 ng, 6.25 ng and 0.625 ng; the amounts of VP24 plasmids were 25 ng, 2.5 ng and 0.25 ng. Twenty-four hours post-transfection, cells were either mock or Sendai virus (SeV)-infected. Firefly and Renilla luciferase activities were determined eighteen hours post-infection using a dual luciferase assay. Fold induction was determined relative to the vector only, mock-infected samples.* ***(B)*** *RO6E cells were assayed as described above, except the amounts of EBOV and MARV VP35, VP40 and VP24 plasmids were 250 ng, 25 ng and 2.5 ng and the amounts of MLAV VP35, VP40 and VP24 plasmids were 125 ng, 12.5 ng and 1.25 ng.* ***(C)*** *HEK293T cells were transfected with 125 ng of empty vector or the indicated protein expression plasmids, mock- or SeV-infected for eighteen hours and endogenous human IFNβ mRNA levels were measured and normalized to human β-actin mRNA levels. For all experiments in A-C, cell lysates were analyzed by western blot with anti-FLAG and anti-β-tubulin antibodies (insets). Experiments were performed in triplicate, error bars represent the SEM for the triplicate, and statistical significance was determined by performing a one-way ANOVA followed with Tukey multiple comparison as compared to SeV-infected control (white bar); **p < 0.0001, * p < 0.001. VPs – viral proteins.* ***(D)*** *HEK293T cells were transfected with empty vector (E) or IRF3 expression plasmid (100 ng), as indicated, and FLAG-tagged EBOV, MARV, MLAV VP35. The amounts of VP35 plasmids were 2,000 ng, 400 ng and 80 ng. Cells were mock or SeV-infected for four hours. Whole cell lysates were analyzed by western blot with anti-pIRF3 (S396), anti-total IRF3, anti-FLAG (VP35), and anti-β-tubulin antibodies.* ***(E)*** *HEK293T cells were transfected with empty vector (E), or plasmids that express FLAG-tagged EBOV VP35, MARV VP35, MLAV VP35, or dsRNA binding mutant EBOV VP35$_{KRA}$ and HA-tagged PACT, as indicated. Immunoprecipitations (IP) were performed with anti-FLAG antibody. Western blots were performed for detection of VP35 (anti-FLAG antibody), PACT (anti-HA antibody), and β-tubulin. WCL, whole cell lysate.* *****Panel (E) Experiment performed by Caroline G. Williams***

2.6.2 MLAV VP35 protein inhibits phosphorylation of PKR in human cells.

To assess whether MLAV VP35 can inhibit activation of PKR, HEK293T cells were transfected with FLAG-tagged EBOV, MARV, and MLAV VP35, or empty vector expression plasmids. Consistent with previous literature, EBOV VP35 and MARV VP35 inhibited SeV-induced PKR phosphorylation (**Figure 11**). MLAV VP35 also inhibited activation of PKR in a concentration dependent manner (**Figure 11**).

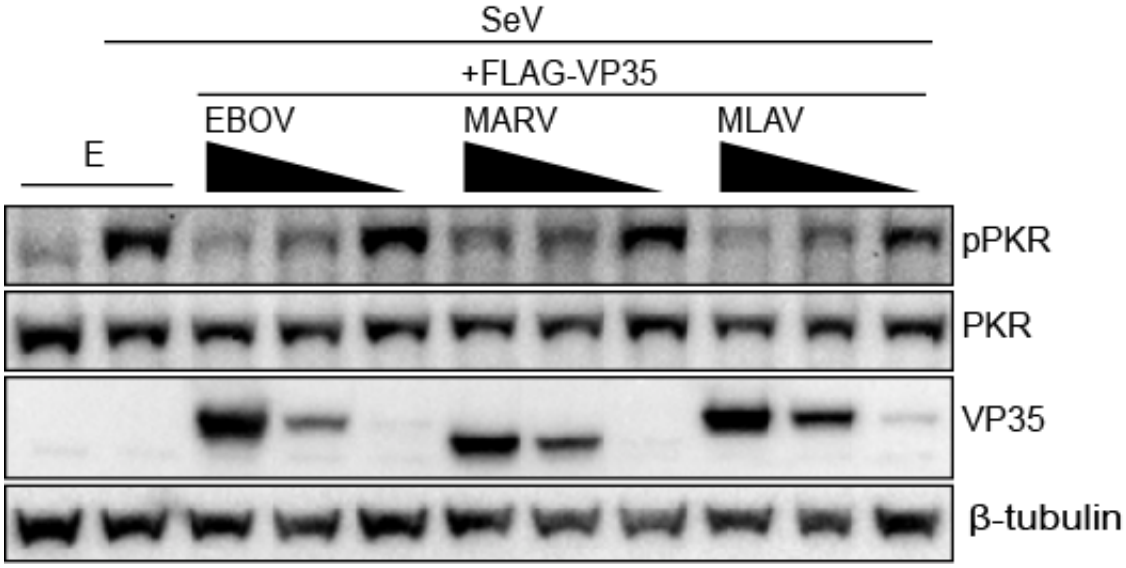

Figure 11 MLAV VP35 inhibits Sendai virus-induced PKR activation.
HEK293T cells were transfected with empty vector (E) or expression plasmids for FLAG-tagged EBOV, MARV and MLAV VP35, as indicated (2000 ng, 400 ng and 80 ng). Twenty-four hours post-transfection, cells were mock- or SeV-infected. Eighteen hours post infection, whole cell lysates were assessed by western blot for levels of total and phosphorylated PKR using anti-FLAG (VP35), anti-total PKR, anti-phospho-PKR (T446) (pPKR) and anti-β-tubulin antibodies. ***Figure 11 performed by Caroline G. Williams***

2.6.3 MLAV VP40 protein inhibits responses to type I IFN in both human and bat cells.

To test the effects of MLAV VP35, VP40 and VP24 on the response of cells to exogenous type I IFN, empty vector or expression plasmids for FLAG-tagged VP35, VP40 and VP24 proteins of EBOV, MARV and MLAV were co-transfected with an IFN-responsive ISG54 promoter firefly luciferase reporter plasmid and a plasmid that constitutively expresses *Renilla* luciferase. Twenty-four hours post-transfection, cells were either mock- or type I IFN-treated. The ISG54 reporter was activated by IFN-treatment in the absence of viral protein expression (**Figure 12A and 12B**). As expected, both MARV VP40 and EBOV VP24 strongly inhibited ISG54 reporter activity in both

human and bat cell lines (**Figure 12A and 12B**). Similar to MARV VP40, MLAV VP40 potently inhibited the ISG54 reporter in both cell types. Each of the VP35s and MARV and MLAV VP24 modestly inhibited the ISG54 reporter when higher amounts of expression plasmid were tested.

To further address this function, endogenous ISG54 transcripts were measured by qRT-PCR. Inhibition of IFN-induced gene expression was demonstrated for MARV VP40, EBOV VP24 and MLAV VP40 (**Figure 12C**), consistent with the reporter gene results. Notably, no inhibition was detected with either MLAV VP35 or MLAV VP24 in this assay.

MARV VP40 has been shown to be a potent inhibitor of IFN-α/β induced phosphorylation of STAT1, whereas EBOV VP24 inhibits this pathway by blocking nuclear transport of pY-STAT1 [348-350]. To determine whether inhibition of IFN responses is due to inhibition of STAT1 phosphorylation, HEK293T cells were co-transfected with empty vector or expression plasmids for FLAG-tagged EBOV, MARV, and MLAV VP24 or VP40. GFP-STAT1 was (**Figure 13A**) or was not (**Figure 13B**) included in the transfection. Addition of IFN triggered the phosphorylation of GFP-STAT1 and endogenous STAT1 in the vector only samples. Among the EBOV and MARV constructs, only MARV VP40 was inhibitory. MLAV VP40 inhibited STAT1 tyrosine phosphorylation to a similar degree as MARV VP40. MLAV VP24 did not detectably affect STAT1 phosphorylation.

MARV VP40 inhibits STAT1 phosphorylation following over-expression of Jak1 [392]. To determine whether MLAV VP40 can prevent Jak1 induced STAT1 phosphorylation, HA-tagged Jak1 was co-transfected with empty vector or FLAG-tagged EBOV, MARV or MLAV VP40. As expected, expression of exogenous Jak1 induced

STAT1 tyrosine phosphorylation, and this was suppressed in the presence of MARV VP40 (**Figure 13C**). Similarly, MLAV VP40 prevented Jak1-dependent STAT1 phosphorylation, suggesting that MLAV VP40 inhibits IFN signaling through mechanisms similar to those used by MARV VP40.

EBOV VP24 interacts with NPI-1 subfamily members of the KPNA nuclear transporters, including KPNA5, to block nuclear import of pY-STAT1 [348-350]. To assess whether MLAV VP24 interacts with KPNA5, co-immunoprecipitation assays were performed in HEK293T cells (**Figure 13D**). KPNA5 did not precipitate in the absence of a co-expressed protein. Among FLAG-tagged EBOV, MARV, and MLAV VP24, only EBOV VP24 detectably interacted with KPNA5. To determine if MLAV VP24 might interact with other KPNA family members, additional co-immunoprecipitation assays were performed between MLAV VP24 and KPNA1-6. EBOV VP24 was used in parallel as a control. As expected, EBOV VP24 co-precipitated with KPNA1, KPNA5, and KPNA6. MLAV VP24 failed to detectably co-precipitate with any of the KPNA family members (**Figure 13E** and **13F**). The absence of MLAV VP24-KPNA interactions is consistent with the inability of MLAV VP24 to inhibit IFN-induced gene expression and identifies a functional difference from EBOV VP24.

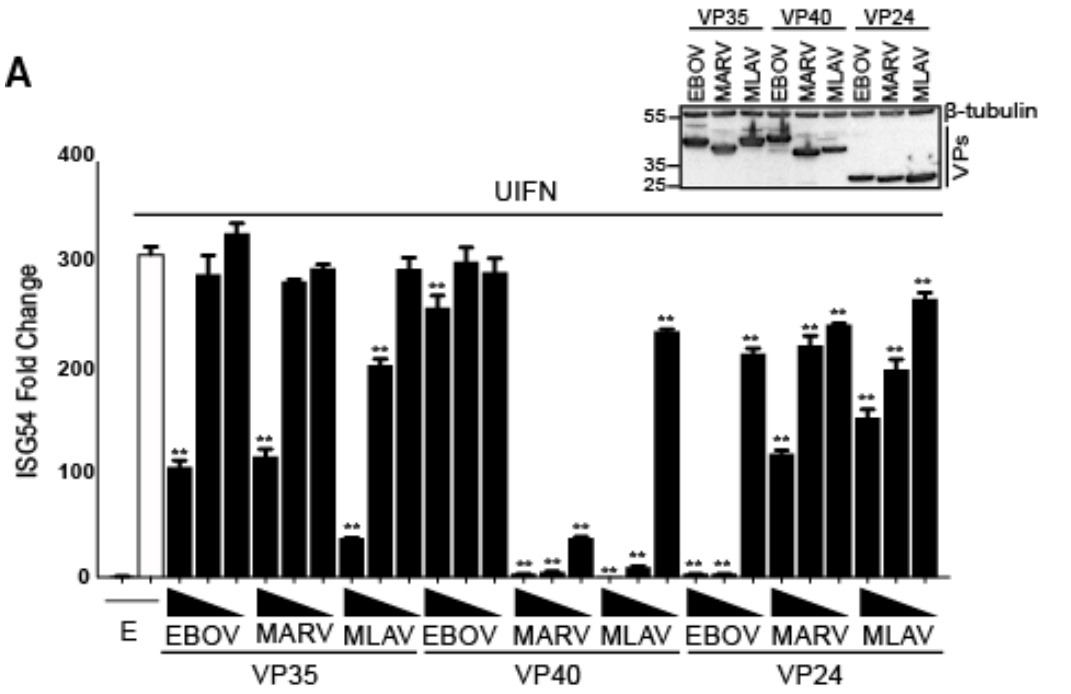
A
VP35
VP40
VP24
EBOV
MARV
MLAV
β-tubulin
VPs
55
35
25
UIFN
ISG54 Fold Change
400
300
200
100
0
E
EBOV
MARV
MLAV
VP35
VP40
VP24

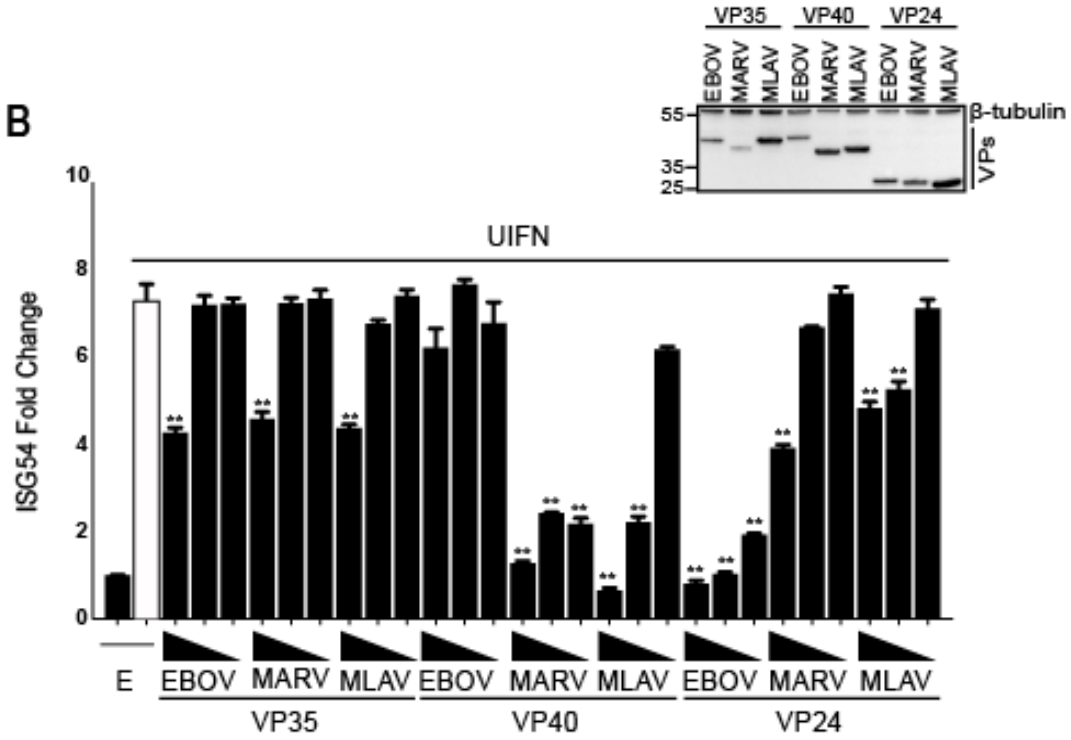
B
VP35
VP40
VP24
EBOV
MARV
MLAV
β-tubulin
VPs
55
35
25
UIFN
ISG54 Fold Change
10
8
6
4
2
0
E
EBOV
MARV
MLAV
VP35
VP40
VP24

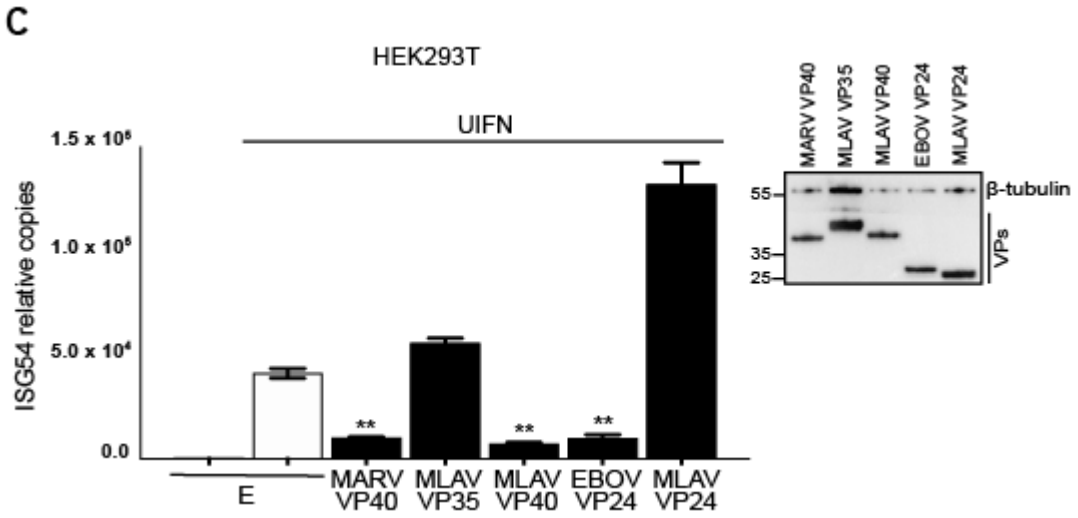

Figure 12 MLAV VP40 protein inhibits responses to type I IFN in both human and bat cells.

(A) *HEK293T cells were transfected with an ISG54 promoter firefly luciferase reporter plasmid, a constitutively-expressed Renilla luciferase reporter plasmid, and either empty vector (E) or the specified FLAG-tagged viral proteins. The amounts of VP35 and VP40 plasmids were 62.5 ng, 6.25 ng, and 0.625 ng; the amounts of VP24 plasmids were 25 ng, 2.5 ng, and 0.25 ng. Twenty-four hours post-transfection, cells were either mock- or UIFN-treated. Eighteen hours post-treatment, firefly, and Renilla luciferase activities were determined. Firefly luciferase values were normalized to Renilla luciferase values, and fold induction was calculated relative to the vector only, mock-treated samples.* ***(B)*** *RO6E cells were transfected as described above, except the amounts of EBOV and MARV VP35, VP40, and VP24 plasmids were 250 ng, 25 ng, and 2.5 ng, and the amounts of MLAV VP35, VP40, and VP24 plasmids were 125 ng, 12.5 ng, and 1.25 ng.* ***(C)*** *HEK293T cells were assessed for endogenous human ISG54 mRNA levels in the presence of empty vector or expression plasmids for the indicated viral proteins, 125 ng. Results were normalized to human β-actin mRNA levels. All experiments were performed in triplicate; error bars represent the SEM for the triplicate. Whole cell lysates were analyzed by western blot with anti-FLAG and anti-β-tubulin antibodies (inset). Statistical significance was determined by performing a one-way ANOVA followed by Tukey's multiple comparison test as compared to UIFN-treated control (white bar); **p < 0.0001, *p < 0.001.*

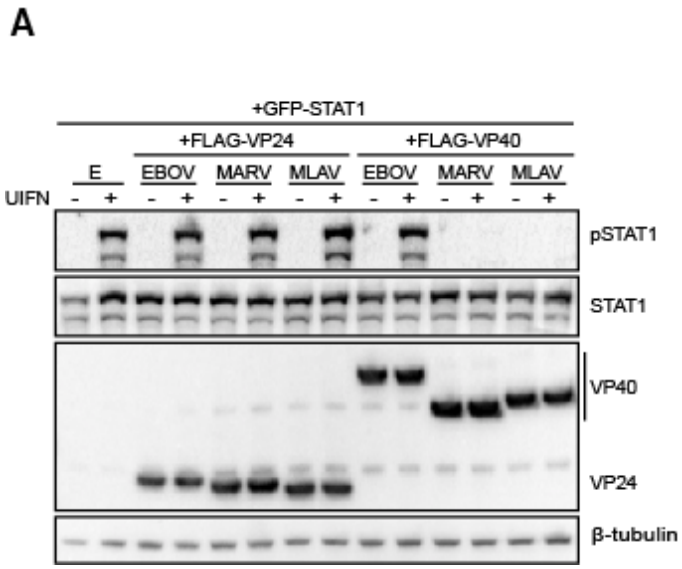
A
+GFP-STAT1
+FLAG-VP24
+FLAG-VP40
E
EBOV
MARV
MLAV
EBOV
MARV
MLAV
UIFN
- + - + - + - + - + - + - +
pSTAT1
STAT1
VP40
VP24
β-tubulin

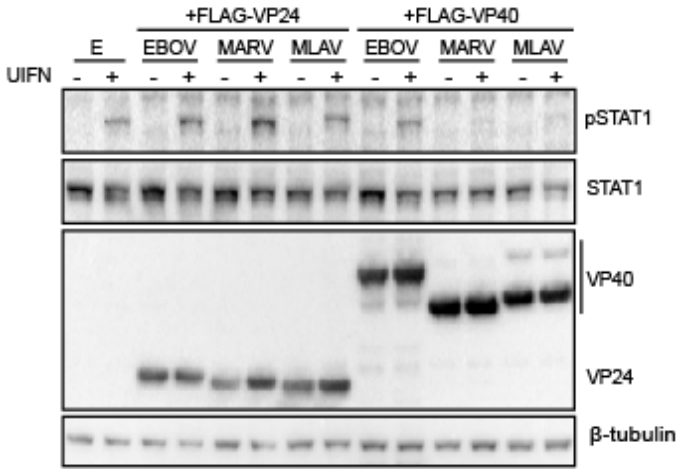
B
+FLAG-VP24
+FLAG-VP40
E
EBOV
MARV
MLAV
EBOV
MARV
MLAV
UIFN
- + - + - + - + - + - + - +
pSTAT1
STAT1
VP40
VP24
β-tubulin

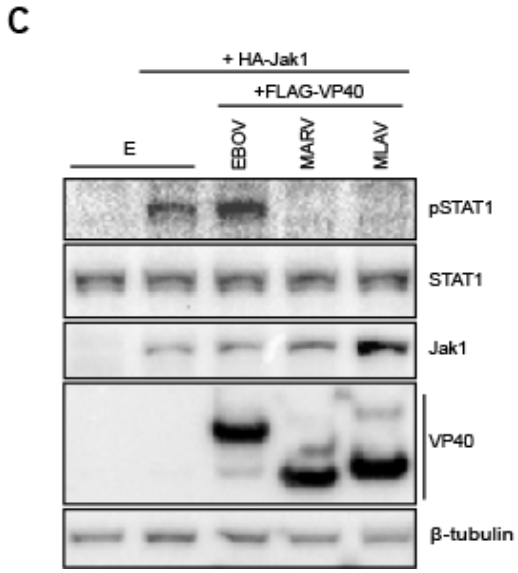
C
+ HA-Jak1
+FLAG-VP40
E
EBOV
MARV
MLAV
pSTAT1
STAT1
Jak1
VP40
β-tubulin

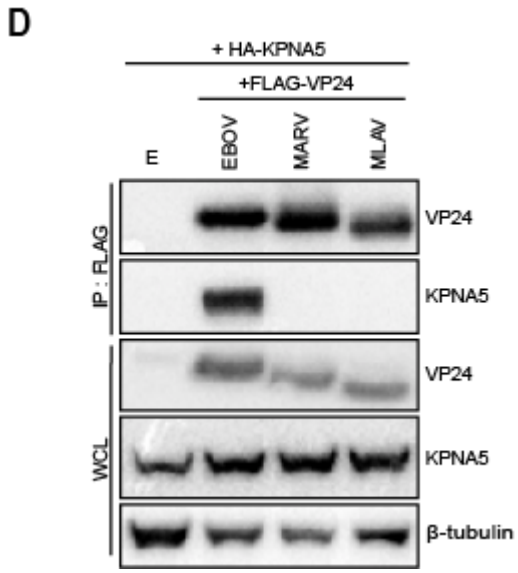
D
+ HA-KPNA5
+FLAG-VP24
E
EBOV
MARV
MLAV
IP : FLAG
WCL
VP24
KPNA5
VP24
KPNA5
β-tubulin

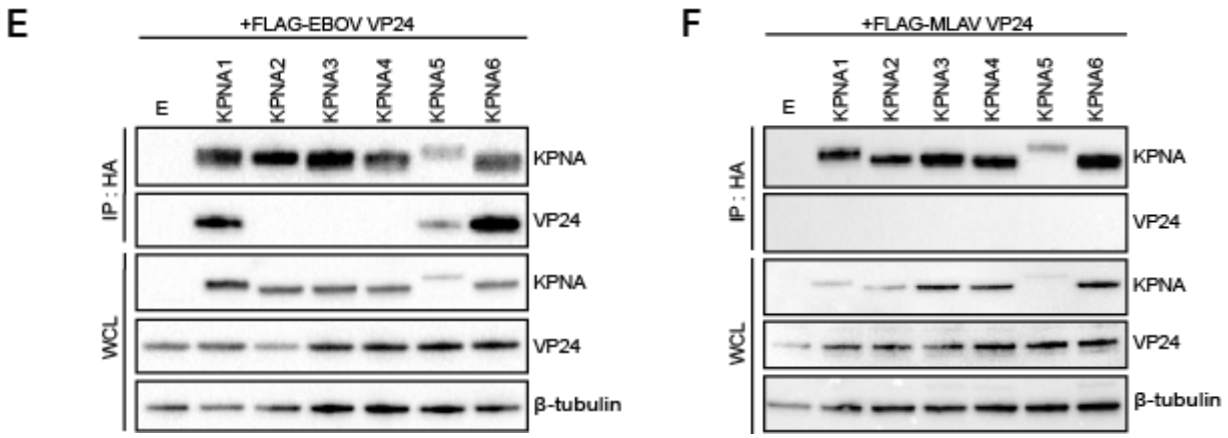

Figure 13 MLAV VP40 protein inhibits type I IFN induced gene expression and Jak-STAT signaling.

HEK293T cells were transfected with empty vector (E), FLAG-tagged VP24s or VP40s from EBOV, MARV and MLAV, as indicated. Twenty-four hours post-transfection, cells were treated with UIFN for 30 minutes and the phosphorylation status of exogenous GFP-STAT1 ***(A)*** *or endogenous STAT1* ***(B)*** *was assessed by western blotting.* ***(C)*** *HEK293T cells were co-transfected with empty vector (E) or FLAG-tagged VP40s from EBOV, MARV and MLAV and HA-tagged Jak1 expression plasmids. Twenty-four hours post-transfection cells were lysed and the phosphorylation status of endogenous STAT1 was analyzed. Western blotting was performed with anti-FLAG, anti-STAT1, anti-pSTAT1 (Y701), and anti-β-tubulin antibodies.* ***(D)*** *HEK293T cells were co-transfected with FLAG-tagged EBOV, MARV, MLAV VP24, and HA-tagged KPNA5. Immunoprecipitation (IP) was performed with anti-FLAG antibody and precipitates and whole cell lysates (WCL) were assessed by western blotting with anti-FLAG (VP24), anti-HA (KPNA5) and anti-β-tubulin antibodies.* ***(E-F)*** *HEK293T cells were co-transfected with either FLAG-tagged EBOV or MLAV VP24, and HA-tagged KPNA1-6. Immunoprecipitation (IP) was performed with anti-HA antibody and precipitates and whole cell lysates (WCL) were assessed by western blotting with anti-FLAG (VP24), anti-HA (KPNA) and anti-β-tubulin antibodies.* *****Figure 13 performed by Caroline G. Williams***

2.6.4 MLAV and MARV VP40 bud with similar efficiencies from human and bat cells.

Filovirus VP40 proteins play a critical role in budding of new virus particles, and expression of VP40 is sufficient for formation and budding of VLPs [143, 144, 146, 401, 402]. MLAV VP40 displays more potent activity than MARV VP40 in several assays. To determine whether this might reflect altered cellular accumulation due to different levels of budding from cells, the capacity of EBOV, MARV and MLAV VP40s to bud as VLPs

was assessed. Upon expression in human and bat cells, each VP40 budded from both cell types. Furthermore, significant portions of the EBOV, MARV, and MLAV VP40 in cell supernatants were only trypsin-sensitive upon addition of Triton X-100 detergent, consistent with the VP40s from both HEK293T and RO6E cells being protected by a membrane, as is characteristic of filovirus particles (**Figure 14A** and **14B**).

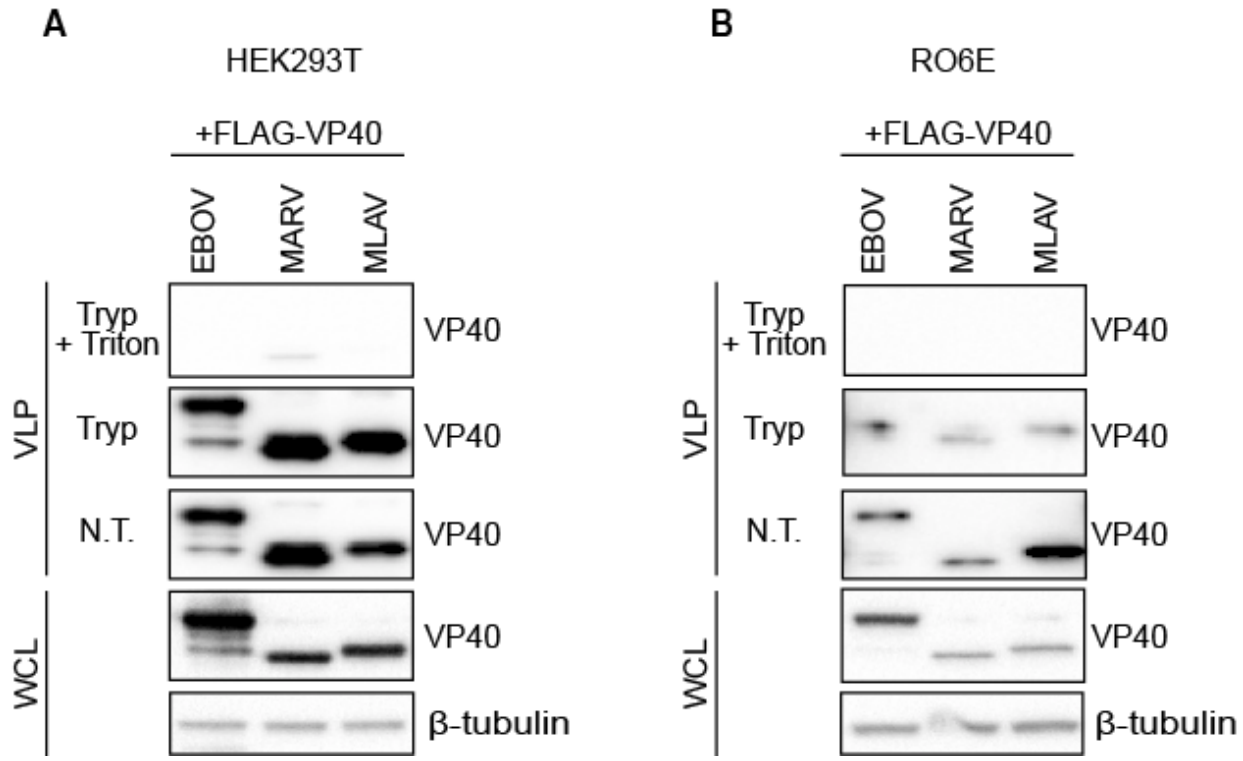

Figure 14 MLAV VP40 is capable of forming virus-like particles from both human and bat cells.

*To compare the budding of EBOV, MARV, and MLAV VP40 proteins from different cell lines, VLP assays were performed in a HEK293T cells **(A)** and RO6E cells **(B)**. Ten percent of each VLP preparation was subjected to treatment with trypsin (Tryp) or trypsin and Triton X-100 (Tryp+Triton) to determine whether VP40 was contained within a membrane. The presence of VP40 in non-treated (N.T.) and treated VLPs and whole cell lysates (WCL) was assessed by western blot with anti-FLAG antibody. Anti-β-tubulin served as a loading control for the WCL. ****Figure 14 performed by Tim Keiffer.***

2.6.5 MLAV VP40 and EBOV VP24 inhibition of IFNβ promoter activation occur independently of Jak-STAT signaling.

The type I IFN response includes a positive feedback loop whereby secreted IFN upregulates pattern recognition receptors, such as RIG-I and transcription factors such as IRF7, to amplify the response [403]. It was therefore of interest to test the hypothesis that MLAV VP40, MARV VP40 and EBOV VP24 inhibit virus-induced induction of the IFN response as a result of their inhibition of IFN-induced positive feedback loop. Activation of the IFNβ promoter by SeV was therefore assessed by reporter gene assay in the absence or presence of the Jak1/Jak2 inhibitor Ruxolitinib. In this experiment, cells were transfected with empty vector or FLAG-tagged expression plasmids for the EBOV VP35, EBOV, MARV and MLAV VP40 and EBOV VP24, pre-treated with DMSO or Ruxolitinib and then mock- or SeV- infected, in the absence or presence of the inhibitor (**Figure 15A**). EBOV VP35 acted as a potent suppressor of IFNβ promoter activation under these conditions. MARV VP40, MLAV VP40, and EBOV VP24 all suppressed IFNβ promoter activation to similar extents in the absence or presence of the Jak kinase inhibitor. To confirm that inhibition of IFN induced signaling was complete, cells transfected with an ISG54 promoter reporter gene were DMSO or Ruxolitinib treated and then mock or IFN-treated. As expected, IFN activated the ISG54 promoter in the presence of DMSO but not Ruxolitinib (**Figure 15B**). To validate the inhibitory activities detected in the reporter gene assays, quantitative RT-PCR was performed to detect expression of the endogenous IFNβ and ISG54 mRNA. Consistent with the reporter assays, IFNβ and ISG54 copy numbers were significantly inhibited in the presence of EBOV VP35, EBOV VP24 and both MARV and MLAV VP40 (**Figure 15C**). It is notable that inhibition of SeV-induced

IFN responses by EBOV VP35 was more robust than for the other proteins. That degrees of inhibition were unaffected by the presence of the Ruxolitinib, these data suggest that MARV VP40, MLAV VP40 and EBOV VP24 all utilize mechanisms independent of inhibition of STAT1 phosphorylation to impair induction of type I IFN responses.

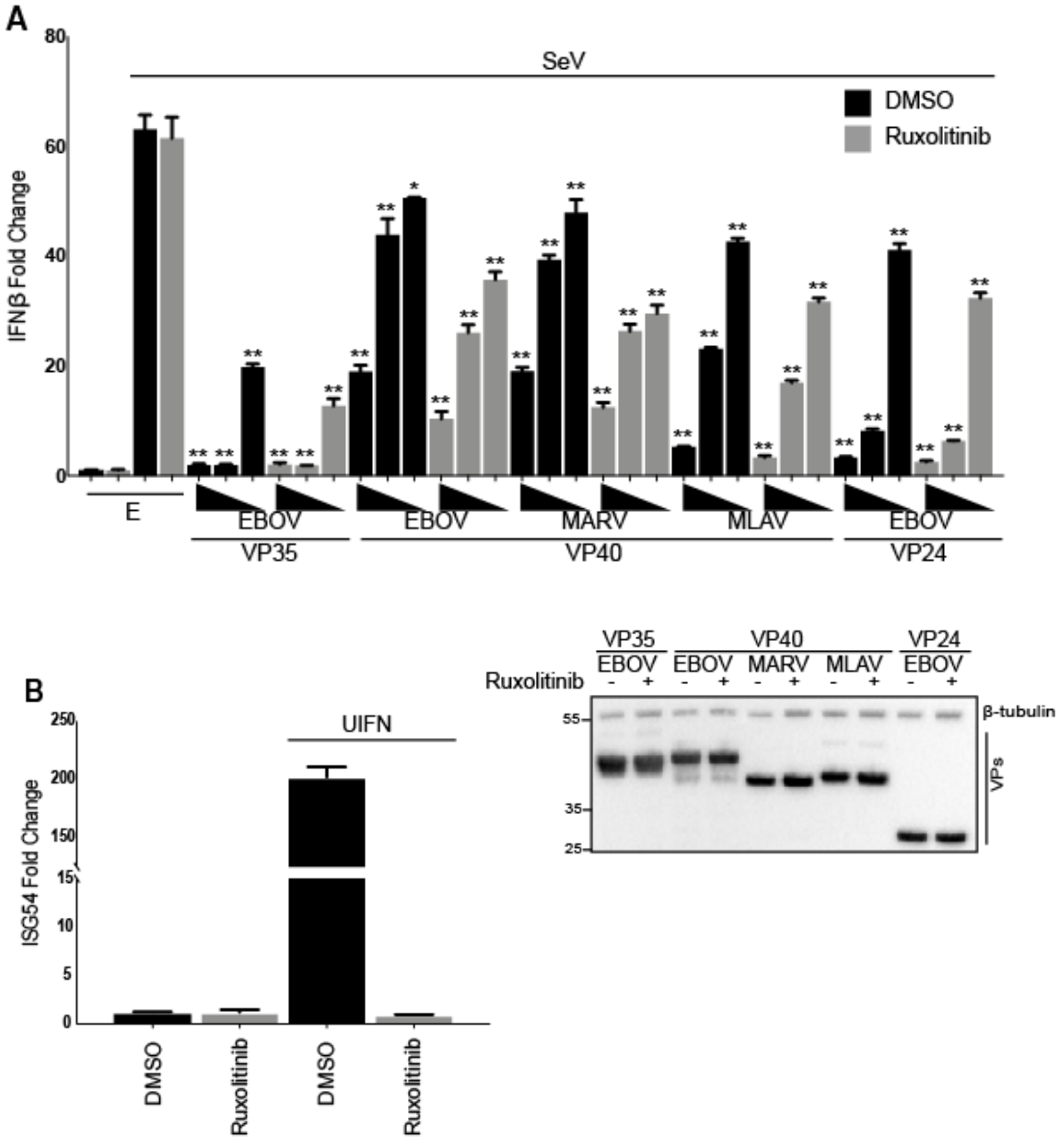

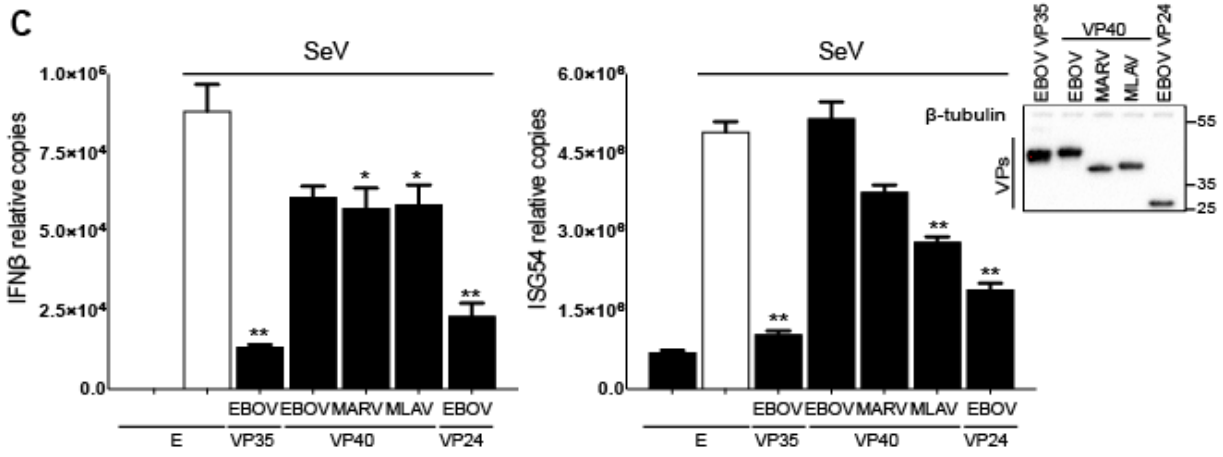

Figure 15 MLAV VP40 blocks Sendai virus-induced IFNβ promoter activation independently of Jak-STAT signaling.

(A) *HEK293T cells were transfected with an IFNβ promoter firefly luciferase reporter plasmid, a constitutively-expressed Renilla luciferase reporter plasmid and either empty vector (E) or the specified FLAG-tagged viral proteins. The amounts of VP35, VP40, and VP24 plasmids were 62.5 ng, 6.25 ng, and 0.625 ng. Twenty-four hours post-transfection, cells were pre-treated with either DMSO or the Jak1/Jak2 inhibitor Ruxolitinib for one hour. Post treatment, cells were mock- or SeV-infected in the presence of DMSO or Ruxolitinib. Firefly and Renilla luciferase activities were determined eighteen hours later using a dual luciferase assay (Promega). Fold induction was determined relative to the DMSO vector only, mock-infected samples. Viral protein expression was confirmed by western blotting with anti-FLAG antibody (inset). Anti-β-tubulin served as a loading control.* ***(B)*** *HEK293T cells were transfected with an ISG54 promotor firefly luciferase reporter plasmid, a constitutively-expressing Renilla luciferase reporter plasmid and empty vector. Twenty-four hours post-transfection, cells were pre-treated with DMSO or Ruxolitinib for one hour. Post-treatment, cells were mock- or UIFN-treated in the presence of DMSO or Ruxolitinib. Firefly and Renilla luciferase activities were determined eighteen hours later using a dual luciferase assay (Promega). Fold induction was determined relative to the DMSO, mock-treated samples.* ***(C)*** *HEK293T cells were assessed for endogenous human IFNβ and ISG54 mRNA levels in the presence of viral expression plasmids, 125 ng. Results were normalized to human β-actin mRNA levels. Assays were performed in triplicate. Cell lysates were analyzed by western blot with anti-FLAG and anti-β-tubulin antibodies (inset). For A and C, error bars represent the SEM for the triplicate. Statistical significance was determined by performing a one-way ANOVA followed with Tukey multiple comparison as compared to SeV-infected control; **p < 0.0001, * p < 0.001.*

2.6.6 MLAV VP24 fails to interact with Keap1 or activate ARE gene expression due to the absence of a Keap1-interacting K-loop.

MARV VP24 interacts with Keap1 to activate ARE promoters [354, 355]. To determine whether MLAV VP24 possesses similar properties, co-immunoprecipitation experiments were performed with HA-tagged human Keap1 (hKeap1) or HA-tagged Keap1 derived from the bat *Myotis lucifugus* (bKeap1), which is 96.8% identical, at the amino acid level, to the predicted *Rousettus aegypticus* Keap1 (data not shown). As previously described, MARV VP24 interacted with both human and bat Keap1, whereas EBOV and MLAV VP24 did not interact (**Figure 16A and 16B**). Consistent with these data, when tested in an ARE promoter reporter gene assay, MARV VP24 activated the ARE reporter, relative to an empty vector control, while neither EBOV nor MLAV VP24 activated the ARE response (**Figure 16C**).

MARV VP24 interaction with Keap1 occurs via a specific motif, the K-loop, and transfer of this sequence to EBOV VP24 confers binding to Keap1 [355]. To determine whether this sequence could confer interaction with Keap1 and activation of ARE responses upon MLAV VP24, the MARV VP24 K-loop sequence (amino acid residues 202-219) was transferred to MLAV VP24, replacing the corresponding amino acid residues (MLAV VP24$_{\text{MARV 202-219}}$). The reverse chimera was also generated, with MLAV sequences replacing the K-loop in MARV VP24 (MARV VP24$_{\text{MLAV 202-219}}$) (**Figure 17A**). Transferring the MARV K-loop sequence to MLAV VP24 conferred the capacity to activate an ARE response while transfer of the MLAV sequence to MARV VP24 abolished the activation (**Figure 17B**). Interaction with human Keap1 (**Figure 17C**) and bat Keap1 (**Figure 17D**) yielded corresponding data, where interaction was dependent on the MARV

VP24 K-loop. Collectively, these data demonstrate that the lack of ARE gene expression by MLAV VP24 is due to the lack of a Keap1 binding motif.

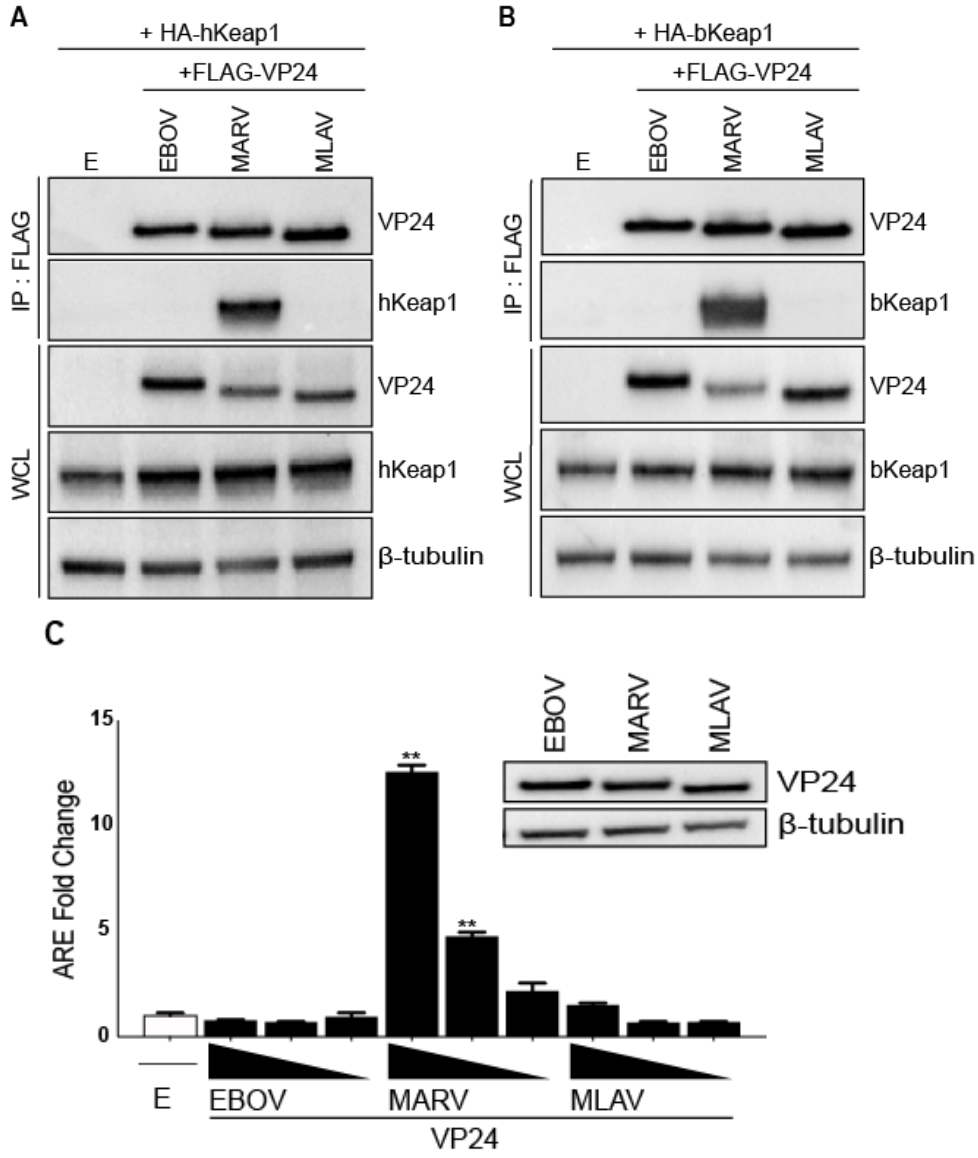

Figure 16 MLAV VP24 does not interact with human or bat KEAP1 or activate the ARE promoter.

(A-B) *HEK293T cells were co-transfected with FLAG-tagged EBOV, MARV, MLAV VP24, as indicated, and HA-tagged human Keap1 (hKeap1)* ***(A)*** *or HA-tagged bat Keap1 (bKeap1)* ***(B)****. Co-immunoprecipitation (IP) was performed with anti-FLAG antibody and precipitates and whole cell lysates (WCL) were assessed by using anti-FLAG (VP24), anti-HA (Keap1) and anti-β-tubulin antibodies.* ***(C)*** *HEK293T cells were transfected with a reporter plasmid with the firefly luciferase gene under the control of an ARE promoter, a reporter plasmid that constitutively expresses Renilla luciferase and either empty vector*

*(E) or the indicated FLAG-VP24 proteins. The amounts of VP24 plasmids were 62.5 ng, 6.25 ng, and 0.625 ng. Firefly and Renilla luciferase activities were determined eighteen hours post-transfection. Firefly luciferase activity was normalized to Renilla luciferase activities, and fold activity is reported relative to the empty vector only sample. Protein expression was analyzed by western blot using anti-FLAG (VP24) and anti-β-tubulin antibodies (inset). The reporter gene assays were performed in triplicate; error bars represent the SEM for the triplicate. Statistical significance was determined by performing a one-way ANOVA followed with Tukey multiple comparisons as compared to vector-only control (white bar); **p < 0.0001, * p < 0.001.*

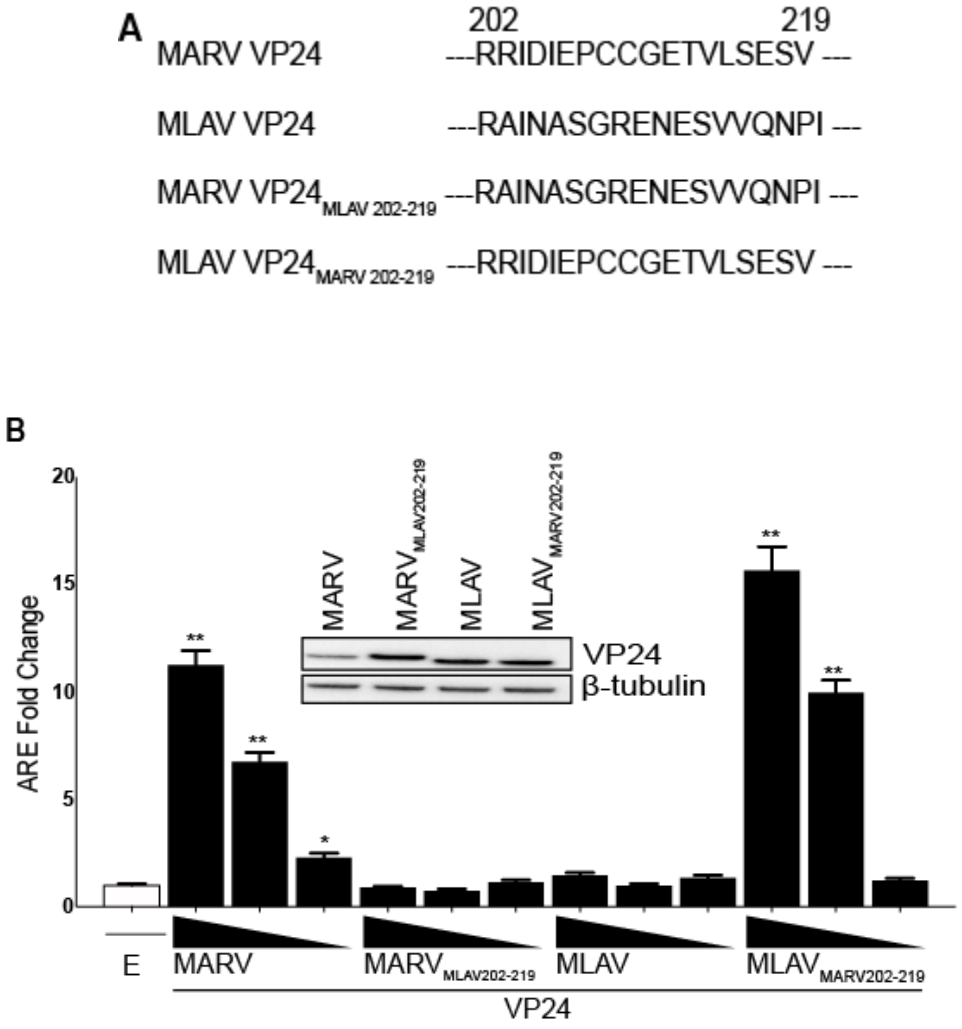

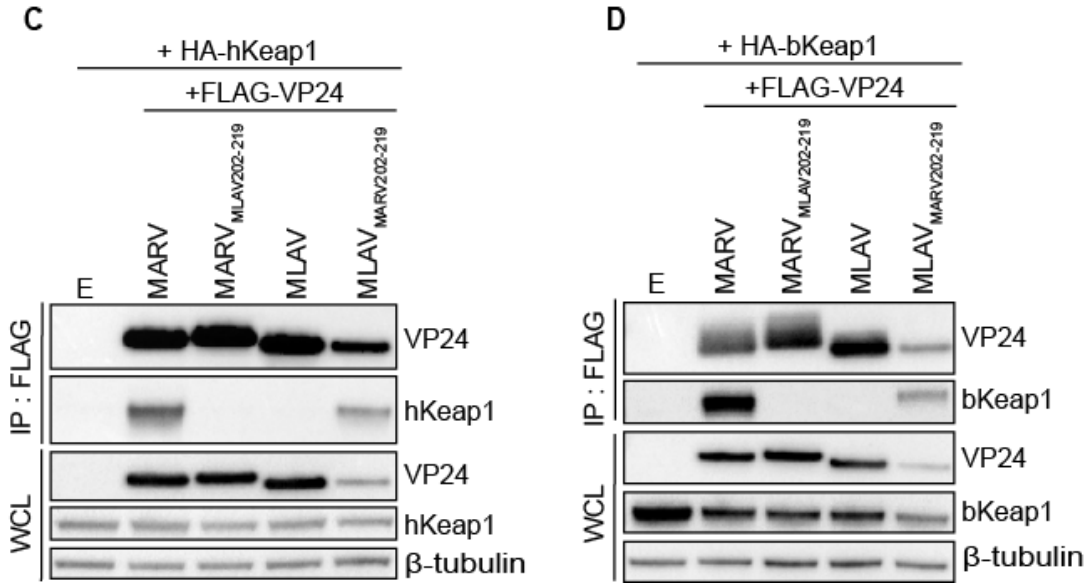

Figure 17 Transfer of the MARV K-Loop sequence confers on MLAV VP24 interaction with Keap1 and activation of ARE signaling.

(A) *Sequences for amino acid residues 202-219, which correspond to the MARV VP24 K-loop, for MARV VP24, MLAV VP24, and the VP24 chimera constructs MLAV VP24 $_{MARV\ 202\text{-}219}$ and MARV VP24$_{MLAV\ 202\text{-}219}$.* ***(B)*** *HEK293T cells were transfected with reporter plasmid with the firefly luciferase gene under the control of an ARE promoter, a reporter plasmid that constitutively expresses Renilla luciferase and either empty vector (E) or the indicated FLAG-VP24 proteins. The amounts of VP24 plasmids were 62.5 ng, 6.25 ng, and 0.625 ng. Firefly and Renilla luciferase activities were determined eighteen hours post-transfection. Firefly luciferase activity was normalized to Renilla luciferase activities, and fold activity is reported relative to the empty vector only sample. The experiment was performed in triplicate; error bars represent the SEM for the triplicate. Statistical significance was determined by performing a one-way ANOVA followed with Tukey multiple comparisons as compared to vector-only control (white bar); **p < 0.0001, * p < 0.001. Cell lysates were analyzed by western blot with anti-FLAG (VP24) and anti-β-tubulin antibodies (Inset).* ***(C-D)*** *HEK293T cells were transfected with FLAG-tagged constructs, as indicated and either* ***(C)*** *HA-tagged human Keap1 (hKeap1) or* ***(D)*** *HA-tagged bat Keap1 (bKeap1). Co-immunoprecipitation (IP) was performed with an anti-FLAG antibody. IPs were analyzed by western blotting with anti-FLAG (VP24), anti-HA (Keap1) and anti-β-tubulin antibodies. WCL, whole cell lysate.*

2.6.7 MLAV VP35 and VP40 maintain their ability to inhibit the IFN response in the presence of other viral proteins.

Both VP35 and VP40 are known to independently interact with the nucleoprotein (NP) and together with the VP24 protein NP and VP35 can form mature nucleocapsids [59, 73, 116, 404]. To determine if the formation of the nucleocapsid complex impacted the ability of VP35 to inhibit IFNβ production, varying amounts of EBOV and MLAV VP35 were transfected in the presence of EBOV or MLAV NP and VP24, respectively. Both EBOV and MLAV VP35 were still able to inhibit SeV-induced activation of the IFNβ promoter in the presence of NP and VP24. (**Figure 18A**). Similarly, to assess if NP could interfere with the ability of VP40 to inhibit IFN production and signaling we co-transfected varying amounts of MARV VP40 or MLAV VP40 in the presence of NP. MLAV VP40 was still a potent repressor of both SeV-induced activation of the IFNβ promoter and the UIFN-induced activation of the ISG54 promoter in the presence of NP (**Figure 18B-C**). Lastly, we evaluated the effect of co-transfecting multiple viral proteins together on the inhibitory capabilities of EBOV, MARV, and MLAV. The respective NP, VP35, VP40, VP30 and VP24 plasmids were transfected together in either the IFNβ or ISG54 promotor assay. Upon activation with either SeV or UIFN, respectively, it was observed that the combination of proteins inhibited the SeV-induced activation of the IFNβ promoter and the UIFN-induced activation of the ISG54 promoter (**Figure 18D-E**).

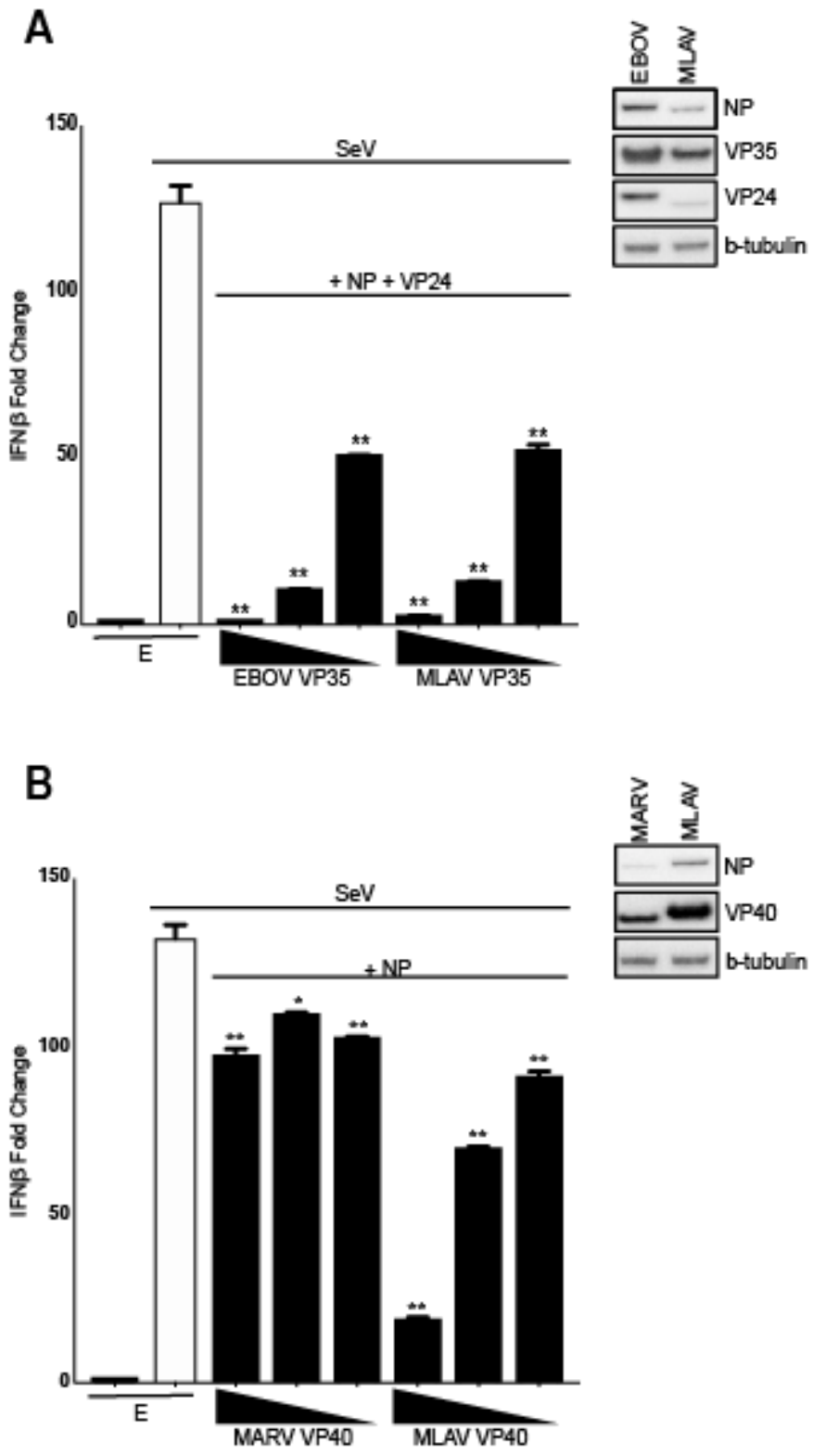
A
EBOV
MLAV
NP
VP35
VP24
b-tubulin
150
100
50
0
IFNβ Fold Change
SeV
+ NP + VP24
**
E
EBOV VP35
MLAV VP35
B
MARV
MLAV
NP
VP40
b-tubulin
150
100
50
0
IFNβ Fold Change
SeV
+ NP
*
**
E
MARV VP40
MLAV VP40

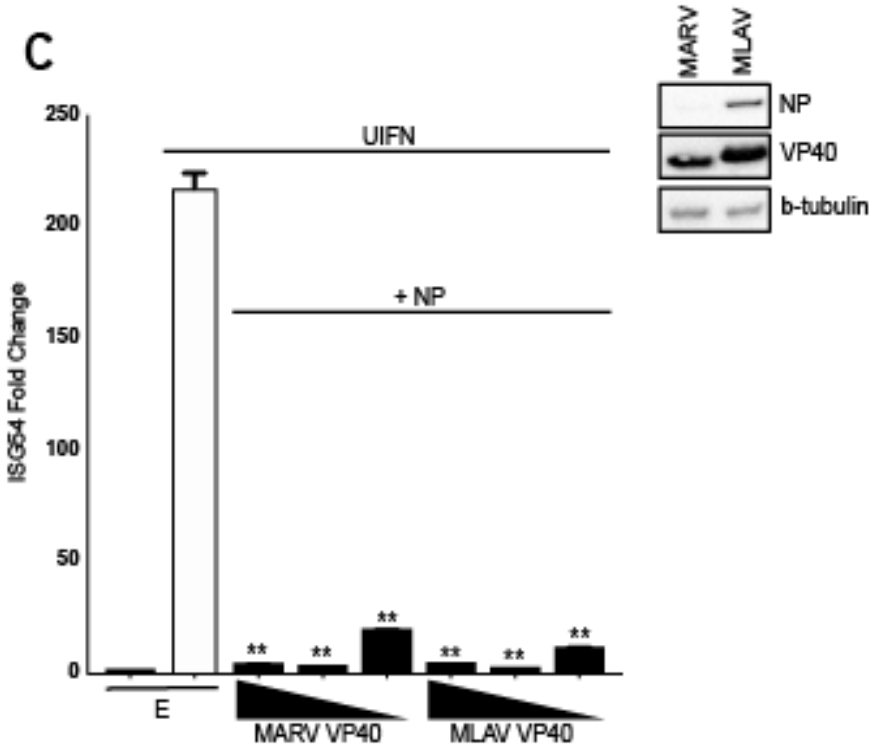
C
MARV
MLAV
NP
VP40
b-tubulin
UIFN
+ NP
ISG54 Fold Change
250
200
150
100
50
0
**
E
MARV VP40
MLAV VP40

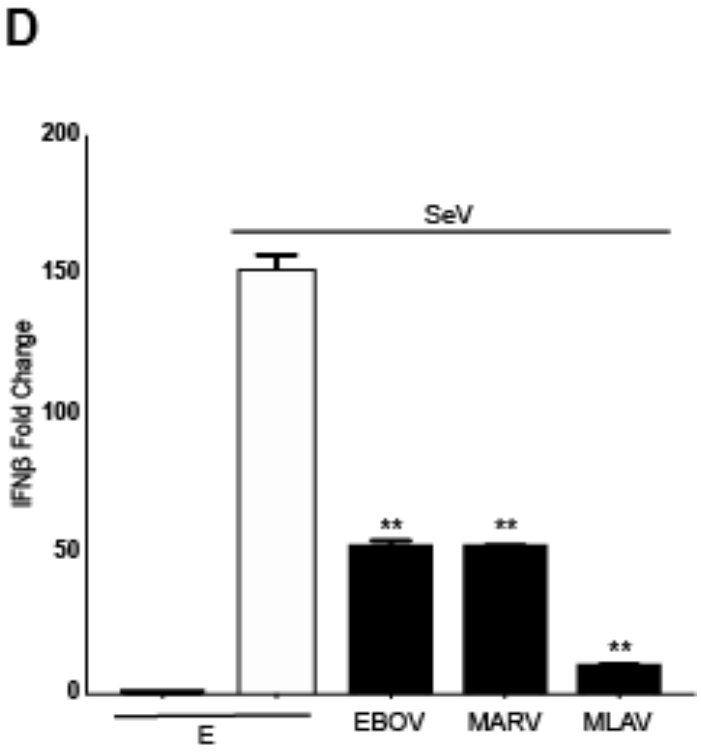
D
SeV
IFNβ Fold Change
200
150
100
50
0
**
E
EBOV
MARV
MLAV

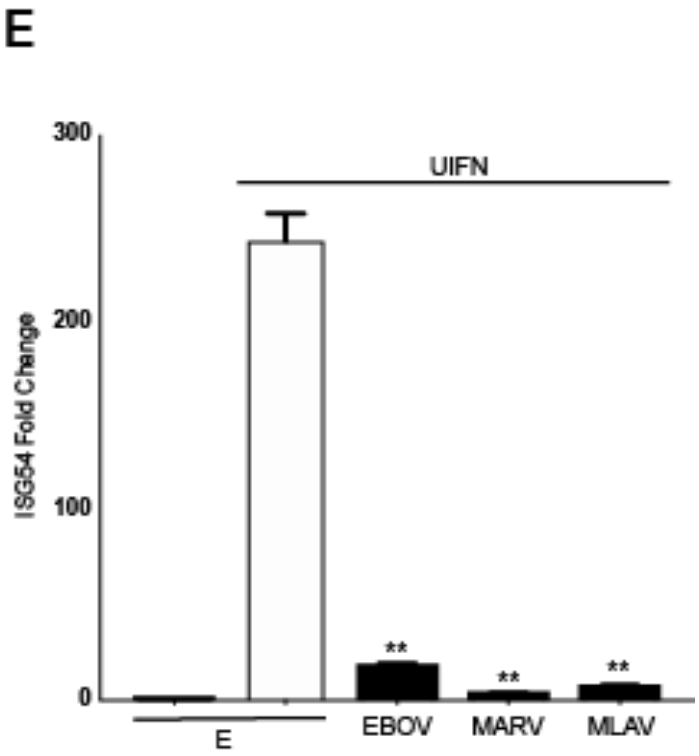

Figure 18 MLAV VP35 and VP40 maintain their ability to inhibit the IFN response in the presence of other viral protein.

(A-C) *HEK293T cells were transfected with either an IFNβ (A-B) or an ISG54 (C) promoter firefly luciferase reporter plasmid, a constitutively-expressed Renilla luciferase reporter plasmid, and either empty vector (E) or the specified FLAG-tagged viral proteins.* ***(A)*** *62.5 ng, 6.25 ng, and 0.625 ng of VP35 plasmid and 6.25 ng of NP and VP24 plasmids.* ***(B-C)*** *62.5 ng, 6.25 ng, and 0.625 ng of VP40 plasmid and 6.25 ng of NP plasmid. Twenty-four hours post-transfection, cells were either mock, SeV-infected (A-B), or UIFN-treated (C). Eighteen hours post-treatment, firefly, and Renilla luciferase activities were determined. Firefly luciferase values were normalized to Renilla luciferase values, and fold induction was calculated relative to the vector only, mock-treated samples.* ***(D-E)*** *HEK293T cells were transfected with either an IFNβ (D) or an ISG54 (E) promoter firefly luciferase reporter plasmid, a constitutively-expressed Renilla luciferase reporter plasmid, and either empty vector (E) or the specified FLAG-tagged viral proteins. 6.25 ng of NP, VP35, VP40, VP30, and VP24 plasmids. Twenty-four hours post-transfection, cells were either mock, SeV-infected (D), or UIFN-treated (E). Eighteen hours post-treatment, firefly, and Renilla luciferase activities were determined. Firefly luciferase values were normalized to Renilla luciferase values, and fold induction was calculated relative to the vector only, mock-treated samples. Whole cell lysates were analyzed by western blot with anti-FLAG and anti-β-tubulin antibodies (insets). Statistical significance was determined by performing a one-way ANOVA followed with Tukey's multiple comparison test as compared to SeV-infected (A-B and D) or UIFN-treated (C, E) control (white bar); **p < 0.0001, *p < 0.001.* ****Panel C&E performed by Caroline G Williams.**

2.7 Discussion

The data in this study provide functional evidence that MLAV is biologically distinct from other filoviruses and support its classification in its own genus. The placement of MLAV in a distinct genus was based on its relatively low sequence identity to other filoviruses [6]. It was also noted to have, compared to other filoviruses, unique gene overlaps and a unique transcription start signal. Despite these distinctions, MLAV mechanisms of entry and RNA synthesis, based on pseudotype and minigenome assays, mirror those of both EBOV and MARV. MLAV also possesses some features that suggest a closer genetic relationship to members of the *Marburgvirus* genus as opposed to the *Ebolavirus* and *Cuevavirus* genera. This includes similarities in Large (L) protein sequence and the absence of RNA editing sites in GP [6]. In addition, MLAV was identified in *Rousettus* bats, and *Rousettus* bats in Africa serve as a reservoir for MARV and RAVV [48]. The present study demonstrates commonalities and distinctions between MLAV and either EBOV or MARV in terms of how viral proteins antagonize the innate immune response in both bat and human cells. Inhibition of RIG-I induced IFN responses is thus far a common feature of filoviruses [405]. The suppression of IFN-induced signaling and gene expression by VP40, rather than via VP24, parallels MARV and draws a functional distinction between MLAV and EBOV. The absence of MLAV VP24 interaction with human or bat Keap1, and its lack of ARE transcriptional activation is consistent with MLAV having evolved unique virus-host interactions that are distinct from MARV. These findings further support placement of MLAV in a distinct genus, but also suggest a closer relationship to MARV than EBOV.

The data also demonstrate that MLAV encodes mechanisms to counteract both type I IFN production and cellular responses to exogenous IFN, and that this virus has the potential to antagonize these innate antiviral responses in both bat and human cells. MLAV VP35 was demonstrated to effectively block activation of the IFNβ promoter in response to SeV infection, a known inducer of the RIG-I signaling pathway. In addition, inhibition of SeV-induced phosphorylation of IRF3 was demonstrated. Together, these data indicate that MLAV can block RIG-I signaling, consistent with the function of other filovirus VP35s [399, 406]. Mechanistically, inhibition of IFN-α/β production by EBOV or MARV VP35 correlates with dsRNA binding activity [330, 331, 335, 342, 343, 380, 381, 383, 386]. This may reflect binding and sequestration of RIG-I activating dsRNAs [343, 386]. The VP35 dsRNA binding domain, also known as the interferon inhibitory domain (IID), directly contacts the phosphodiester backbone of dsRNA, via residues that comprise a central basic patch, to mediate this interaction [330, 335, 336, 381, 382, 385]. EBOV VP35 also caps the ends of dsRNA in a manner that likely masks 5'-triphosphates, which contribute to recognition of RNAs by RIG-I [335, 336]. VP35 interaction with host protein PACT, which interacts with and facilitates activation of RIG-I, also contributes to inhibition [343, 407]. Because the residues that make up the central basic patch are conserved between MLAV and other filoviral VP35s (1), MLAV is likely to bind to dsRNA. Given that it also interacts with PACT (**Figure 10E**), its mechanisms of inhibition are likely similar to other filoviral VP35s.

EBOV, MARV and LLOV VP35 have also been demonstrated to inhibit activation of PKR, an IFN-induced, dsRNA-activated protein kinase that exerts antiviral effects by suppressing translation [340, 351, 387-389]. The mechanism by which VP35s inhibit PKR

remains ambiguous, however, mutation of multiple central basic patch residues in EBOV or MARV VP35 disrupts the inhibitory activity [340, 388]. In contrast, single point mutations that disrupt EBOV VP35 dsRNA binding activity leave PKR inhibition intact, suggesting that inhibition of PKR is not dependent upon VP35-dsRNA interaction or sequestration [387, 388]. Consistent with PKR inhibition being an important function for filoviruses, this activity is conserved in MLAV as well. That the inhibition can occur in human cells further supports the likelihood that MLAV could counter human innate antiviral defenses.

The IFN-inhibitory activities of both EBOV and MARV VP35 have been demonstrated to be important for efficient virus replication in IFN-competent systems [383, 400]. In addition to blocking the production of antiviral IFNs, VP35 inhibition of RIG-I also suppresses maturation of dendritic cells when expressed alone or in the context of EBOV infection [384, 408, 409]. This activity impairs adaptive immunity to EBOV [410, 411]. Therefore, VP35 likely inhibits adaptive, as well as innate, antiviral defenses. Disruption of VP35 anti-IFN function in the context of recombinant EBOVs has been demonstrated to render the virus avirulent in mice, guinea pigs and non-human primates [383, 412, 413]. Based on these data, VP35 suppression of RIG-I signaling appears to be critical for virulence. The effective function in human cells of MLAV VP35 satisfies one apparent criterion for virulence in humans. It should be noted however, that suppression of RIG-I signaling by VP35 is not sufficient on its own to confer virulence. Even though MARV VP35 functions in *Rousettus* cells and likely has evolved in this species, MARV does not appear to cause significant disease in these animals [414-416]. It does seem

likely that in the reservoir host, VP35 IFN-antagonist function will be important for efficient replication and transmission, although this remains to be tested experimentally.

For MARV, either infection or VP40 expression alone blocks IFN induced phosphorylation of Jak kinases, inhibiting activation and downstream signaling. The absence of these phosphorylation events in response to IFN-α/β or IFNγ is consistent with the phenotype of Jak1-deficient cells, suggesting that Jak1 function may be targeted by MARV VP40, although there is no evidence to date of VP40-Jak1 interaction [392]. Consistent with MARV VP40 impairing Jak1 function, MARV VP40 expression is sufficient to prevent phosphorylation of STAT proteins following Jak1 over-expression or treatment by IFN-α/β or IFNγ (type II IFN) [392]. MLAV VP40 likewise blocks ISG expression and inhibits STAT1 phosphorylation following IFN treatment or over-expression of Jak1. Therefore, inhibition of IFN signaling by MLAV VP40 seems likely to proceed by a mechanism similar to that employed by MARV VP40.

MARV VP24 binds directly to Keap1, a cellular substrate adaptor protein of the Cullin-3/Rbx1 E3 ubiquitin ligase complex [354, 355, 396, 417]. Keap1 regulates the cellular antioxidant response [418]. Under homeostatic conditions, Keap1 promotes Nrf2 polyubiquitination and degradation. Cell stresses, including oxidative stress, disrupt the Keap1-mediated ubiquitination of Nrf2, stabilizing it and promoting Nrf2 dependent expression of antioxidant response genes. Biophysical studies demonstrated that MARV VP24 interacts with the Keap1 Kelch domain at a site that overlaps the region that binds Nrf2 [396]. This interaction disrupts Nrf2-Keap1 interaction and activates ARE gene expression [354, 355, 396]. Keap1 similarly interacts with host kinase IKKβ to repress NF-κB responses and MARV VP24 can also disrupt this interaction, thereby relieving

Keap1 repression on the NF-κB transcriptional response [397]. In contrast, EBOV and LLOV VP24 targets KPNA proteins in a manner that prevents pY-STAT1 nuclear transport, inhibiting ISG expression [348-351, 391].

Given that MLAV VP40 mirrored MARV VP40 in its inhibition of the IFN response, it was of interest to determine whether MLAV VP24 would similarly mimic MARV VP24 in terms of interaction with the Keap1-Nrf2 pathway. However, MLAV VP24 lacks a sequence that resembles the MARV VP24 K-loop and, correspondingly, did not interact with human or a bat-derived Keap1 and did not activate an ARE promoter. Chimeric MARV-MLAV VP24 proteins confirmed that the absence of the K-loop sequence can explain the lack of MLAV VP24 effects on antioxidant responses. Furthermore, consistent with the absence of MLAV VP24 inhibitory activity in IFN-signaling assays, it also fails to interact with KPNA1, 5 and 6, which can mediate nuclear import of pY-STAT1. The interface between EBOV VP24 and KPNA covers a large surface area and involves multiple points of contact [348]. This precluded the mapping of specific amino acid residues that explain the lack of MLAV VP24-KPNA interactions. Nonetheless, these data presented here indicate that MLAV VP24 does not reflect the functions of either MARV or EBOV VP24. It will be of interest to determine whether MLAV VP24 engages different host signaling pathway(s).

The inhibition of IFNβ promoter activity by MLAV VP40 parallels the inhibition by EBOV VP24 and MARV VP40, although inhibition by MLAV VP40 appeared to be more potent. Interestingly, MLAV VP40 inhibits SeV-induced IFNβ gene expression with an efficiency comparable to EBOV VP35, although MLAV VP35 appears to be more potent than MLAV VP40 in this assay. It will be of interest to determine to what extent VP35 and

VP40 contribute to suppression of IFN induction in MLAV infected cells. MARV VP40 and EBOV VP24 inhibition of IFN-α/β production and, in the case of EBOV VP24, production of IFN-λ as well, have been previously reported [353, 395]. However, the mechanism(s) for these inhibitory activities are incompletely defined, although EBOV VP24 was implicated as having an effect post-IRF3 phosphorylation [395]. Inhibition of STAT1 activation and IFN-induced gene expression would be expected to impair the positive feedback loop in which IFN-α/β induces expression of IFN stimulated genes, including RIG-I and IRF7, to amplify IFN responses [403]. This prompted additional experiments to determine whether the detected inhibition was a product of blocking a positive feedback loop involving Jak-STAT signaling. Treatment of empty vector-transfected cells with a Jak1/Jak2 inhibitor did not inhibit SeV-induced IFNβ promoter activation, suggesting that in the system used, Jak-STAT signaling does not contribute to the IFNβ response. Further, the dose response of EBOV VP24, MARV VP40 and MLAV VP40 in the IFNβ promoter assay were unaffected. These data suggest MLAV VP40 has an additional mechanism(s) of IFN antagonism that requires further exploration.

Infectious MLAV is not available to allow us to confirm that suppression of IFN responses occurs in infected cells. As an alternative, we asked whether other viral proteins might modulate these activities. We co-transfected MLAV VP35 and MLAV VP40 with other viral proteins that, based on data from EBOV and MARV, would be expected to form functional complexes. VP35, when co-expressed with NP and VP24, forms nucleocapsid structures [59, 73, 116]. Despite this, NP and VP24 co-expression did not prevent inhibition of the IFNβ promoter by either EBOV or MLAV. Similarly, VP40 interacts with NP [404]. However, NP affected neither VP40 suppression of the IFNβ nor the ISG54

promoter. Additionally, co-expression of the internal viral proteins except the Large (L) protein which is expressed at low levels in filovirus-infected cells, also did not prevent suppression of IFN responses. These findings suggest that these innate immune evasion functions will be active during MLAV infection.

Cumulatively, the present study has identified several functions of MLAV proteins that, in conjunction with previously published data, indicate a compatibility with infection of humans. These include the capacity of MLAV GP to mediate entry into human cells via interaction with NPC1 and suppression of IFN responses through several mechanisms [6]. Notably, given that MLAV VP24 does not detectably interact with the KPNAs or Keap1, it is likely that it may make unique interactions with host cells. Therefore, the existing data also suggests that the outcome of MLAV infection in humans could differ from that of the typical outcome of EBOV or MARV infection.

2.8 Acknowledgments

The following reagent was obtained through BEI Resources, NIAID, NIH: RO6E, Rousettus aegyptiacus (Egyptian fruit bat), Immortalized Fetal Cell Line, NR-49168. This work was supported by NIH grants P01AI120943 and U19AI109945 and Department of the Defense, Defense Threat Reduction Agency grant HDTRA1-16-1-0033. The content of the information does not necessarily reflect the position or the policy of the federal government, and no official endorsement should be inferred.

3 MECHANISMS OF ANTI-VESICULAR STOMATITIS VIRUS ACTIVITY OF DEAZANEPLANOCIN AND ITS 3-BROMINATED ANALOGUES

Submitted to Antiviral Research as of 3/19/2021

3.1 Author figure contributions

The below outlines the figure contribution of each author.

Joyce Sweeney Gibbons - Figure 19 A-E, Figure 20 A-E, Figure 21, Figure 22 A-C, Figure 23 A-B, Figure 24, Figure 25, and Figure 26 A-C.

Sudip Khadka - Figure 26 A-C - Lysates, sucrose-gradients, polysome profiling and fraction collection.

Lin Wang - Figure 22 A-C - *De novo* assembly of WT-VSV-GFP and mutant viruses.

3.2 Abstract

3-deazaneplanocin A (DzNep) and its 3-brominated analogues inhibit replication of several RNA viruses. This antiviral activity is attributed to inhibition of S-adenosyl homocysteine hydrolase (SAHase) and consequently inhibition of viral methyltransferases, impairing translation of viral transcripts. The L-enantiomers of some derivatives retain antiviral activity despite dramatically reduced inhibition of SAHase *in vitro*. To better understand the mechanisms by which these compounds exert their antiviral effects, we compared DzNep, its 3-bromo-derivative, CL123, and the related enantiomers, CL4033 and CL4053, for their activities towards the model negative-sense RNA virus vesicular stomatitis virus (VSV). In cell culture, DzNep, CL123 and CL4033 each exhibited 50 percent inhibitory concentrations (IC50s) in the nanomolar range whereas the IC50 for the L-form, CL4053, was 34-85 fold higher. When a CL123-resistant mutant (VSV^R) was selected, it exhibited cross-resistance to each of the neplanocin

analogs, but retained sensitivity to the adenosine analog BCX4430, an RNA chain terminator. Sequencing of VSV^R identified a mutation in the C-terminal domain (CTD) of the viral Large (L) protein, a domain implicated in regulation of L protein methyltransferase activity. CL123 inhibited parent VSV viral mRNA 5' cap methylation, impaired viral protein synthesis and decreased association of viral mRNAs with polysomes. Modest impacts on viral transcription were also demonstrated. VSV^R exhibited partial resistance in each of these assays but its replication was impaired, relative to the parent VSV, in the absence of the inhibitors. These data suggest that DzNep, CL123 and CL4033 inhibit VSV through impairment of viral mRNA cap methylation and that the L-form, CL4053, based on the cross-resistance of VSV^R, may act by a similar mechanism.

3.3 Introduction

The synthesis and biological activity of derivatives of DzNep, 3-bromo-3-deazaneplanocin, CL123, and 3-bromo-1',6'-isoneplanocin isomers, CL4033 and CL4053 have been described [228, 229]. Each of these analogs contains unique structural modifications relative to the parent compound, DzNep [225, 419]. Specifically, all analogs are brominated at the C-3 position of the nucleobase and the "D-Like" CL4033 and "L-Like" CL4053 isomers have a double bond in the cyclopentenyl moiety at the 1',6' position instead of the 1',4' position [228, 229].

Compounds from this series have demonstrated broad-spectrum antiviral activity against DNA and RNA viruses [218, 270]. The non-segmented negative-sense RNA viruses (NNSVs) are particularly sensitive to this class of compounds with notable activity demonstrated against Ebola virus (EBOV) both *in vitro* and *in vivo* [218, 226, 227]. The antiviral activity of neplanocin derivatives has been attributed to their capacity to inhibit

S-adenosylhomocysteine (SAH) hydrolase (SAHase, E.C.3.3.1.1). In *in vitro* assays, DzNep, CL123 and CL4033 have low nanomolar IC50s against SAHase. However, the L-enantiomer, CL4053, is approximately 1000-fold less inhibitory, relative to the D-enantiomer, CL4033 [228].

SAHase is a critical cellular enzyme in the methylation cycle that hydrolyzes SAH derived from S-adenosylmethionine (SAM)-dependent methyltransferase reactions into homocysteine and adenosine [218, 230, 275]. In the absence of SAH hydrolysis, intracellular levels of SAH increase [231, 232]. The accumulating SAH acts as a feedback inhibitor of SAM-dependent methyltransferases [420]. Inhibition of viral SAM-dependent methyltransferases is proposed to diminish methylation of viral mRNA and thereby impair viral protein synthesis [270].

In this study, we sought to address the mechanisms by which DzNep, CL123, CL4033 and CL4053 inhibit NNSVs by using vesicular stomatitis virus (VSV), a prototypical NNSV. VSV is sensitive to neplanocin congeners [421-423], and there is a strong correlation (r = 0.986) between inhibition of VSV and SAHase [218]. Our data indicate that VSV is inhibited by DzNep, CL123 and CL4033 at low nM IC50s. The anti-VSV activity of the L-form, CL4053, is 85 times higher than the D-form, CL4033. A CL123-resistant mutant, VSV^R, displayed cross-resistance against DzNep and all three DzNep derivatives, including CL4053. Analysis of VSV^R revealed a non-synonymous mutation, I1905R, within the CTD of the L protein. CL123 inhibited the methylation of parental VSV 5' methylated caps and viral mRNA associated with polysomes. For parental VSV, DzNep, CL123 and CL4033 caused minor inhibition of viral mRNA transcription as well as impaired protein synthesis. VSV^R demonstrated reduced sensitivity in all these assays.

3.4 Materials and Methods

3.4.1 Compounds

Compounds were dissolved in dimethyl sulfoxide (DMSO) and diluted to 20 mM stock concentrations. All compounds were > 95% pure.

3.4.2 Cell culture, compound treatments and virus infections

Vero 76 cells (ATCC) were cultured in Dulbecco's Modified Eagle's Medium supplemented with 10% fetal bovine serum (FBS). For all virus infections, excluding plaque assays, cells were pre-treated for 1 hour prior to infection with either DMSO or 1 μM or the indicated compound concentrations in 2% FBS. Monolayers were infected for 1 hour at 37 °C, 5% CO_2, washed twice with PBS and compounds were added back at the indicated concentrations. Multi-step growth kinetics were performed as described previously [424] at MOI 0.002. The initial infection to generate the CL123-resistant VSV was performed at MOI 0.005. All other infections were performed at MOI 10.

3.4.3 Plaque assays

Ten-fold serial dilutions of virus were adsorbed at 37 °C, 5% CO_2 for 1 hour. Post-adsorption, the inoculum was removed, monolayers were washed twice with PBS and overlayed with DMEM, 1% SeaPlaque™ Agarose (Lonza), and 2% FBS. Plates were incubated at 37 °C, 5% CO_2 for 48 hours. Monolayers were fixed with 4% paraformaldehyde for 30 minutes at room temperature, followed by agarose plug removal and staining with crystal violet stain (19% methanol, 9.5% of 1% crystal violet) for 30 minutes. Plates were dunked in water to remove excess stain and dried at room temperature before counting plaques.

3.4.4 Determining IC50 and CC50 values

To obtain IC50 and CC50 values, cells were pre-treated with five-fold compound serial dilutions starting at 30 μM. Infections were performed at MOI 0.002. Viral supernatants were collected 21 hpi and stored at -80 °C until titers were determined by plaque assay. Cell viability was determined with the CellTiter-Glo® assay (Promega) on uninfected cells using the same compound dilutions as described for determining the IC50.

3.4.5 Selection of a CL123-resistant VSV

VSV^R was selected by serially passaging WT-VSV-GFP in the presence of 1 μM CL123 (>IC90). GFP expression serves as a visual measure for viral replication and was used as a gauge for development of CL123 resistance. The initial infection was performed at MOI 0.005. Twenty-four hpi, viral supernatants were serially passaged onto cells that had been pre-treated for 1 hour with 1 μM CL123. At the thirteenth passage, the effect of CL123 on virus replication (GFP expression) appeared to be reduced and a plaque assay was performed on the cell supernatants. Twelve plaques were isolated and amplified twice in the presence of 1 μM CL123. All titers were determined by plaque assay.

3.4.6 Viral genome amplification and sequencing

Viral RNA was extracted using Trizol™ LS Reagent (Thermo Fisher Scientific). First strand cDNA was synthesized using Accuscript High Fidelity 1st Strand cDNA Synthesis Kit (Agilent) and PCR amplification was performed with Phusion® High Fidelity DNA Polymerase (New England Biolabs). Primers used for first strand cDNA synthesis and PCR amplification have been previously described [425]. PCR products were agarose gel-purified and eluted PCR products were then diluted to 5 ng/ul with a

NanoDrop spectrophotometer (Thermo Fisher Scientific) and further quantified with Qubit (Thermo Fisher Scientific). Viral sequencing libraries were prepared with 1 ng of the PCR products using the Nextera XT DNA library preparation kit (FC-131-1024, Illumina). All protocols were carried out as per manufacturer protocols. Analysis of reads was performed using CLC Genomics Workbench 10.0 (Qiagen, Hilden, Germany). The raw reads were assessed for coverage, length, and quality. Adapters were trimmed and default settings were used to trim remaining reads that did not meet the quality thresholds - limit = 0.02, removal of ambiguous nucleotides, maximal 1 nucleotide allowed, and removal of sequences of length with a minimum of 20 nucleotides. Approximately 99.5% (4,776,544 reads) of WT-VSV-GFP total reads (average read length of ~140 base pairs) were *de novo* assembled using the *de novo* assembly function of CLC Genomics Workbench and used as a reference genome to assemble the sequencing reads of the clones. The mapped reads of the clones were locally re-aligned automatically, ends with sequencing errors discarded and duplicate reads removed with default settings. Genome-wide SNP variants with average base quality scores over 20.0 and forward to reverse reads ratio over 0.05 were called and compared to the reference genome and clones run in parallel to identify unique variants.

3.4.7 Determining m^7G capped viral mRNA levels

Post CL123 treatment and infection, cells were harvested at 3 hpi, and total RNA was Trizol-extracted. Protein G beads (Pierce™ Protein G Magnetic Beads, Thermo Fisher Scientific) were pre-conjugated overnight at 4 °C with either an anti-m^7G cap monoclonal antibody (MBL International) or a control mouse IgG2a (MBL International). 40 µg of RNA was incubated with each antibody for 3 hours at 4 °C with gentle rocking.

Samples were washed and eluted from the beads using the RIP-Assay kit (RN1005, MBL International). First strand cDNA was generated with oligo dT primers (SuperScript™ IV kit, Thermo Fisher Scientific). The reactions were carried out as per the manufacturers' protocol with the exception of halving all reagents. The cDNA was diluted 10 fold in nuclease free water and used as a template for quantitative PCR (qPCR). PerfeCTa® SYBR Green FastMix® (VWR Scientific) was used to determine levels of viral genes and β-actin. The final concentration of primers in the reaction was 0.25 μM. Input RNA, prior to the RNA IP, was also assessed for viral gene expression and the ratio of m^7G cap RNA to input RNA was determined.

3.4.8 Quantifying viral RNA synthesis

To assess the effect of the compounds on RNA synthesis, monolayers were compound treated, infected and RNA was harvested at the indicated timepoints (1 and 6 hpi) using the RNeasy® Mini Kit (Qiagen). cDNA synthesis and qPCR were performed as described above.

3.4.9 Pulse-chase analysis of viral protein synthesis

Monolayers were compound treated and infected. One hour prior to each timepoint collection, cell media was replaced with DMEM lacking methionine and cysteine (30 minutes) and the cells were radioactively labeled with 20 μCi/ml of EasyTag™ EXPRESS ^{35}S Protein Labeling Mix (PerkinElmer) (30 minutes). Whole cell lysates were prepared on ice with NP40 buffer (50mM Tris-HCl [pH 8.0], 280mM NaCl, 0.5% NP-40) supplemented with cOmplete™ protease inhibitor cocktail (Roche). Lysates were incubated for ten minutes on ice and clarified for ten minutes at 21,100 x g at 4 °C. Lysates were resolved on a 4-12% polyacrylamide gel which was fixed for 30 minutes in

20% methanol / 7% acetic acid and dried for two hours. Labeled bands were visualized with a phosphorimager.

3.4.10 Polysome profiling

Polysome analysis was performed as previously described [426]. Monolayers were compound treated and infected. Three hpi the media was replaced with media containing 100 ug/ml cycloheximide and incubated for ten minutes at 37 °C, 5% CO_2. Monolayers were washed twice with PBS containing 100 ug/ml cycloheximide. Cell lysates were prepared with NP40 buffer supplemented with cOmplete™ protease inhibitor cocktail (Roche) and RiboLock RNase inhibitor (40 U/μL) (Thermo Fisher Scientific). Lysates were layered over a 10-50% sucrose gradient and centrifuged at 4 °C, 200,000 x g for two hours. One milliliter (ml) fractions were collected using the BR-188 Density Gradient Fractionation System (Brandel). From the 1 ml fractions, 200 μL of RNA was extracted using Trizol LS and oligo dTs were used to generate first strand cDNA. Viral gene expression was determined by qPCR as described above.

3.4.11 Experimental design and statistics

All experiments, except where stated, were performed in triplicate and the error bars represent the SEM for the replicates. Statistics were determined using a student t-test as compared to DMSO-treated-infected controls unless otherwise stated; *** $p < 0.0002$, ** $p < 0.0021$, * $p < 0.0332$.

3.5 Results

3.5.1 Neplanocin analogs are potent inhibitors of WT-VSV-GFP.

To assess the antiviral activity of CL123, CL4033, CL4053, and DzNep, we determined the IC50 of each compound against VSV. Relative to the DMSO control,

CL123, CL4033 and DzNep inhibited WT-VSV-GFP with low nanomolar IC50s (**Figure 19A-B, D)**. CL4053 inhibited WT-VSV-GFP, however, its IC50 was approximately 100-fold higher as compared to the D-enantiomer CL4033 (**Figure 19C**). Additionally, we evaluated the antiviral activity of the adenosine analog and known nascent RNA chain-terminator BCX4430 [191, 192]. BCX4430 inhibited WT-VSV-GFP with an IC50 of 14.9 μM (**Figure 19E**). In parallel, the effects on cell viability were assessed. The fifty percent cytotoxic concentrations (CC50s) for all compounds were greater than 30 μM (**Figure 19A-E,** red curves).

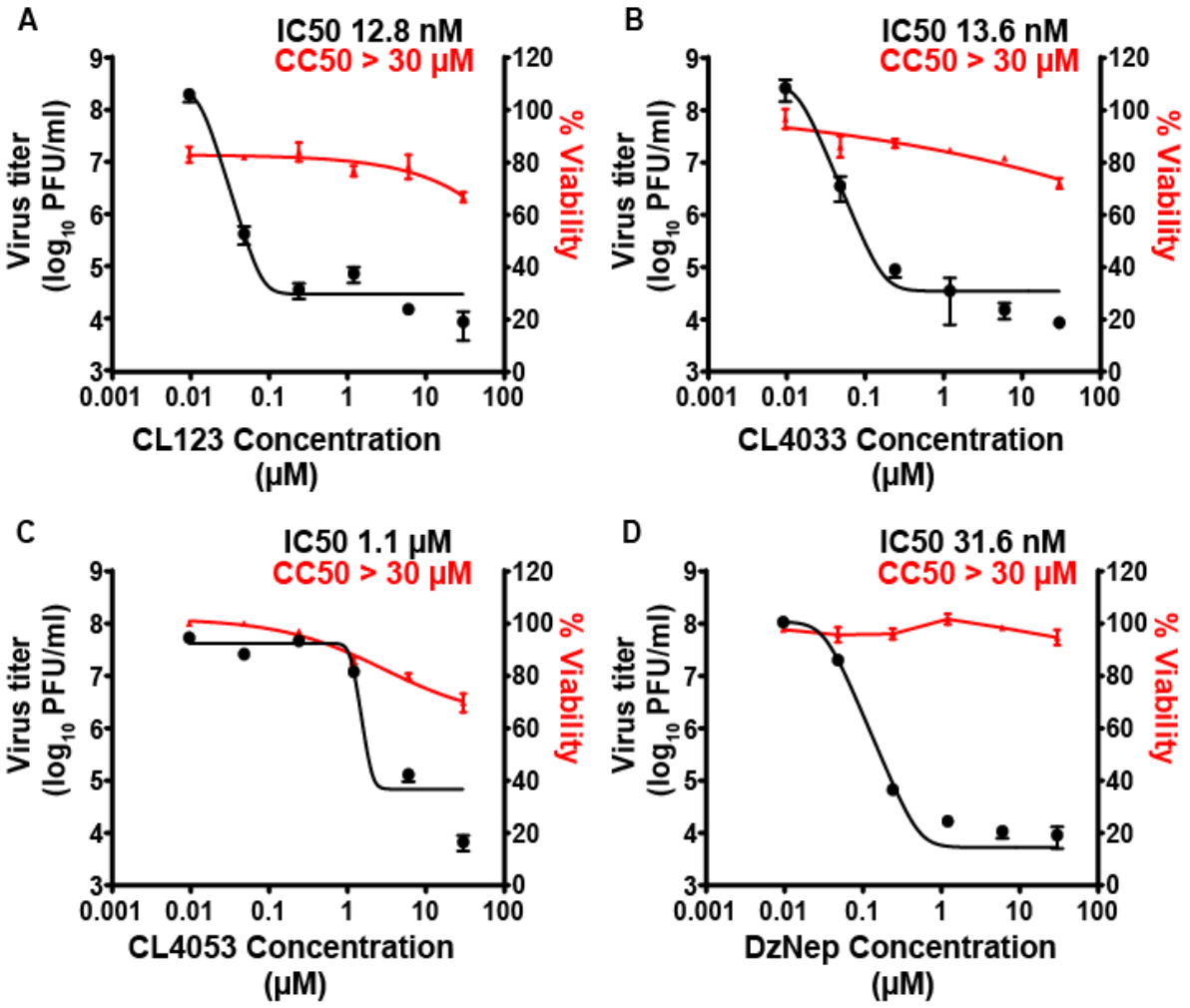

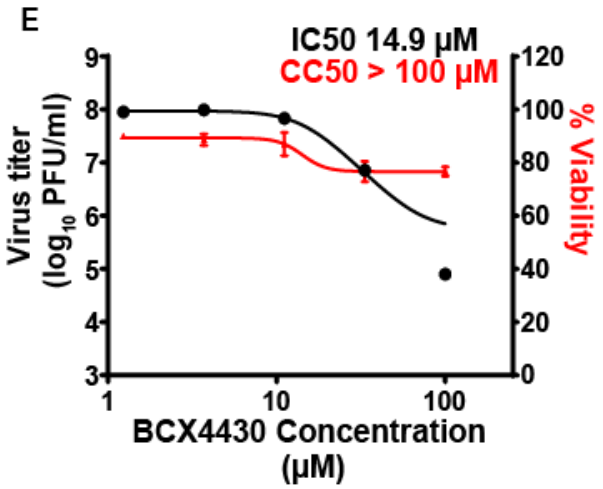

Figure 19 Neplanocin analogs are potent inhibitors of WT-VSV-GFP.
*Levels of infectious virus and percent viability of cells treated with the indicated concentrations of **(A)** CL123, **(B)** CL4033, **(C)** CL4053, **(D)** DzNep and **(E)** BCX4430 are presented. Vero 76 cells were pre-treated for one hour with the compounds at the indicated concentrations and infected with WT-VSV-GFP at MOI 0.002. Twenty-one hours post-infection, supernatants were collected, and levels of infectious virus were determined by plaque assay. Cell viability was determined in the absence of viral infection. The experiment was performed in triplicate and the error bars represent the standard error of the mean (SEM) for the triplicate.*

3.5.2 VSV^R demonstrates cross-resistance to all neplanocin derivatives.

To gain insight into the antiviral mechanism of these compounds, we serially passaged WT-VSV-GFP in the presence of CL123 and obtained a resistant virus, VSV^R. VSV^R exhibited increased resistance to each of the compounds, with IC50s shifting to greater than 30 µM (**Figure 20A-D**). We isolated 11 additional plaque-purified clones, and all exhibited similar resistance against CL123 (data not shown). BCX4430 inhibited VSV^R, to a similar extent as WT-VSV-GFP with an IC50 of 11.3 µM (**Figure 20E**). This suggests that the neplanocin analogs having a different mechanism of inhibition than BCX4430.

To determine whether VSR^R exhibited any growth impairment, its multi-cycle growth kinetics (MOI 0.002) were compared to WT-VSV-GFP (**Figure 21**). In the presence of DMSO, VSV^R exhibited a significant lag in its replication relative to WT-VSV-GFP, with 100- and 10-fold lower titers at 12 and 24 hours post-infection, but by 36 hours, VSV^R titers were equivalent to those of WT-VSV-GFP. CL123 severely inhibits WT-VSV-GFP, decreasing viral titers 2-5 $\log_{10}$ fold; however, the antiviral effect of CL123 was absent with VSV^R (**Figure 21**).

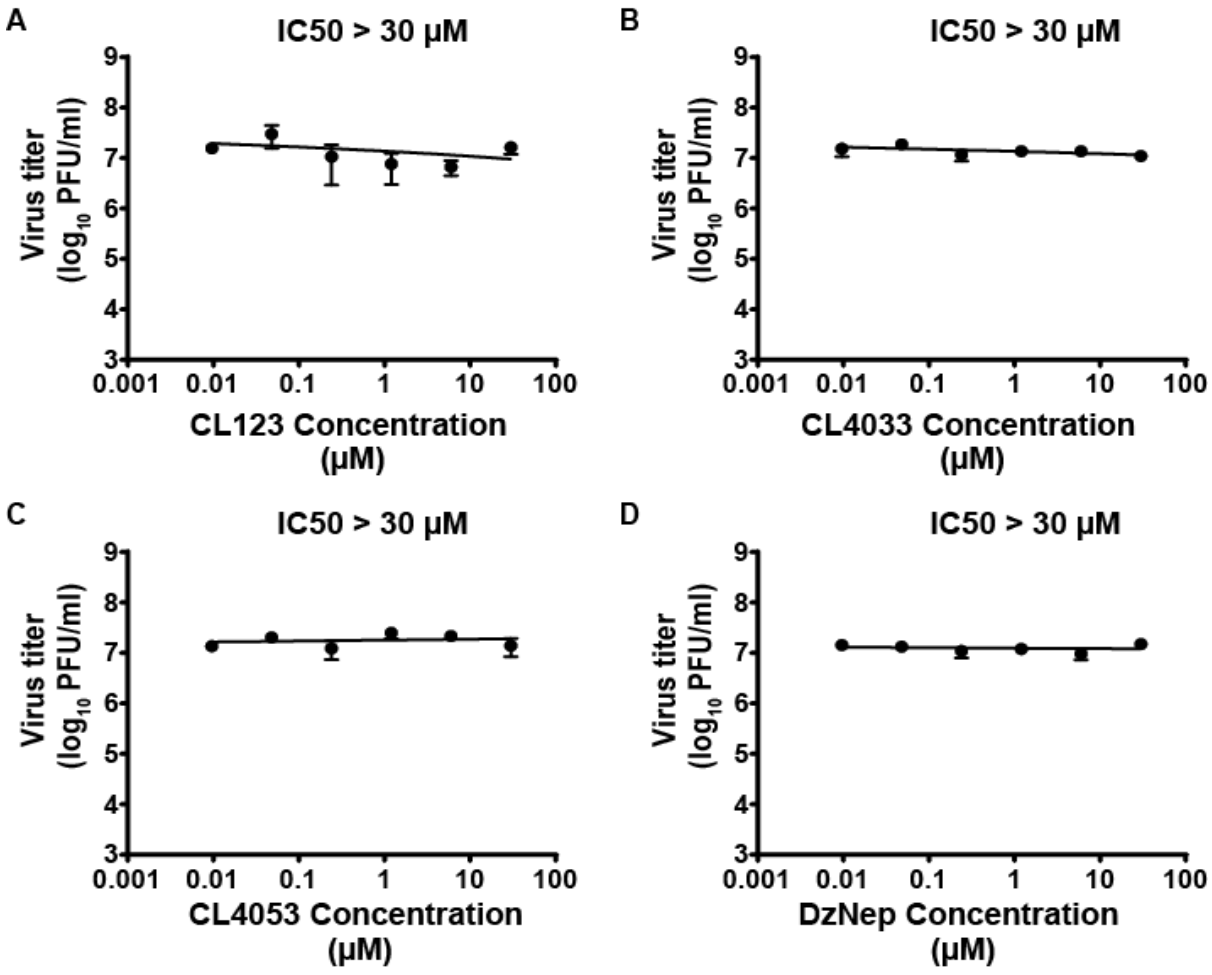

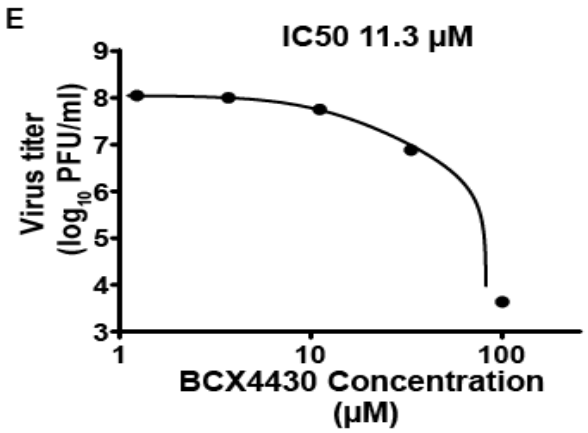

Figure 20 VSV^R exhibits cross-resistance to all four neplanocin analogs.
Levels of infectious VSV^R after growth in the presence of the indicated concentrations of ***(A)*** *CL123,* ***(B)*** *CL4033,* ***(C)*** *CL4053,* ***(D)*** *DzNep and* ***(E)*** *BCX4430. Vero 76 cells were pre-treated for one hour with the compounds at the given concentrations and infected with VSV^R at MOI 0.002 for twenty-one hours. Supernatants were collected and levels of infectious virus were determined by plaque assay. The experiment was performed in triplicate and the error bars represent the SEM for the triplicate.*

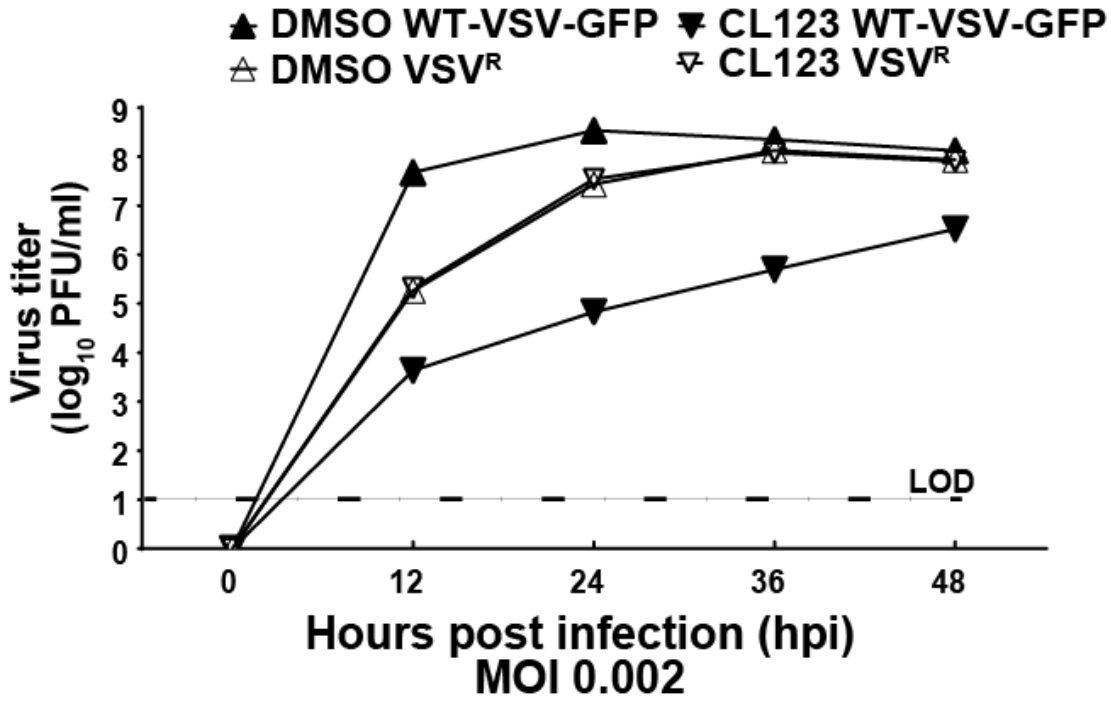

Figure 21 VSV^R is impaired early during infection.

WT-VSV-GFP and VSV^R multi-step growth kinetics in Vero 76 cells at MOI 0.002 in the absence and presence of 1 µM CL123 are presented. Cell culture supernatants were collected at the indicated timepoints and the titers were determined by plaque assay. The limit of detection (LOD) is indicated on the graph. The experiment was performed in triplicate and the error bars represent the SEM for the triplicate.

3.5.3 VSV^R possesses a mutation in the CTD of the L protein.

We performed deep sequencing on all twelve isolated clones. All mutations obtained from the 12 sequenced clones are provided in *Table 3.1.1*. The non-synonymous mutations with single nucleotide polymorphism (SNP) frequencies greater than 10% in the characterized VSV^R (clone 5), are indicated in **Figure 22A**. In comparison to WT-VSV-GFP, the only non-synonymous mutation, which was present in all 12 resistant clones, was a T to G SNP at nucleotide position 11,286. This gave rise to a non-synonymous substitution, I1905R, within the L protein (**Figure 22B**). This mutation occurred at high SNP frequency (>98%) in all of the clones. Residue 1905 is located within the CTD (**Figure 22B-C**, red colored domain), which is adjacent to the L methyltransferase domain (MTD, orange colored) [131]. The amino acid residues that are involved in SAM binding and catalysis are included within the MTD for comparison (**Figure 22C**).

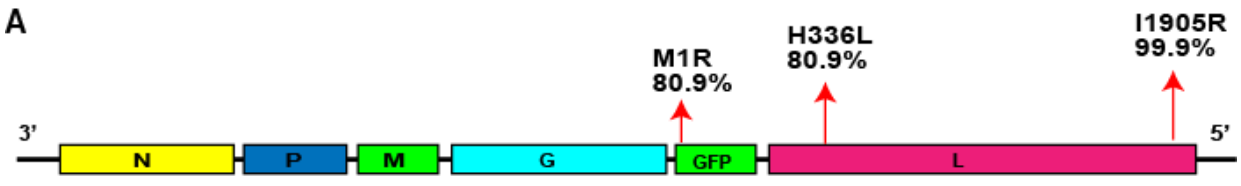

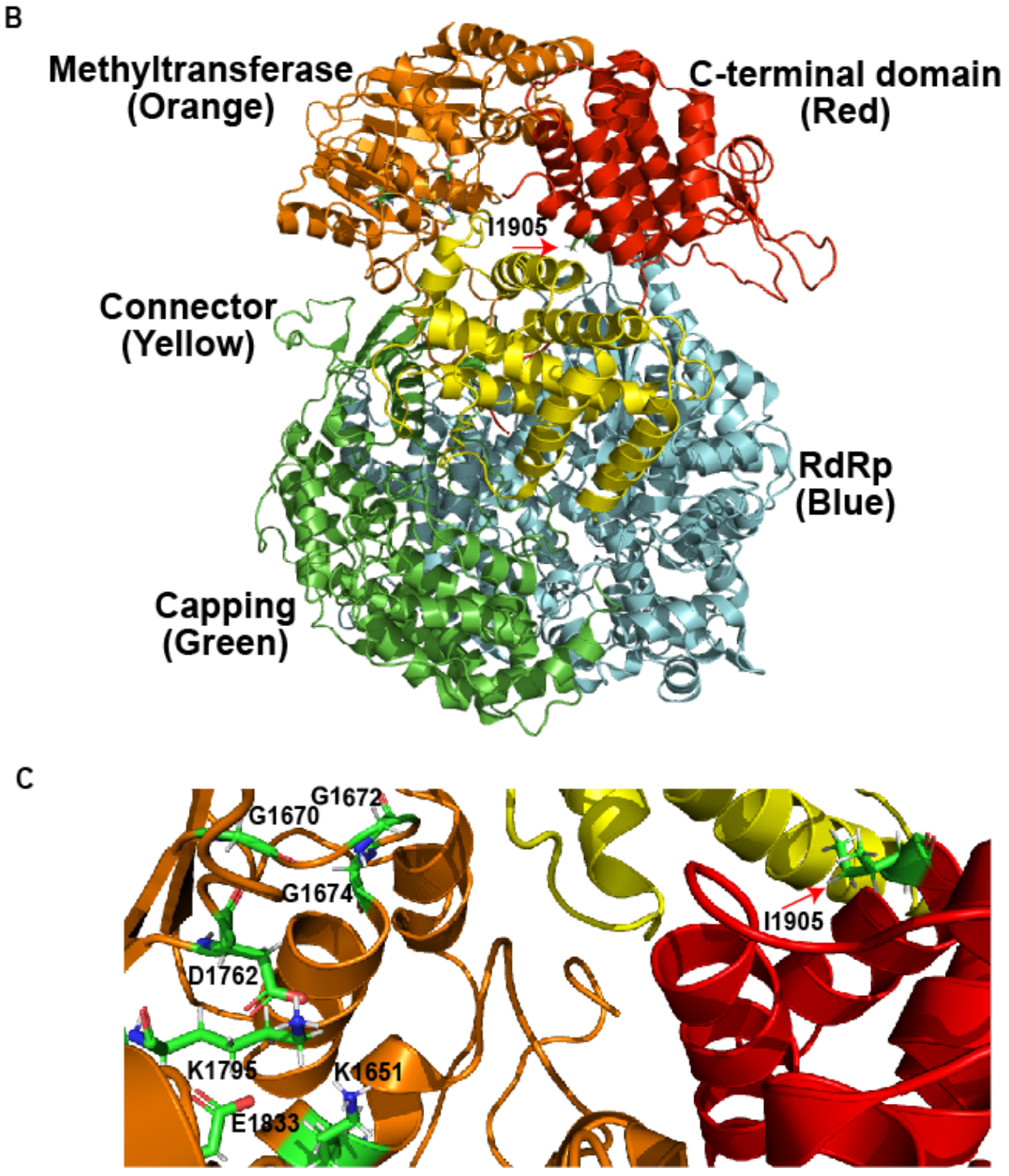

Figure 22 VSV^R mutation I1905R is located in the CTD of the L protein.
The location of non-synonymous mutations found in VSV^R. ***(A)*** *Schematic of the VSV^R genome with non-synonymous mutations that were present in at least 10% of reads are labeled.* ***(B)*** *Structure of VSV L with the location of amino acid residue I1905 indicated*

(C) *Amino acid residue I1905 with SAM binding motif and methyltransferase catalytic residues labeled; oxygen red-color, nitrogen blue-color, carbon green-color, and hydrogen white-color.* ***B*** *and* ***C*** *are PyMOL renderings based on PDB: 5A22.*

Table 3.1.1 Identified mutations, location on the viral genome and allele frequency.

Type[a]	***Nucleotide[b]***	***Gene***	***Protein***	***% SNP Frequency (Clone)***
SNV	*11286 T:G*	*L*	*Ile1905Arg*	*> 98 (1-12)*
SNV	*6579 A:T*	*L*	*His336Leu*	*81 (5); 5 (6)*
SNV	*6069 A:G*	*L*	*Lys166Arg*	*96 (8); 95 (1); 35 (2); 9 (3); 6 (5)*
SNV	*7265 C:T*	*L*	*Pro565Ser*	*96 (8)*
SNV	*6157 T:A*	*L*	*His195Gln*	*25 (4)*
SNV	*7863 A:G*	*L*	*Asp764Gly*	*8-12 (2-4; 6-12)*
SNV	*5654 G:T*	*L*	*Asp28Tyr*	*3-5 (1-4;6-12)*
SNV	*6837 T:A*	*L*	*Phe422Tyr*	*2-5 (4,6,8-12)*
SNV	*6872 G:T*	*L*	*Ala434Ser*	*8 (7)*
SNV	*11850 C:A*	*L*	*Ser2093Tyr*	*2 (4)*
SNV	*10934 G:T*	*L*	*Glu1788STOP*	*2 (2, 4)*
SNV	*11870 G:T*	*L*	*Asp2100Tyr*	*2 (2)*
SNV	*3084 T:C*	*G*	*Cys3Arg*	*97 (2); 37 (4) 7 (5); 97 (8); 6 (11)*
SNV	*5039 C:A*	*GFP*	*Asn106Lys*	*100 (1) 4 (2)*
SNV	*4723 T:G*	*GFP*	*Met1Arg*	*81 (5)*
SNV	*4737 G:T*	*GFP*	*Glu6STOP*	*25 (6);10 (5)*
SNV	*5406 G:A*	*GFP*	*Gly229Arg*	*20 (7)*
Del	*7865 G*	*L*	*Asp765fs*	*8-12 (2-4; 6-12)*
Del	*8635 T*	*L*	*Leu1023fs*	*2 (1,3,6,9-11)*
Ins	*11974^11975T*	*L*	*NCR*	*12 (4); 5 (5)*
Ins	*11935^11936A*	*L*	*NCR -TT*	*2-4 (1-5; 7-12)*
Ins	*8479^8480A*	*L*	*Cys972fs*	*3-8 (1-4; 6-12)*
Ins	*7494^7493T*	*L*	*Glu643fs*	*2-3 (1-4, 6-12)*
Ins	*4633^4634A*	*G*	*NCR-TT*	*4-9 (1-12)*
Ins	*3039^3040A*	*M*	*NCR-TT*	*2-3 (1-8, 10)*
Ins	*5538^5539T*	*GFP*	*NCR*	*73 (12); 5 (10)*
Ins	*5553^5554A*	*GFP*	*NCR-TT*	*2-4 (1-4; 6-12)*
SNV	*717 T:A*	*N*	*Silent*	*82 (5)*
SNV	*2112 A:C*	*P*	*Silent*	*82 (5)*
SNV	*3824 A:T*	*G*	*Silent*	*3 (5)*
SNV	*7687 T:C*	*L*	*Silent*	*80 (10); 18 (11); 3 (9)*
SNV	*9289 C:T*	*L*	*Silent*	*78 (9)*
SNV	*10219 A:G*	*L*	*Silent*	*77 (12)*
SNV	*10321 T:G*	*L*	*Silent*	*79 (5)*
SNV	*10669 G:A*	*L*	*Silent*	*79 (5); 4 (6); 3 (12)*
SNV	*11981 A:T*	*L*	*Silent*	*67 (12)*
SNV	*11797 A:G*	*L*	*Silent*	*25 (7)*
SNV	*9574 T:G*	*L*	*Silent*	*11 (5)*
SNV	*8017 T:G*	*L*	*Silent*	*5 (4)*

Type[a]	*Nucleotide*[b]	*Gene*	*Protein*	*% SNP Frequency (Clone)*
SNV	*8224 T:A*	*L*	*Silent*	*4 (2)*

[a] SNV - single nucleotide variants; Del - deletion; Ins - insertion; [b] Nucleotide numbering is based off of the *de novo* assembly of our WT-VSV-GFP; fs - frameshift; NCR-TT- non-coding region- transcription terminator sequence.

3.5.4 Neplanocin congeners modestly impact VSV transcription.

We next sought to address whether the neplanocin congeners might impact viral RNA and protein synthesis. For these studies, infections were performed at MOI=10 to ensure a robust signal and to ensure robust shutoff of host protein synthesis. Under these conditions, inhibition by the less potent L-isomer CL4053 was not readily achieved. Therefore, CL4053 was not included in these studies.

A point of consideration is that DMSO-treated mutant and parental VSV have differences in viral mRNA levels at each assessed timepoint. Viral mRNAs for DMSO-treated VSV^R as compared to DMSO-treated WT-VSV-GFP were 10-18 fold less at one hpi and 3-5 fold less at six hpi, depending on the viral gene. This is consistent with the impairment seen for VSV^R as compared to parental VSV in the viral kinetics and protein synthesis (**Figure 21** and **24**).

At 1 hpi, for each of the WT-VSV-GFP viral genes tested, moderate decreases in viral mRNA levels (5-10 fold, depending on the viral gene) were observed in the presence of 1 μM of the compounds as compared to the DMSO control (**Figure 23A**). This inhibition at early times post-infection was not observed with VSV^R (**Figure 23A**). At 6 hpi, viral mRNA levels were significantly enhanced in the presence of the analogs for WT-VSV-GFP and to a much less extent for VSV^R (**Figure 23B**).

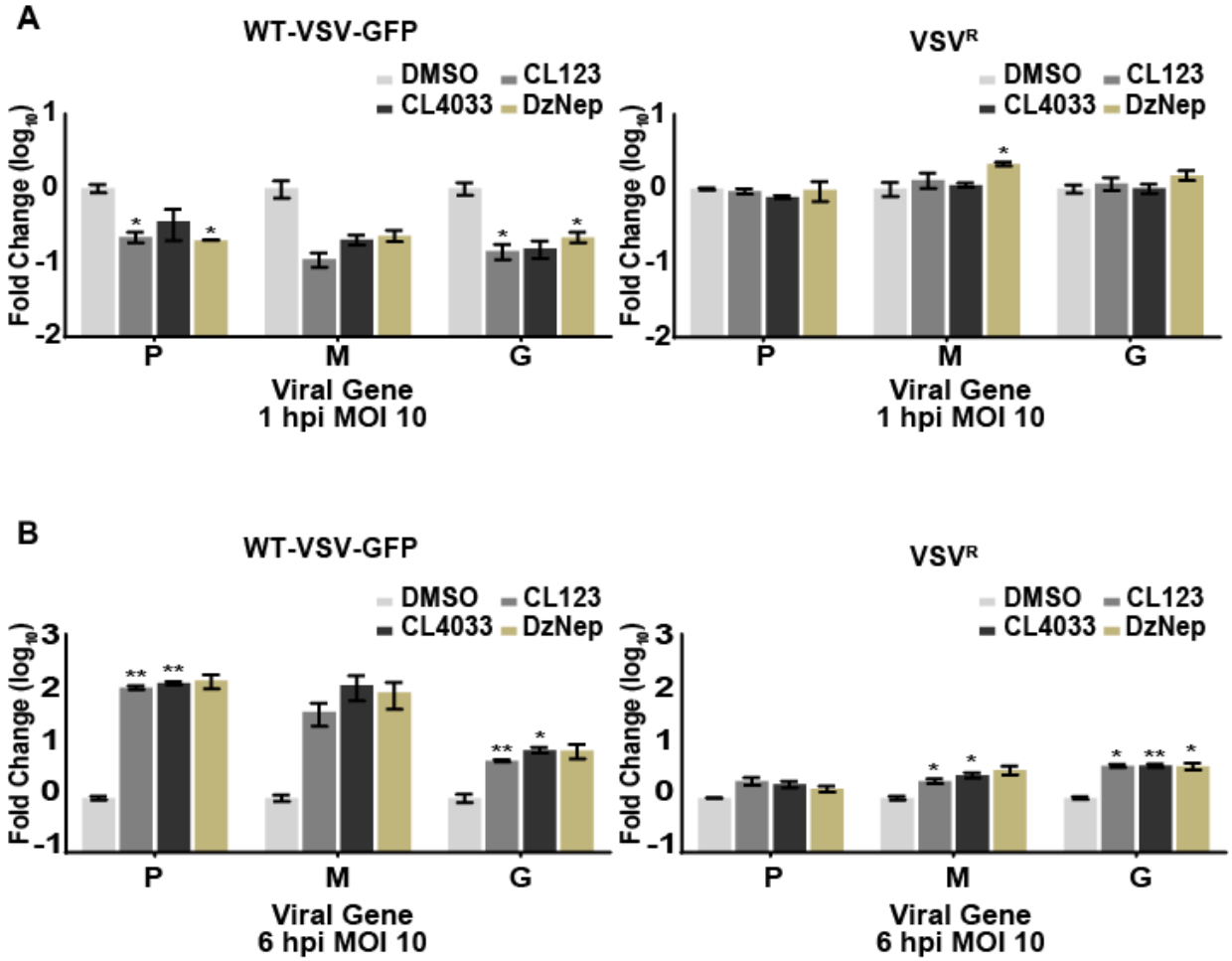

Figure 23 Analogs have a minor impact on transcription.

*The effect of the indicated compounds on viral mRNA was determined at one hpi **(A)** or six hpi **(B)** for WT-VSV-GFP and VSV^R. Monolayers were pre-treated with 1 μM of each indicated compound and infected with each virus at MOI=10. Total RNA was harvested at the indicated timepoints and reverse transcription-qPCR, was performed with gene specific primers. Viral mRNA levels were normalized to β-actin mRNA levels and are presented as fold-change relative to the DMSO treated control for each virus. The experiment was performed in triplicate and the error bars represent the SEM for the triplicate. Statistical significance was determined by performing a student t-test as compared to DMSO virus-infected control (light grey bar); ** $p < 0.0021$, * $p < 0.0332$.*

3.5.5 VSV protein expression is impaired in the presence of neplanocin like compounds.

To determine any effects of our compounds on viral protein synthesis, we conducted ^{35}S metabolic labeling experiments. In the presence of DMSO, WT-VSV-GFP protein levels increased throughout the course of the infection (**Figure 24**). VSV L was weakly expressed, as expected [170, 427-429]. For each of the analogs, WT-VSV-GFP viral protein synthesis was impeded. This was most notable at earlier timepoints during infection. As the infection progressed, the inhibitory effect of the analogs began to diminish, particularly for the N and P genes. In contrast, expression of GFP and M, which co-migrate, and of G was still clearly inhibited at 6 hpi. This pattern of inhibition correlates with the VSV transcription gradient, where N and P genes are transcribed at higher levels than other genes [170, 427-429]. DMSO-treated VSV^R proteins also increased throughout the course of infection. When treated with the neplanocin analogs, expression of VSV^R proteins was less impaired as compared to WT-VSV-GFP (**Figure 24**) demonstrating that resistance correlates with sustained viral protein synthesis.

.

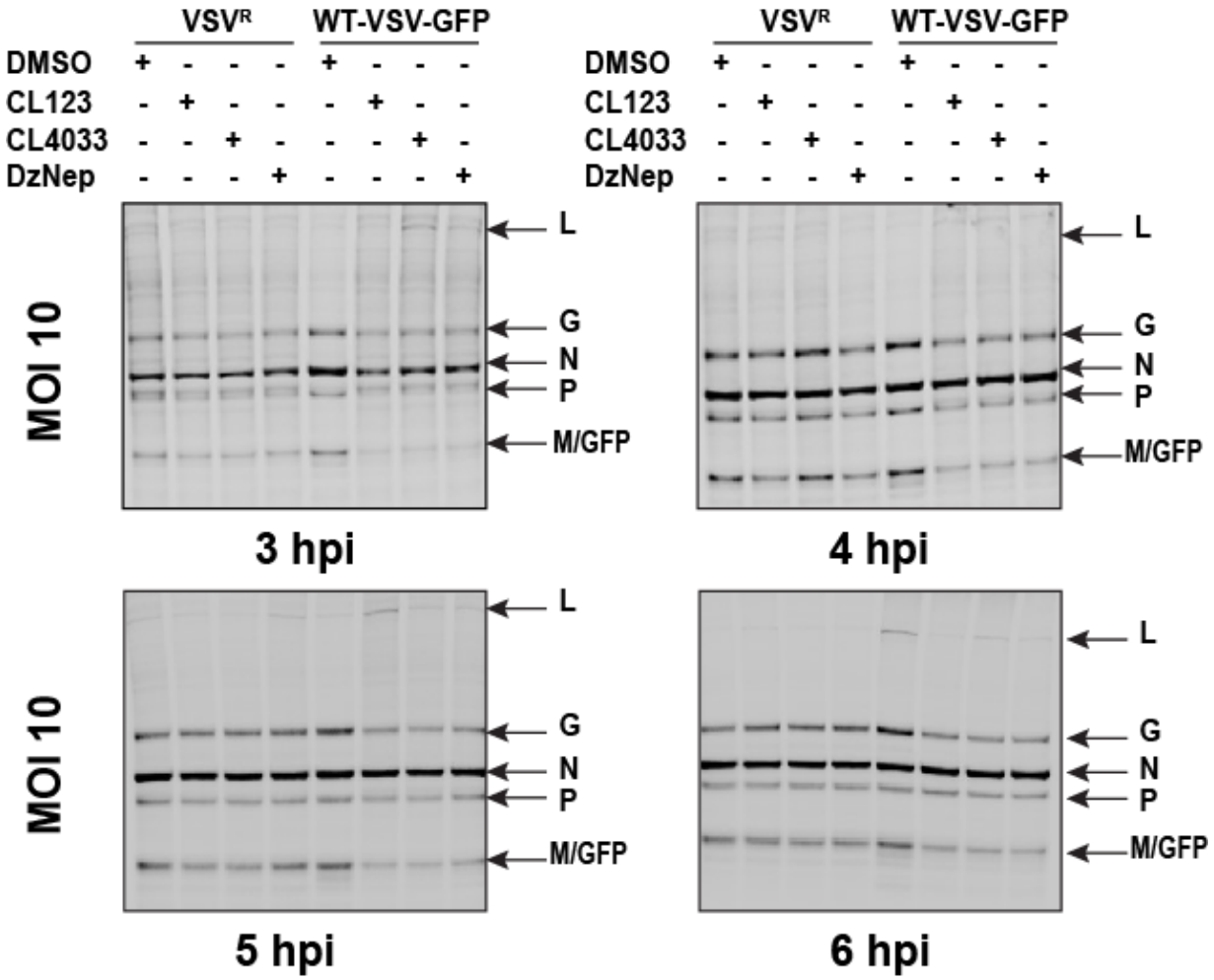

Figure 24 Each of the compounds inhibits WT-VSV-GFP protein expression. *The effect of the indicated compounds at 1 μM on viral protein synthesis was evaluated for both WT-VSV-GFP and VSV^R (MOI=10). At the indicated timepoints poot-infection, the cells were starved of methionine and cysteine for thirty minutes and then labeled with ^{35}S methionine and cysteine for 30 minutes. Whole cell lysates were prepared for the indicated timepoints and then separated on 4-12% gradient gels. Gels were fixed for thirty minutes, dried for two hours, and visualized using a phosphorimager.*

3.5.6 CL123 diminishes parental VSV mRNA cap methylation and RNA association with polysomes.

Since our neplanocin derivatives are known to inhibit SAHase [228, 229], we directly assessed the effect of CL123 on viral mRNA cap methylation and on viral mRNA

association with polysomes. We focused only on CL123 for these experiments as our mutant VSV^{R} was generated using this analog.

To directly assess the impact of CL123 on mRNA cap methylation, we performed RNA immunoprecipitations (IPs) with an anti-m^{7}G cap monoclonal antibody and quantified mRNA levels by reverse-transcription-quantitative PCR (qPCR). The DMSO-treated WT-VSV-GFP infection produced more mRNA with methylated cap than other conditions, and levels of mRNA with methylated caps decreased in the presence of CL123 (**Figure 25A**). For VSV^{R} in DMSO-treated cells, levels of mRNA with methylated caps were reduced relative to the DMSO-treated WT-VSV-GFP condition and more similar to WT-VSV-GFP in CL123-treated cells. However, CL123 had less impact on absolute levels of mRNA with methylated caps for VSV^{R} (**Figure 25A**). When levels of mRNA with methylated cap were compared to total levels of mRNA, CL123 was found to have a greater impact on the ratio of methylated capped to total mRNA for WT-VSV-GFP as compared to VSV^{R}. However, some inhibition of cap methylation was present for VSV^{R}, as well (**Figure 25B**).

Next, the effect of CL123 on translation of viral mRNAs was evaluated by polysome analysis. DMSO-treated WT-VSV-GFP infected cells actively translated more mRNA relative to CL123-treated, infected cells, as is seen by the higher absorbance in the polysome fractions (**Figure 26A and 26B**). For VSV^{R} both the DMSO and CL123-treated cells had near equivalent amounts of mRNA associated with polysomes (**Figure 26A and 26B**). Examination of the distribution of viral mRNAs revealed greater association with polysomes for WT-VSV-GFP N mRNA in the presence of DMSO as compared to the WT-VSV-GFP infected, CL123-treated samples (**Figure 26C**). In the CL123-treated samples,

there was also a shift of N mRNA towards the monosome fractions. In contrast, differences between DMSO and CL123 treatments were nearly absent when VSV^R was used (**Figure 26C**). The overall polysome profiles for both the DMSO and CL123-treated VSV^R samples were more similar to the CL123-treated WT-VSV-GFP profile. For both the DMSO and CL123-treated VSV^R samples, a larger 80S monosome peak was apparent, as compared to the DMSO-treated WT-VSV-GFP samples (**Figure 26A**). The viral genes, P, M and G mRNAs were also measured and behaved in a similar fashion as the N gene (data not shown). Overall, these data demonstrate that CL123 impairs WT-VSV-GFP mRNA cap methylation and protein synthesis while, VSV^R mRNA cap methylation and translation are somewhat resistant to the effects of CL123 but that, even in the absence of CL123, cap methylation and translation are reduced for VSV^R.

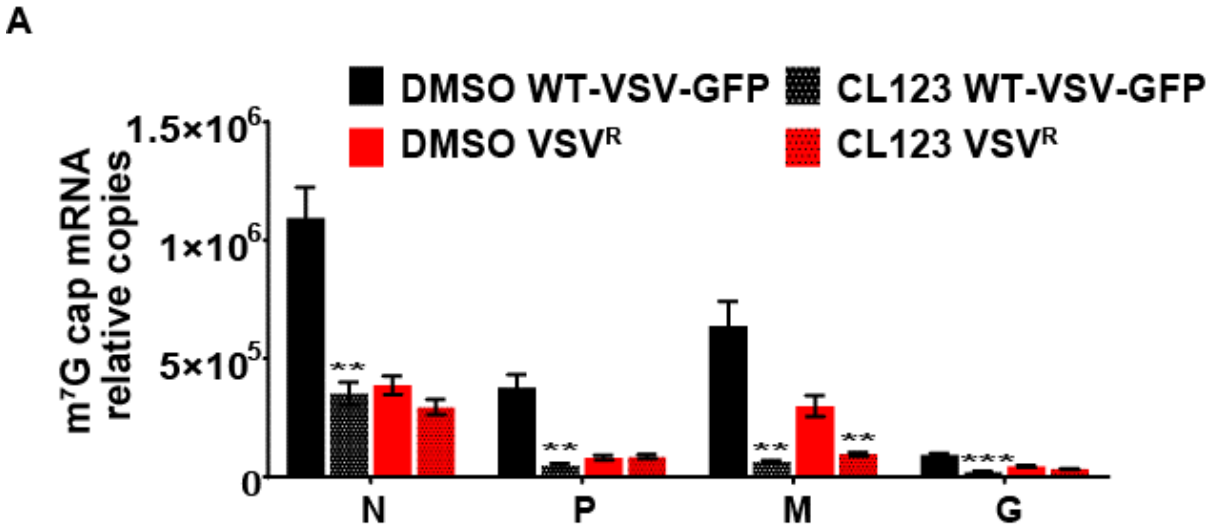

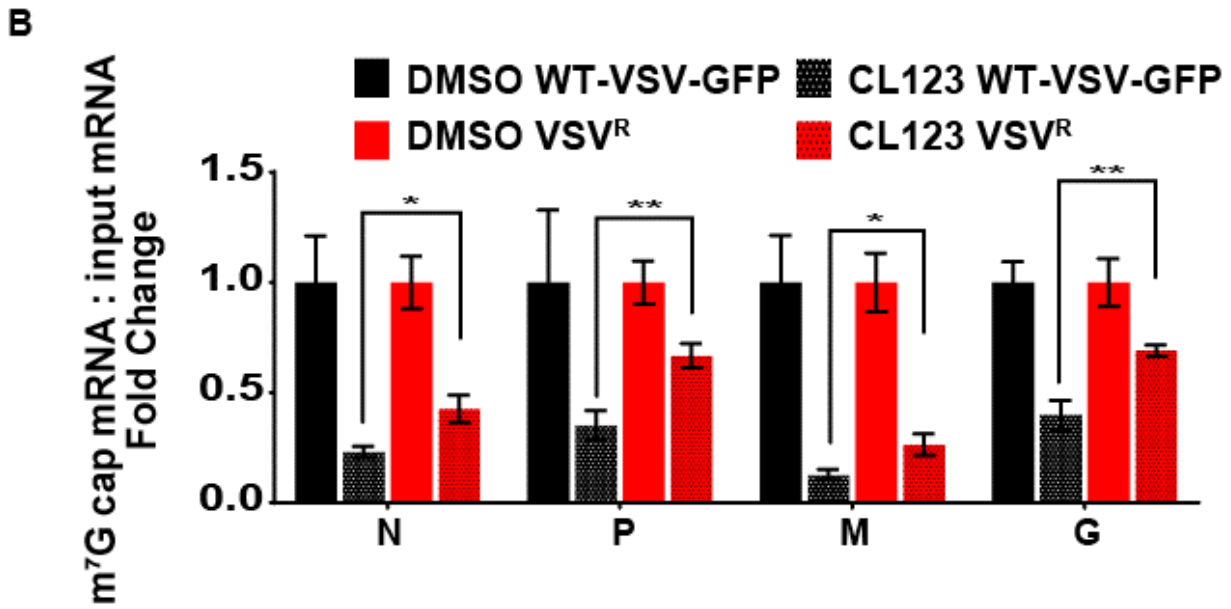

Figure 25 CL123 decreases levels of VSV mRNA cap methylation.
*m^7G cap mRNA relative copies **(A)**, and ratios of m^7G capped mRNA to input mRNA **(B)** were calculated. The ratios of each DMSO-treated virus was averaged and the DMSO and CL123-virus-infected ratios were compared to these averages for each respective virus. The concentration of CL123 was 1 μM. Total RNA was harvested at three hpi (MOI 10) and samples were incubated with either an IgG control antibody or a monoclonal anti-m^7G cap antibody. Reverse transcription-qPCR was performed, and viral mRNA levels were normalized to β-actin mRNA levels to determine relative copies of mRNAs. The experiment was performed in sextuplicate and the error bars represent the SEM for the sextuplicate. Statistical significance was determined by performing a student t-test as compared to each DMSO-virus-infected sample (black or red bar) (**A**), or CL123 virus-infected sample (black hash or red hash bar) (**B**); *** $p < 0.0002$, ** $p < 0.0021$, * $p < 0.0332$.*

A

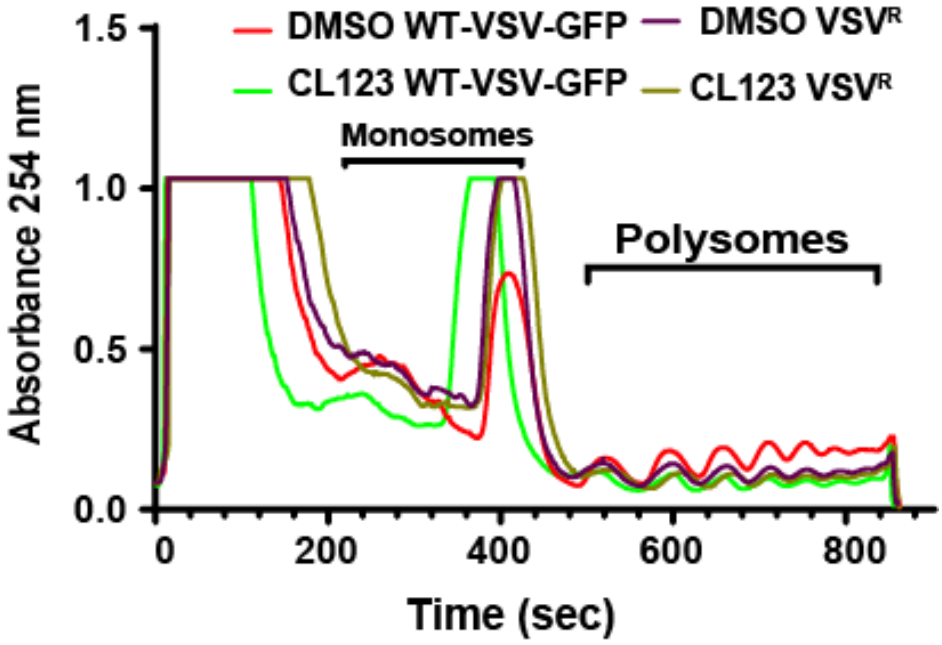
DMSO WT-VSV-GFP
DMSO VSV^R
CL123 WT-VSV-GFP
CL123 VSV^R
Monosomes
Polysomes
Absorbance 254 nm
1.5
1.0
0.5
0.0
0
200
400
600
800
Time (sec)

B

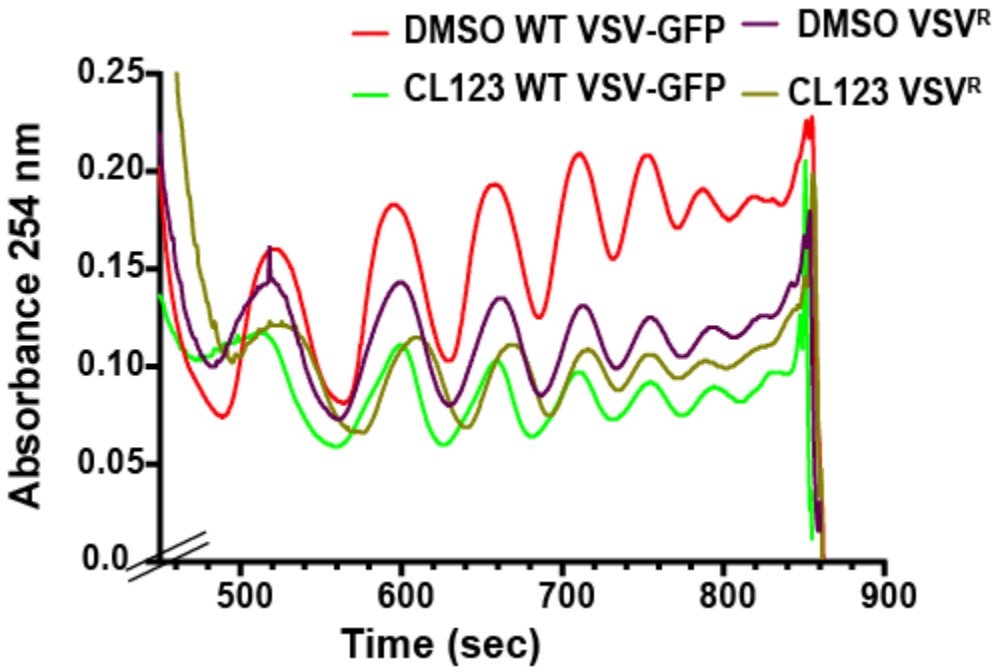
DMSO WT VSV-GFP
DMSO VSV^R
CL123 WT VSV-GFP
CL123 VSV^R
Absorbance 254 nm
0.25
0.20
0.15
0.10
0.05
0.0
500
600
700
800
900
Time (sec)

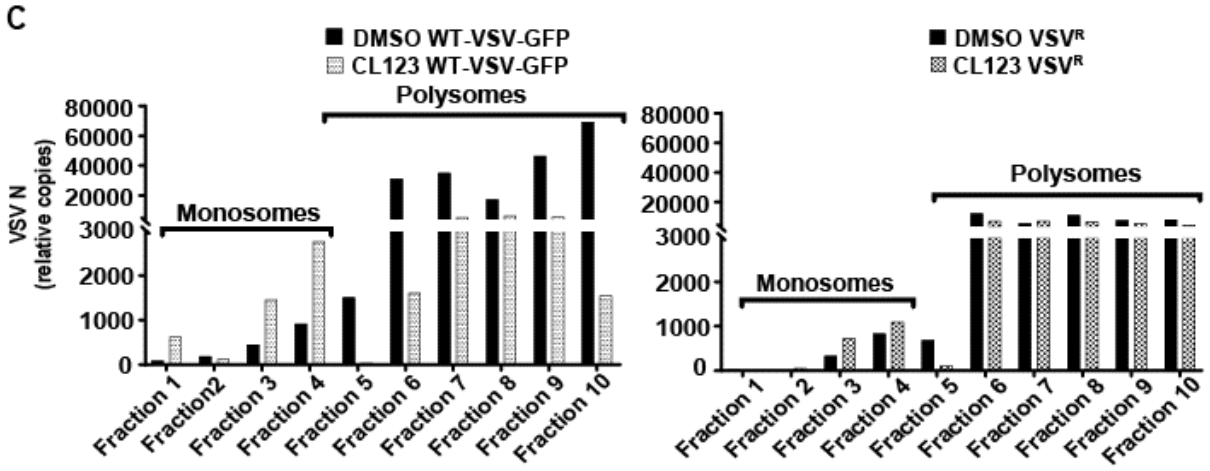

Figure 26 CL123 diminishes the amount of WT-VSV-GFP RNA associated with polysomes.

Changes in viral RNA association with monosome and polysome fractions was determined. Both WT-VSV-GFP and VSV^R infections were performed at MOI 10 in the presence of DMSO or 1 μM CL123. Three hours post infection, translating RNA was immobilized on the ribosomes using cycloheximide. Whole cell lysates were harvested and centrifuged at 200,000 x g for two hours through a 10-50% sucrose gradient. Fractions were collected using the BR-188 Density Gradient Fractionation System, RNA was extracted with Trizol and reverse transcription qPCR was performed with primers specific to viral genes. ***(A)*** *Ribosome traces of all tested conditions.,* ***(B)*** *Ribosome traces with x axis cut at 450 sec.* ***(C)*** *Relative copy numbers of VSV N were determined by reverse transcription q-PCR. The experiment was performed two independent times and the data shown is representative of both experiments.*

3.6 Discussion

This study characterized the mechanisms by which DzNep, CL123 and the enantiomeric pair CL4033 and CL4053 inhibit VSV. It has been proposed that neplanocin and derivatives thereof lead to a block in 5' methylation of viral mRNA due to their inhibition of SAHase [218, 270, 280]. This would result in impaired translation of viral mRNAs. Because CL4053 has decreased inhibitory activity towards SAHase, it has been suggested that it might have alternate antiviral mechanisms. Our data indicate that VSV is inhibited primarily by decreased mRNA cap methylation and protein synthesis, with only

modest effects of the compounds on viral RNA synthesis. Based on the cross resistance observed with VSV^R against both the D- and L-enantiomers, these compounds may inhibit by similar mechanisms.

All analogs strongly inhibited WT-VSV-GFP without causing significant cell toxicity at the tested concentrations. Our IC50 results are analogous to antiviral activity obtained for previously described SAHase inhibitors [218, 228, 229, 430, 431]. For the enantiomeric pair, the IC50s against WT-VSV-GFP are less different (85-fold) than those IC50s obtained against SAHase *in vitro* (approximately 770-fold) [228]. What accounts for this difference remains to be determined.

The selection of VSV^R allowed additional discernment into the mechanism of the different compounds tested. For each of the compounds, the IC50 for VSV^R was shifted more than 1,000-fold when compared to parental VSV IC50s. These data suggest that all of our compounds are working through a similar mechanism of inhibition, although we cannot definitively rule out additional mechanisms. To ensure specificity of selection of VSV^R, we evaluated BCX4430, in parallel. BCX4430, similar to the neplanocin analogs, is an adenosine analog; however, its mechanism of inhibition is as a non-obligate RNA chain-terminator [191, 192]. Our results indicate that BCX4430 inhibited VSV^R to a similar extent as parental VSV, thereby further confirming the specificity of resistance of VSV^R against CL123.

We did observe differences between WT-VSV-GFP and VSV^R in their growth kinetics. At early times post-infection, VSV^R lags in growth as compared to WT-VSV-GFP; however, as the infections progress these differences abate. Consistent with these data, impairment of VSV^R protein synthesis was also observed at early times post-

infection as compared to WT-VSV-GFP. The reduced protein synthesis is also reflected in the cap methylation and polysome analyses where the VSV^R more closely resembled that of CL123-treated WT-VSV-GFP samples than the DMSO-treated WT-VSV-GFP samples. These data suggest that the CL123 resistant virus is compromised in its replication, perhaps due to less efficient mRNA cap methylation.

The neplanocin analogs caused a modest inhibition of viral transcription for WT-VSV-GFP at early times post-infection. The early time point was chosen such that measurements could be made before significant viral protein synthesis had occurred, thus isolating effects on viral RNA synthesis. This inhibition suggests some effect of the analogs on viral transcription. Curiously, at later time points, the compounds significantly enhanced the total WT-VSV-GFP mRNA levels but not for VSV^R. This phenotype may be driven by increased lengths of the poly A tails on viral mRNAs because increased levels of SAH have previously been shown to lead to lengthening of VSV poly A tails [432-434]. Eukaryotic mRNAs with longer poly A tails have longer half-lives [435-438]. The increased viral mRNA levels may therefore be due to diminished viral mRNA turnover.

A significant reduction in m^7G viral mRNA levels was found in parental VSV infected and CL123-treated cells. m^7G mRNA contributes to efficient translation of viral mRNAs [263, 439-441] and inhibiting VSV 5' cap methylation can attenuate pathogenesis *in vivo* [442]. Interestingly, our polysome profiling shows that in CL123-treated and WT-VSV-GFP infected cells, the viral mRNA is shifted into the 80S fraction (**Figure 26A and C, Fraction 4**). This would suggest that the viral mRNA is able to associate with the 80S ribosome and translational initiation stalling may be occurring in CL123-treated cells. This effect is also observed for both DMSO and CL123-treated VSV^R (**Figure 26A**). Additional

work would need to be done to confirm this hypothesis. A consideration for interpretation of both the cap methylation and the polysome analyses, as well as the metabolic labeling studies, is that the infections were performed at much higher multiplicities of infection as compared to the assays that directly measured virus growth. This approach was taken because it facilitates the detection of viral RNAs and proteins. An outcome of this experimental approach is that the effects of the compounds may be less dramatic than if less virus was used.

Finally, the I1905R mutation in VSV^R, which was the highest frequency mutation found in all resistant purified virus isolates, may contribute to resistance by impacting viral methyltransferase activity. In the available VSV L cryoEM structures [131, 132, 375], I1905R lies within the CTD and is approximately 20 Å from critical amino acids involved in SAM binding and methyl transfer (**Figure 22C**) during VSV mRNA methylation [138, 139, 367, 372, 443, 444]. There are examples from VSV, paramyxovirus and filovirus studies where amino acid residues in non-MTase domains of NNSV L proteins affect the methylation status of viral mRNA [133, 137, 372, 445]. In a VSV minigenome system, exchanging the CTD of the two different species of VSV (Indiana and New Jersey), abrogated minigenome activity, and the MT with its respective CTD had to be co-exchanged to maintain polymerase activity [446]. Further, deletion of the CTD of the *Sudan ebolavirus* L protein abolished methyltransferase activity [133, 445]. Finally, within the paramyxoviruses, human metapneumovirus (hMPV) was found to contain residues within the CTD that were required for MTase activity [137]. Additional non-synonymous mutations were found in the L protein (*Table 3.1.1*); however, since these were not present throughout all clones that demonstrated CL123 resistance or were present at low

SNP frequency we do not believe these mutations were contributing to virus resistance. Additional work would need to be done to confirm this hypothesis.

In summary, our data points to inhibition of mRNA cap methylation and subsequently impaired viral protein synthesis as the primary mechanism of action of the compounds tested, consistent with the prevailing model of action for the D-like neplanocin derivatives. It also demonstrates the capacity of VSV to develop resistance to such compounds. However, for VSV^R, resistance is associated with decreased viral fitness, likely due to less efficient mRNA cap methylation.

3.7 Acknowledgments

This work was supported in part by NIH grants AI125453 and P01AI120943 (Amarasinghe) to C.F.B.

4 DISCUSSION AND FUTURE DIRECTIONS

4.1 Characterizing novel Filovirus proteins

Filoviruses are lethal zoonotic RNA viruses and depending on the virus species can have a case fatality rate upward of 90% in humans [13]. In addition to loss of life, the economic burden associated with outbreaks can be devastating to affected countries. The 2014-2016 West African EBOV outbreak had an estimated economic impact of $2.8 billion to Guinea, Liberia, and Sierra Leone [447].

In the last decade alone, the *Filoviridae* family has tripled in size, growing from the two founding members (*Ebolavirus* and *Marburgvirus*) each classified in a separate genus to six genera today, 2011 *Cuevavirus* (LLOV), 2018 *Striavirus* (XILV) and *Thamnovirus* (HUJV), and 2019 *Dianlovirus* (MLAV) [2, 6, 8, 10]. A salient health concern is the emergence and the potential for a spillover transmission event of a new filovirus resulting

in infection and disease in humans [49, 448]. A facet that needs to be considered in a "successful" zoonotic spillover occurrence is the innate immune response of a potential host. If the innate immunity of the prospective host is capable of shutting down any part of the virus' life cycle to the point where the virus cannot establish a successful replication and transmission cycle, then the zoonotic spillover event will be unfruitful for the virus [449]. For filoviruses, one factor that contributes to host virulence and species virus replication restriction is the ability to subvert the innate immune pathway [128]. Recently, it was determined that disruptions in VP35's ability to suppress the RIG-I signaling pathway produced a severely attenuated infection, relative to wild-type VP35, in cynomolgus macaques (*Macaca fascicularis*) [450]. These results are consistent with previous literature showing that mutations in VP35 that impair its dsRNA binding and thereby its IFN antagonism function, resulted in reduced levels of virulence in mice and avirulence in guinea pigs [332, 412]. Finally, filoviruses have to be mouse-adapted to adult immunocompetent mice to render the mice susceptible to infection. This mouse-adapted virus is accomplished by continually passaging the virus until a lethal infection is obtained in the mouse [451, 452]. Sequencing of these mouse-adapted virus genomes revealed that MARV VP40, RAVV VP40 and EBOV VP24, which are all capable of inhibiting the type I IFN pathway, were implicated in virulence and mouse virus replication restriction [322-324, 453-455].

Chapter 2 of this dissertation characterizes the type I IFN antagonism of MLAV VP35, VP40 and VP24 in comparison to their EBOV and MARV equivalents. MLAV VP35 behaves very similarly to the previously described antagonism functions of EBOV and MARV VP35 [128]. In a dose dependent manner, MLAV VP35 can potently suppress 1)

the SeV-induced activation of an IFNβ promoter, and 2) phosphorylation of IRF3 and PKR. It can also co-precipitate with the cellular protein PACT (**Figure 10 and Figure 11**). Based on these data, presumably, MLAV VP35's main mode of IFN inhibition is interaction and sequestration of dsRNA and functioning as a decoy receptor for TBK1 and IKKε [128]. Future studies demonstrating interaction between MLAV VP35 and dsRNA are warranted to confirm that this interaction is contributing to MLAV VP35s inhibition of the type I IFN pathway. Interestingly, solved crystal structures of EBOV and MARV VP35 complexed with dsRNA show distinct binding interactions. MARV VP35 coats the sugar-phosphate backbone of the RNA whereas EBOV VP35 not only coats the sugar-phosphate backbone but caps the phosphate ends of the RNA [329, 336, 456-458]. This difference in dsRNA binding is thought to contribute to differences between EBOV and MARV VP35 in inhibitory efficiency of RIG-I signaling [327]. Determining how MLAV VP35 engages with dsRNA would further contribute to our understanding of its mechanisms of type I IFN inhibition.

We have also determined that MLAV VP40 strongly suppresses the activation of type I IFN signaling (**Figure 12**) and does so by abrogating phosphorylation of STAT1 induced either through treatment with UIFN or overexpression of Jak1 (**Figure 13**). MLAV VP40 abrogation of STAT1 phosphorylation is similar to that of MARV VP40 [324, 352]. The exact mechanism by which MARV VP40 inhibits STAT1 and Jak1 phosphorylation is not yet understood. We do know that the late domain motif (PPPY) that assists in the MARV VP40 budding process [173] is not required for the type I IFN antagonism [352]. MLAV VP40 and to a lesser extent MARV VP40 were also determined to inhibit the IFNβ production pathway. This inhibition is independent of its type I IFN signaling inhibition as

described above (**Figure 10 and Figure 15**). Previous literature has confirmed that MARV VP40 can indeed inhibit the IFNβ production pathway [459]. The mechanism of this inhibition is not understood and is currently being investigated. One approach to determining how MLAV and MARV VP40 inhibit the IFNβ production pathway is described below.

Curiously, transfected MARV VP40 can localize to the nucleus [460] and personal observation. Transfected MLAV VP40 can also localize to the nucleus and it does so more robustly than that of MARV VP40 (personal observation). If nuclear localization is a component of the mechanism of either, or both, the antagonism of type I IFN signaling and the IFNβ production pathway, MLAV VP40 could prove to be a useful research tool given that the nuclear localization phenotype is more robust than that of MARV VP40. Previously, the matrix (M) proteins of other NNS RNA viruses have been shown to localize to the nucleus. Of the mechanisms we understand, the biological ramifications of M protein nuclear localization can be diverse [461-475]. For VSV M, nuclear localization results in inhibition of the export of cellular mRNA transcripts through interaction with nucleoporin proteins [468, 469]. For respiratory syncytial virus (RSV), it is thought that nuclear localization of its M protein may be involved in regulation of cellular transcription, similar to VSV M [463, 465, 466, 476]. In the *Paramyxoviridae* family, several viral M proteins have been found in the nucleus, including the relevant animal and human pathogens, Newcastle disease virus (NDV), Hendra virus and Nipah virus (NiV) [477, 478]. For the NiV M protein it has been shown that cytoplasmic-nuclear trafficking correlates with efficient budding of Nipah VLPs. M protein sequence alignment of several virus species within the *Paramyxoviridae* family identified a highly conserved lysine

residue (K258) that was found to be critical for NiV M nuclear import, export and VLP budding. Specifically, the ubiquitination of the M protein within the nucleus is thought to aid in NiV VLP budding [462]. In a separate study, NiV M was also shown to be capable of inhibiting the type I IFN response. Specifically, antagonism of the type I IFN pathway by NiV M is mediated by degradation of TRIM6, an E-3-ubiquitin ligase that helps with the activation of IKKε, a kinase involved in type I IFN induction. Curiously, the same K258 residue described above, was found to be critical for NiV M's subversion of the type I IFN [479]. The functional significance of MARV and MLAV VP40's nuclear localization could be determined several ways experimentally. As described above, for NiV M, the identification, and the subsequent mutation of the K258 residue involved in nuclear shuttling helped generate a mutant phenotype (diminished Nipah VLP budding), thereby allowing determination of its functional relevance [462]. The K258 residue was readily identified as part of the NiV M putative bipartite nuclear localization signal (NLS) [480, 481]. Neither MLAV nor MARV VP40 contain putative NLSs. However, nuclear trafficking could be mediated by non-classical NLSs, which has been found in DNA virus proteins and several host proteins [482-485]. Basic residue patches tend to be involved in nuclear transport [480] and MLAV and MARV's VP40s C-terminal domain does contain several conserved lysine and arginine residues (personal determination). Systematically mutating these basic residues and determining VP40s' cellular localization as well as any effects on MLAV and MARV VLPs could help identify the functional significance of the VP40 within the nucleus. Additionally, if the identification of residues involved in the nuclear shuttling of VP40 proves unfruitful, leptomycin B, a compound that inhibits protein nuclear export [486], could also be employed. The biological consequences of both MARV and

MLAV VP40's nuclear trafficking would warrant future studies as it may aid in the identification of potential therapeutic targets for MARV infections. Finally, it is worth noting that nuclear localization may very well not be involved in the type I IFN antagonism of MLAV and MARV VP40. If this is the case then systematically assessing the different components of the RIG-I signaling pathway (RIG-I, MAVS, TBK1, IKKε, etc.) should be performed to help further identify the mechanism of inhibition.

The MLAV VP24 protein did not detectably interact with any tested KPNAs or human and bat Keap1 (**Figure 12, 13, 16 and 17**). Given that both EBOV and MARV VP24s interfere with distinct cellular processes, type I IFN signaling inhibition and antioxidant response activation, respectively [128], MLAV VP24 could be interacting with different cellular pathways. Previously, for EBOV and MARV VP24, affinity purification coupled with mass spectrometry and bioinformatics helped identify several known and novel host protein interactors of EBOV and MARV VP24 [487, 488]. Using a similar approach for MLAV VP24, we could determine cellular protein interactors and ultimately if these interactors can be implicated in important cellular processes such as host restriction.

4.2 DzNep derivatives as antivirals against NNS RNA viruses

Currently, there are no pan-filovirus antivirals [185]. An antiviral that targets a common functionality of filovirus infections would be of interest as a therapeutic strategy. Nucleotide analogs are attractive therapeutic candidates for their ability to inhibit both EBOV and MARV infections *in vitro* and *in vivo* [185, 186]. Recently, GS-5734 and T-705 were approved for emergency and compassionate care use during the 2014-2016 West African and the 2018-2020 DRC EBOV outbreaks [199-201, 210-215]. During the 2018-

2020 DRC outbreak, use of GS-5734 was halted due to the better results obtained with treatment by Ebanga (Ridgeback Biotherapeutics' monoclonal EBOV antibody) and Inmazeb (Regeneron's cocktail of three monoclonal EBOV antibodies) [199]. GS-5734 is currently in phase 2 clinical trials to determine its safety profile and antiviral efficacy in male EBOV survivors with persistent EBOV in their semen [489]. As mentioned previously, a concrete resolution of the efficacy of T-705 during the 2014-2016 outbreak was unattainable, primarily due to the trials not being randomized and issues with administration of the correct dosages [210-215].

C-nucleoside adenosine analogs are also of particular interest given their broad-spectrum antiviral activities against a number of NNS RNA viruses [185, 218]. DzNep has shown very good antiviral activity in an *in vivo* mouse model for lethal mouse-adapted EBOV infections [227] and recently, in cell culture, halogenated derivatives of DzNep inhibited the replication of both EBOV and MARV with low micromolar 50 percent effective concentrations (EC50s) [490].

In Chapter 3 of this dissertation, we investigated the antiviral mechanisms of DzNep and three of its brominated analogs - CL123, CL4033 and CL4053. Working with EBOV or MARV to determine antiviral mechanisms can be quite burdensome given they are biosafety level 4 (BSL-4) pathogens, and so we opted to use the common surrogate for NNS RNA viruses, VSV. Our results indicate that DzNep, CL123, CL4033 and CL4053 inhibit VSV replication and appear to derive their antiviral effects through impaired methylation of viral mRNA caps (**Figure 25A-B**). The generation and subsequent sequencing of our VSV CL123 resistant mutant (VSV^R) suggested mechanisms of inhibition of our analogs (**Figure 20 and Figure 22**). Strikingly, DzNep, CL123, CL4033

and CL4053 showed shifted IC50s (>1000 fold) against VSV^R and this is suggestive of a common mechanism of virus inhibition for all these compounds, particularly since BCX4430 could inhibit both parental and mutant VSV (**Figure 19 and Figure 20**). This conclusion is of particular interest for our isomers, CL4033 and CL4053.

As described previously, CL4033 and CL4053 are identical in all chemical aspects except the direction of rotation of plane polarized light (**Figure 5**). Mechanistically it was thought that these isomers may have different antiviral activities due to discrepancies between antiviral activity against EBOV and the hypothesized cellular target, SAHase [228]. Our data also shows a large difference between VSV and SAHase IC50s – CL4053 has a ~85 fold higher VSV IC50 and a ~800 fold higher SAHase IC50, both relative to CL4033 (Figure 16) [228]. This large discrepancy between the two IC50s is intriguing and may be driven by the type of inhibition of SAHase. It is known that two different modes of SAHase inhibitors exist. A type I mechanism inhibitor reduces the hydrolases' required co-factor, NAD+, to NADH and in the process becomes oxidized at the 3' position of the sugar moiety. A type II mechanism inhibitor also reduces NAD+ to NADH but can covalently attach itself to the hydrolase. Type I inhibition is reversible, whereas type II inhibition, due to the covalent modification of the SAHase, is irreversible [218]. Differences in how the enantiomers are engaging with the SAHase may be driving the observable effects in their antiviral activities. To date, there are numerous crystal structures of SAHase complexed with various SAHase inhibitors [491-501]. Co-crystallization of each isomer with the SAHase would provide valuable insight into any differences in SAHase binding modes and may also help answer the discrepancy between antiviral and SAHase IC50s. Additionally, structural knowledge of how the

compounds are interacting with their cellular targets is useful in 1) determining modes of inhibition and 2) allowing for more rational structure-activity relationship (SAR) development.

The I1905R mutation found in VSV^R may contribute to the viruses' resistance to CL123. The change from a non-polar moiety (isoleucine) to a charged, bulky guanidino group (arginine) could potentially alter the I1905 microenvironment. Residue 1905 is located in the VSV CTD [131, 132, 375]. In the published cryoEM structure, the I1905R is approximately 10-20 Å from residues involved either directly (SAM binding and methyltransferase activity) or indirectly in VSV mRNA methylation [133, 137-139, 367, 372, 443-446]. Note that the point of comparison for the above calculations was performed using a VSV L cryo-EM that was co-crystalized with the P co-factor [131] and does not contain the SAM or SAH substrates. Binding of these substrates to the MTD may significantly alter the VSV L configuration. Recently, amino acids that contribute to the methylation status of viral mRNA in non-MT domains have been identified [133, 137, 372, 445, 446]. In chapter 3, we described previously identified CTD residues for VSV, EBOV and hMPV that contribute to viral mRNA methylation [133, 137, 445, 446]. Additionally, residues within the connector domain (CD) of VSV have also been identified in contributing to VSV mRNA methylation. For G1481R, a mutation responsible for the phenotype of heat resistant (*hr*)*8*, the viral mRNA was near devoid of methylation. Notably our I1905R residue is located within 10 Å of G1481R (personal calculation) [372]. Finally, contributions of the viruses' polymerase mode (replicase versus transcriptase) should be considered [136]. Since the polymerase both transcribes and replicates the viral genome it presumably adopts different conformations for the transcription and replication

functions. The cryo-EM structure of the complexed L-P for parainfluenza virus 5 (PIV5) suggests that the solved L-P structure may be that of a transcriptase polymerase. It is suggested that the orientation of the MT-CTD could potentially function as a switching mechanism between the two different modes of the polymerase [136]. Alternatively, if the VSV L cryo-EM is a replicase versus a transcriptase polymerase, the orientation of methyltransferase residues involved in SAM binding and catalysis could be very different. For future studies, a VSV infectious clone system could be employed to further build on our above findings. The VSV infectious clone system has been well established and contains all the necessary components to rescue a live recombinant VSV [424, 502, 503]. A recombinant VSV containing the I1905R mutation could be generated to further confirm the contribution of this residue in the development of the VSV^R resistance against CL123, CL4033, CL4053 and DzNep. Additionally, *in vitro* assays for VSV RNA transcription and assessment of VSV methylated cap structures are available [285, 504]. Both of these techniques could be utilized to determine if the I1905R disrupts the methylation status of the VSV 5'cap structure.

The viability of SAHase inhibitors as antivirals requires further assessment, particularly for efficacy in *in vivo* studies. These class of inhibitors are advantageous in that they are quite potent against numerous RNA viruses, both in cell culture and in mouse-models [185, 227, 271]. They also indirectly target a common function of NNS RNA viruses [218], which lends itself to the possibility of a pan-antiviral. However, our data for VSV show that DzNep and its brominated analogs are not sterilizing inhibitors (**Figure 19 and Figure 21**). Under our conditions, our compounds were incapable of completely abrogating the production of infectious virus particles. This non-sterilizing

characteristic in conjunction with our ability to generate a CL123-VSV resistant mutant, would not bode well in the context of developing drug resistant viruses. However, this assessment is in the context of a cell culture system. We cannot rule out that *in vivo* models evaluating SAHase inhibitors could prove useful in determining additional contributing components that aid in SAHase inhibitors' antiviral efficacy. As previously described, contributions by *in vivo* factors were best demonstrated by the 2002 study showing a single dose of DzNep, administered after infection with a lethal mouse-adapted EBOV, fully protected mice from EBOV lethality while simultaneously producing large amounts of IFNα. [227].

4.3 Concluding remarks

In conclusion, this dissertation has determined that the newest addition to the filovirus family, MLAV, has the ability to modulate type I IFN responses in human and bat cells. These results suggest that MLAV has the capacity to become a human pathogen. Mechanistic knowledge of the basis of this antagonism could lead to the identification and development of filovirus therapeutics, and the discovery of novel host restriction factors. We have also determined antiviral mechanisms of DzNep analogs against VSV, addressing an important gap in knowledge regarding this class of compounds. Our results with the CL4033 and CL4053 enantiomers strongly suggest that both compounds are inhibiting VSV through a shared mechanism. Ideally, these results could prove useful in guiding the direction of the design of future enantiomers as broad-spectrum therapeutics against NNS RNA viruses.

REFERENCES

1. Maes, P., et al., *Taxonomy of the order Mononegavirales: second update 2018.* Arch Virol, 2019. **164**(4): p. 1233-1244.
2. Kuhn, J.H., et al., *ICTV Virus Taxonomy Profile: Filoviridae.* J Gen Virol, 2019. **100**(6): p. 911-912.
3. Bào, Y., et al., *Implementation of Objective PASC-Derived Taxon Demarcation Criteria for Official Classification of Filoviruses.* Viruses, 2017. **9**(5).
4. Towner, J.S., et al., *Marburgvirus Genomics and Association with a Large Hemorrhagic Fever Outbreak in Angola.* Journal of Virology, 2006. **80**(13): p. 6497.
5. Brauburger, K., et al., *Forty-Five Years of Marburg Virus Research.* Viruses, 2012. **4**(10).
6. Yang, X.L., et al., *Characterization of a filovirus (Mengla virus) from Rousettus bats in China.* Nat Microbiol, 2019. **4**(3): p. 390-395.
7. Hume, A.J. and E. Mühlberger, *Distinct Genome Replication and Transcription Strategies within the Growing Filovirus Family.* Journal of Molecular Biology, 2019. **431**(21): p. 4290-4320.
8. Shi, M., et al., *The evolutionary history of vertebrate RNA viruses.* Nature, 2018. **556**(7700): p. 197-202.
9. Kemenesi, G., et al., *Re-emergence of Lloviu virus in Miniopterus schreibersii bats, Hungary, 2016.* Emerg Microbes Infect, 2018. **7**(1): p. 66.
10. Negredo, A., et al., *Discovery of an Ebolavirus-Like Filovirus in Europe.* PLOS Pathogens, 2011. **7**(10): p. e1002304.
11. Martini, G.A., *Marburg agent disease: In man.* Transactions of The Royal Society of Tropical Medicine and Hygiene, 1969. **63**(3): p. 295-302.
12. Smith, C.E., et al., *Fatal human disease from vervet monkeys.* Lancet, 1967. **2**(7526): p. 1119-21.
13. Languon, S. and O. Quaye, *Filovirus Disease Outbreaks: A Chronological Overview.* Virology : research and treatment, 2019. **10**: p. 1178122X19849927-1178122X19849927.
14. Bausch, D.G., et al., *Marburg hemorrhagic fever associated with multiple genetic lineages of virus.* N Engl J Med, 2006. **355**(9): p. 909-19.
15. Timen, A., et al., *Response to imported case of Marburg hemorrhagic fever, the Netherland.* Emerg Infect Dis, 2009. **15**(8): p. 1171-5.
16. Centers for Disease, C. and Prevention, *Imported case of Marburg hemorrhagic fever - Colorado, 2008.* MMWR Morb Mortal Wkly Rep, 2009. **58**(49): p. 1377-81.
17. Nikiforov, V.V., et al., *[A case of a laboratory infection with Marburg fever].* Zh Mikrobiol Epidemiol Immunobiol, 1994(3): p. 104-6.
18. *Ebola haemorrhagic fever in Sudan, 1976. Report of a WHO/International Study Team.* Bull World Health Organ, 1978. **56**(2): p. 247-70.
19. *Ebola haemorrhagic fever in Zaire, 1976.* Bull World Health Organ, 1978. **56**(2): p. 271-93.
20. Pattyn, S., et al., *Isolation of Marburg-like virus from a case of haemorrhagic fever in Zaire.* Lancet, 1977. **1**(8011): p. 573-4.

21. Johnson, K.M., et al., *ISOLATION AND PARTIAL CHARACTERISATION OF A NEW VIRUS CAUSING ACUTE HÆMORRHAGIC FEVER IN ZAIRE.* The Lancet, 1977. **309**(8011): p. 569-571.
22. Bowen, E.T., et al., *Viral haemorrhagic fever in southern Sudan and northern Zaire. Preliminary studies on the aetiological agent.* Lancet, 1977. **1**(8011): p. 571-3.
23. Jacob, S.T., et al., *Ebola virus disease.* Nature Reviews Disease Primers, 2020. **6**(1): p. 13.
24. Organization, W.H., *Ebola virus disease – Guinea*, W.H. Organization, Editor. 2021, World Health Organization: https://www.who.int/csr/don/17-february-2021-ebola-gin/en/.
25. Kupferschmidt, K., *New Ebola outbreak likely sparked by a person infected 5 years ago*, in *The Scientist*. 2021, The Scientist: https://www.sciencemag.org/news/2021/03/new-ebola-outbreak-likely-sparked-person-infected-5-years-ago.
26. Prevention, C.f.D.C.a., *2021 Democratic Republic of the Congo, North Kivu Province*, V.S.P. Branch, Editor. 2021, Centers for Disease Control and Prevention https://www.cdc.gov/vhf/ebola/outbreaks/drc/2021-february.html.
27. Frontieres, M.S., *Twelfth outbreak declared in North Kivu province*. 2021: https://www.msf.org/drc-ebola-outbreak-crisis-update.
28. Olival, K.J., C.C. Weekley, and P. Daszak, *Are Bats Really "Special" as Viral Reservoirs? What We Know and Need to Know*, in *Bats and Viruses*. 2015. p. 281-294.
29. Swanepoel, R., et al., *Studies of reservoir hosts for Marburg virus.* Emerging infectious diseases, 2007. **13**(12): p. 1847-1851.
30. Pourrut, X., et al., *Large serological survey showing cocirculation of Ebola and Marburg viruses in Gabonese bat populations, and a high seroprevalence of both viruses in Rousettus aegyptiacus.* BMC infectious diseases, 2009. **9**: p. 159-159.
31. Towner, J.S., et al., *Marburg virus infection detected in a common African bat.* PloS one, 2007. **2**(8): p. e764-e764.
32. Leroy, E.M., et al., *Fruit bats as reservoirs of Ebola virus.* Nature, 2005. **438**(7068): p. 575-576.
33. Pourrut, X., et al., *Spatial and Temporal Patterns of Zaire ebolavirus Antibody Prevalence in the Possible Reservoir Bat Species.* The Journal of Infectious Diseases, 2007. **196**(Supplement_2): p. S176-S183.
34. Hayman, D.T.S., et al., *Long-Term Survival of an Urban Fruit Bat Seropositive for Ebola and Lagos Bat Viruses.* PLOS ONE, 2010. **5**(8): p. e11978.
35. Hayman, D.T.S., et al., *Ebola virus antibodies in fruit bats, Ghana, West Africa.* Emerging infectious diseases, 2012. **18**(7): p. 1207-1209.
36. Mari Saez, A., et al., *Investigating the zoonotic origin of the West African Ebola epidemic.* EMBO Mol Med, 2015. **7**(1): p. 17-23.
37. Kuzmin, I.V., et al., *Marburg virus in fruit bat, Kenya.* Emerging infectious diseases, 2010. **16**(2): p. 352-354.
38. Amman, B.R., et al., *Isolation of Angola-like Marburg virus from Egyptian rousette bats from West Africa.* Nature Communications, 2020. **11**(1): p. 510.

39. Amman, B.R., et al., *Marburgvirus resurgence in Kitaka Mine bat population after extermination attempts, Uganda.* Emerging infectious diseases, 2014. **20**(10): p. 1761-1764.
40. Amman, B.R., et al., *Seasonal Pulses of Marburg Virus Circulation in Juvenile Rousettus aegyptiacus Bats Coincide with Periods of Increased Risk of Human Infection.* PLOS Pathogens, 2012. **8**(10): p. e1002877.
41. Towner, J.S., et al., *Isolation of genetically diverse Marburg viruses from Egyptian fruit bats.* PLoS pathogens, 2009. **5**(7): p. e1000536-e1000536.
42. Pawęska, J.T., et al., *Marburg Virus Infection in Egyptian Rousette Bats, South Africa, 2013-2014(1).* Emerging infectious diseases, 2018. **24**(6): p. 1134-1137.
43. Kajihara, M., et al., *Marburgvirus in Egyptian Fruit Bats, Zambia.* Emerging Infectious Disease journal, 2019. **25**(8): p. 1577.
44. Changula, K., et al., *Seroprevalence of Filovirus Infection of Rousettus aegyptiacus Bats in Zambia.* The Journal of Infectious Diseases, 2018. **218**(suppl_5): p. S312-S317.
45. Swanepoel, R., et al., *Experimental inoculation of plants and animals with Ebola virus.* Emerging infectious diseases, 1996. **2**(4): p. 321-325.
46. Smith, D.H., et al., *MARBURG-VIRUS DISEASE IN KENYA.* The Lancet, 1982. **319**(8276): p. 816-820.
47. Conrad, J.L., et al., *Epidemiologic Investigation of Marburg Virus Disease, Southern Africa, 1975.* The American Journal of Tropical Medicine and Hygiene, 1978. **27**(6): p. 1210-1215.
48. Schuh, A.J., B.R. Amman, and J.S. Towner, *Filoviruses and bats.* Microbiol Aust, 2017. **38**(1): p. 12-16.
49. Olival, K.J. and D.T.S. Hayman, *Filoviruses in bats: current knowledge and future directions.* Viruses, 2014. **6**(4): p. 1759-1788.
50. Olival, K.J., et al., *Ebola virus antibodies in fruit bats, bangladesh.* Emerging infectious diseases, 2013. **19**(2): p. 270-273.
51. Yuan, J., et al., *Serological evidence of ebolavirus infection in bats, China.* Virology journal, 2012. **9**: p. 236-236.
52. Taniguchi, S., et al., *Reston Ebolavirus antibodies in bats, the Philippines.* Emerging infectious diseases, 2011. **17**(8): p. 1559-1560.
53. Pourrut, X., et al., *The natural history of Ebola virus in Africa.* Microbes and Infection, 2005. **7**(7): p. 1005-1014.
54. Jayme, S.I., et al. *Molecular evidence of Ebola Reston virus infection in Philippine bats*. Virology journal, 2015. **12**, 107 DOI: 10.1186/s12985-015-0331-3.
55. Goldstein, T., et al., *The discovery of Bombali virus adds further support for bats as hosts of ebolaviruses.* Nature Microbiology, 2018. **3**(10): p. 1084-1089.
56. Yang, X.L., et al., *Genetically Diverse Filoviruses in Rousettus and Eonycteris spp. Bats, China, 2009 and 2015.* Emerg Infect Dis, 2017. **23**(3): p. 482-486.
57. Sugita, Y., et al., *Cryo-EM structure of the Ebola virus nucleoprotein-RNA complex at 3.6 Å resolution.* Nature, 2018. **563**(7729): p. 137-140.
58. Wan, W., et al., *Structure and assembly of the Ebola virus nucleocapsid.* Nature, 2017. **551**(7680): p. 394-397.

59. Bharat, T.A., et al., *Structural dissection of Ebola virus and its assembly determinants using cryo-electron tomography.* Proc Natl Acad Sci U S A, 2012. **109**(11): p. 4275-80.
60. Bharat, T.A., et al., *Cryo-electron tomography of Marburg virus particles and their morphogenesis within infected cells.* PLoS Biol, 2011. **9**(11): p. e1001196.
61. Noda, T., et al., *Characterization of the Ebola virus nucleoprotein-RNA complex.* J Gen Virol, 2010. **91**(Pt 6): p. 1478-83.
62. Noda, T., et al., *Assembly and budding of Ebolavirus.* PLoS pathogens, 2006. **2**(9): p. e99-e99.
63. Geisbert, T.W. and P.B. Jahrling, *Differentiation of filoviruses by electron microscopy.* Virus Res, 1995. **39**(2-3): p. 129-50.
64. Beniac, D.R., et al., *The organisation of Ebola virus reveals a capacity for extensive, modular polyploidy.* PLoS One, 2012. **7**(1): p. e29608.
65. Welsch, S., et al., *Electron tomography reveals the steps in filovirus budding.* PLoS Pathog, 2010. **6**(4): p. e1000875.
66. Luque, D., et al., *Infectious bursal disease virus is an icosahedral polyploid dsRNA virus.* Proceedings of the National Academy of Sciences, 2009. **106**(7): p. 2148.
67. Hosaka, Y., H. Kitano, and S. Ikeguchi, *Studies on the pleomorphism of HVJ virons.* Virology, 1966. **29**(2): p. 205-21.
68. Volchkov, V.E., et al., *Characterization of the L gene and 5' trailer region of Ebola virus.* Journal of General Virology, 1999. **80**(2): p. 355-362.
69. Bukreyev, A.A., et al., *The complete nucleotide sequence of the Popp (1967) strain of Marburg virus: a comparison with the Musoke (1980) strain.* Arch Virol, 1995. **140**(9): p. 1589-600.
70. Booth, T.F., M.J. Rabb, and D.R. Beniac, *How do filovirus filaments bend without breaking?* Trends Microbiol, 2013. **21**(11): p. 583-93.
71. Becker, S., et al., *Interactions of Marburg virus nucleocapsid proteins.* Virology, 1998. **249**(2): p. 406-17.
72. Watt, A., et al., *A novel life cycle modeling system for Ebola virus shows a genome length-dependent role of VP24 in virus infectivity.* J Virol, 2014. **88**(18): p. 10511-24.
73. Huang, Y., et al., *The assembly of Ebola virus nucleocapsid requires virion-associated proteins 35 and 24 and posttranslational modification of nucleoprotein.* Mol Cell, 2002. **10**(2): p. 307-16.
74. Groseth, A., et al., *The Ebola virus ribonucleoprotein complex: a novel VP30-L interaction identified.* Virus research, 2009. **140**(1-2): p. 8-14.
75. Dolnik, O., et al., *Tsg101 is recruited by a late domain of the nucleocapsid protein to support budding of Marburg virus-like particles.* J Virol, 2010. **84**(15): p. 7847-56.
76. Noda, T., et al., *Mapping of the VP40-binding regions of the nucleoprotein of Ebola virus.* Journal of virology, 2007. **81**(7): p. 3554-3562.
77. Noda, T., et al., *Ebola virus VP40 drives the formation of virus-like filamentous particles along with GP.* J Virol, 2002. **76**(10): p. 4855-65.
78. Stahelin, R.V., *Membrane binding and bending in Ebola VP40 assembly and egress.* Front Microbiol, 2014. **5**: p. 300.

79. Hofmann-Winkler, H., F. Kaup, and S. Pohlmann, *Host cell factors in filovirus entry: novel players, new insights.* Viruses, 2012. **4**(12): p. 3336-62.
80. Olejnik, J., et al., *Intracellular events and cell fate in filovirus infection.* Viruses, 2011. **3**(8): p. 1501-31.
81. Manicassamy, B., et al., *Characterization of Marburg virus glycoprotein in viral entry.* Virology, 2007. **358**(1): p. 79-88.
82. Kuhn, J.H., et al., *Conserved receptor-binding domains of Lake Victoria marburgvirus and Zaire ebolavirus bind a common receptor.* J Biol Chem, 2006. **281**(23): p. 15951-8.
83. Feldmann, H., et al., *Glycosylation and oligomerization of the spike protein of Marburg virus.* Virology, 1991. **182**(1): p. 353-6.
84. Hume, A.J. and E. Mühlberger, *Distinct Genome Replication and Transcription Strategies within the Growing Filovirus Family.* J Mol Biol, 2019. **431**(21): p. 4290-4320.
85. Sanchez, A., et al., *Sequence analysis of the Ebola virus genome: organization, genetic elements, and comparison with the genome of Marburg virus.* Virus Res, 1993. **29**(3): p. 215-40.
86. Feldmann, H., et al., *Marburg virus, a filovirus: messenger RNAs, gene order, and regulatory elements of the replication cycle.* Virus Res, 1992. **24**(1): p. 1-19.
87. Emanuel, J., A. Marzi, and H. Feldmann, *Filoviruses: Ecology, Molecular Biology, and Evolution.* Adv Virus Res, 2018. **100**: p. 189-221.
88. Elliott, L.H., M.P. Kiley, and J.B. McCormick, *Descriptive analysis of Ebola virus proteins.* Virology, 1985. **147**(1): p. 169-76.
89. Sanchez, A., et al., *The nucleoprotein gene of Ebola virus: cloning, sequencing, and in vitro expression.* Virology, 1989. **170**(1): p. 81-91.
90. Kiley, M.P., et al., *Conservation of the 3' terminal nucleotide sequences of Ebola and Marburg virus.* Virology, 1986. **149**(2): p. 251-4.
91. Kirchdoerfer, R.N., et al., *Filovirus Structural Biology: The Molecules in the Machine.* Curr Top Microbiol Immunol, 2017. **411**: p. 381-417.
92. Enterlein, S., et al., *The marburg virus 3' noncoding region structurally and functionally differs from that of ebola virus.* J Virol, 2009. **83**(9): p. 4508-19.
93. Weik, M., et al., *The Ebola virus genomic replication promoter is bipartite and follows the rule of six.* J Virol, 2005. **79**(16): p. 10660-71.
94. Mühlberger, E., et al., *Comparison of the transcription and replication strategies of marburg virus and Ebola virus by using artificial replication systems.* J Virol, 1999. **73**(3): p. 2333-42.
95. Mühlberger, E., et al., *Three of the Four Nucleocapsid Proteins of Marburg Virus, NP, VP35, and L, Are Sufficient To Mediate Replication and Transcription of Marburg Virus-Specific Monocistronic Minigenomes.* Journal of Virology, 1998. **72**(11): p. 8756.
96. Bach, S., et al., *Hexamer phasing governs transcription initiation in the 3'-leader of Ebola virus.* RNA, 2020. **26**(4): p. 439-453.
97. Gutsche, I., P. le Mercier, and D. Kolakofsky, *A paramyxovirus-like model for Ebola virus bipartite promoters.* PLoS Pathog, 2020. **16**(11): p. e1008972.
98. Mühlberger, E., et al., *Termini of all mRNA species of Marburg virus: sequence and secondary structure.* Virology, 1996. **223**(2): p. 376-80.

99. le Mercier, P. and D. Kolakofsky, *Bipartite promoters and RNA editing of paramyxoviruses and filoviruses.* Rna, 2019. **25**(3): p. 279-285.
100. Manhart, W.A., et al., *A Chimeric Lloviu Virus Minigenome System Reveals that the Bat-Derived Filovirus Replicates More Similarly to Ebolaviruses than Marburgviruses.* Cell reports, 2018. **24**(10): p. 2573-2580.e4.
101. Neumann, G., S. Watanabe, and Y. Kawaoka, *Characterization of Ebolavirus regulatory genomic regions.* Virus Res, 2009. **144**(1-2): p. 1-7.
102. Brauburger, K., et al., *Analysis of the highly diverse gene borders in Ebola virus reveals a distinct mechanism of transcriptional regulation.* J Virol, 2014. **88**(21): p. 12558-71.
103. Zhu, W., et al., *The Roles of Ebola Virus Soluble Glycoprotein in Replication, Pathogenesis, and Countermeasure Development.* Viruses, 2019. **11**(11).
104. Sanchez, A., et al., *The virion glycoproteins of Ebola viruses are encoded in two reading frames and are expressed through transcriptional editing.* Proceedings of the National Academy of Sciences of the United States of America, 1996. **93**(8): p. 3602-3607.
105. Volchkov, V.E., et al., *GP mRNA of Ebola virus is edited by the Ebola virus polymerase and by T7 and vaccinia virus polymerases.* Virology, 1995. **214**(2): p. 421-30.
106. Takamatsu, Y., L. Kolesnikova, and S. Becker, *Ebola virus proteins NP, VP35, and VP24 are essential and sufficient to mediate nucleocapsid transport.* Proceedings of the National Academy of Sciences, 2018. **115**(5): p. 1075.
107. Enterlein, S., et al., *Rescue of recombinant Marburg virus from cDNA is dependent on nucleocapsid protein VP30.* J Virol, 2006. **80**(2): p. 1038-43.
108. Martin, B., et al., *Filovirus proteins for antiviral drug discovery: Structure/function of proteins involved in assembly and budding.* Antiviral Research, 2018. **150**: p. 183-192.
109. Martin, B., et al., *Filovirus proteins for antiviral drug discovery: A structure/function analysis of surface glycoproteins and virus entry.* Antiviral Res, 2016. **135**: p. 1-14.
110. Wu, L., et al., *The two-stage interaction of Ebola virus VP40 with nucleoprotein results in a switch from viral RNA synthesis to virion assembly/budding.* Protein Cell, 2020.
111. Leung, D.W., et al., *An Intrinsically Disordered Peptide from Ebola Virus VP35 Controls Viral RNA Synthesis by Modulating Nucleoprotein-RNA Interactions.* Cell Rep, 2015. **11**(3): p. 376-89.
112. Kirchdoerfer, R.N., et al., *Assembly of the Ebola Virus Nucleoprotein from a Chaperoned VP35 Complex.* Cell reports, 2015. **12**(1): p. 140-149.
113. Dong, S., et al., *Insight into the Ebola virus nucleocapsid assembly mechanism: crystal structure of Ebola virus nucleoprotein core domain at 1.8 Å resolution.* Protein Cell, 2015. **6**(5): p. 351-62.
114. DiCarlo, A., et al., *Nucleocapsid formation and RNA synthesis of Marburg virus is dependent on two coiled coil motifs in the nucleoprotein.* Virology Journal, 2007. **4**(1): p. 105.

115. Martin, B., B. Canard, and E. Decroly, *Filovirus proteins for antiviral drug discovery: Structure/function bases of the replication cycle.* Antiviral Res, 2017. **141**: p. 48-61.
116. Watanabe, S., T. Noda, and Y. Kawaoka, *Functional mapping of the nucleoprotein of Ebola virus.* J Virol, 2006. **80**(8): p. 3743-51.
117. Fields, B.N., D.M. Knipe, and P.M. Howley, *Fields virology*. 2013, Philadelphia: Wolters Kluwer Health/Lippincott Williams & Wilkins.
118. Miyake, T., et al., *Ebola Virus Inclusion Body Formation and RNA Synthesis Are Controlled by a Novel Domain of Nucleoprotein Interacting with VP35.* Journal of Virology, 2020. **94**(16): p. e02100-19.
119. Hoenen, T., et al., *Inclusion Bodies Are a Site of Ebolavirus Replication.* Journal of Virology, 2012. **86**(21): p. 11779.
120. Baskerville, A., et al., *Ultrastructural pathology of experimental Ebola haemorrhagic fever virus infection.* J Pathol, 1985. **147**(3): p. 199-209.
121. Nanbo, A., et al., *The spatio-temporal distribution dynamics of Ebola virus proteins and RNA in infected cells.* Scientific Reports, 2013. **3**(1): p. 1206.
122. Dong, S., et al., *Crystal structure of the Měnglà virus VP30 C-terminal domain.* Biochemical and Biophysical Research Communications, 2020. **525**(2): p. 392-397.
123. Batra, J., et al., *Protein Interaction Mapping Identifies RBBP6 as a Negative Regulator of Ebola Virus Replication.* Cell, 2018. **175**(7): p. 1917-1930.e13.
124. Xu, W., et al., *Ebola virus VP30 and nucleoprotein interactions modulate viral RNA synthesis.* Nat Commun, 2017. **8**: p. 15576.
125. Kirchdoerfer, R.N., et al., *The Ebola Virus VP30-NP Interaction Is a Regulator of Viral RNA Synthesis.* PLOS Pathogens, 2016. **12**(10): p. e1005937.
126. Hartlieb, B., et al., *Crystal structure of the C-terminal domain of Ebola virus VP30 reveals a role in transcription and nucleocapsid association.* Proceedings of the National Academy of Sciences, 2007. **104**(2): p. 624.
127. Olejnik, J., et al., *Filovirus Strategies to Escape Antiviral Responses.* Curr Top Microbiol Immunol, 2017. **411**: p. 293-322.
128. Messaoudi, I., G.K. Amarasinghe, and C.F. Basler, *Filovirus pathogenesis and immune evasion: insights from Ebola virus and Marburg virus.* Nat Rev Microbiol, 2015. **13**(11): p. 663-76.
129. Kolesnikova, L., et al., *Inside the Cell: Assembly of Filoviruses*, in *Marburg- and Ebolaviruses: From Ecosystems to Molecules*, E. Mühlberger, L.L. Hensley, and J.S. Towner, Editors. 2017, Springer International Publishing: Cham. p. 353-380.
130. Whelan, S.P., J.N. Barr, and G.W. Wertz, *Transcription and replication of nonsegmented negative-strand RNA viruses.* Curr Top Microbiol Immunol, 2004. **283**: p. 61-119.
131. Liang, B., et al., *Structure of the L Protein of Vesicular Stomatitis Virus from Electron Cryomicroscopy.* Cell, 2015. **162**(2): p. 314-327.
132. Rahmeh, A.A., et al., *Molecular architecture of the vesicular stomatitis virus RNA polymerase.* Proceedings of the National Academy of Sciences, 2010. **107**(46): p. 20075.
133. Valle, C., et al., *First insights into the structural features of Ebola virus methyltransferase activities.* Nucleic Acids Research, 2021.

134. Pan, J., et al., *Structure of the human metapneumovirus polymerase phosphoprotein complex.* Nature, 2020. **577**(7789): p. 275-279.
135. Horwitz, J.A., et al., *Structure of a rabies virus polymerase complex from electron cryo-microscopy.* Proceedings of the National Academy of Sciences, 2020. **117**(4): p. 2099.
136. Abdella, R., et al., *Structure of a paramyxovirus polymerase complex reveals a unique methyltransferase-CTD conformation.* Proceedings of the National Academy of Sciences, 2020. **117**(9): p. 4931.
137. Paesen, G.C., et al., *X-ray structure and activities of an essential Mononegavirales L-protein domain.* Nature Communications, 2015. **6**(1): p. 8749.
138. Ferron, F., et al., *Viral RNA-polymerases — a predicted 2'-O-ribose methyltransferase domain shared by all Mononegavirales.* Trends in Biochemical Sciences, 2002. **27**(5): p. 222-224.
139. Bujnicki, J.M. and L. Rychlewski, *In silico identification, structure prediction and phylogenetic analysis of the 2'-O-ribose (cap 1) methyltransferase domain in the large structural protein of ssRNA negative-strand viruses.* Protein Engineering, Design and Selection, 2002. **15**(2): p. 101-108.
140. Ogino, T. and T.J. Green, *RNA Synthesis and Capping by Non-segmented Negative Strand RNA Viral Polymerases: Lessons From a Prototypic Virus.* Frontiers in Microbiology, 2019. **10**(1490).
141. Schmidt, M.L. and T. Hoenen, *Characterization of the catalytic center of the Ebola virus L polymerase.* PLoS Negl Trop Dis, 2017. **11**(10): p. e0005996.
142. Kolesnikova, L., et al., *The Matrix Protein of Marburg Virus Is Transported to the Plasma Membrane along Cellular Membranes: Exploiting the Retrograde Late Endosomal Pathway.* Journal of Virology, 2004. **78**(5): p. 2382.
143. Kolesnikova, L., et al., *VP40, the matrix protein of Marburg virus, is associated with membranes of the late endosomal compartment.* J Virol, 2002. **76**(4): p. 1825-38.
144. Timmins, J., et al., *Vesicular release of ebola virus matrix protein VP40.* Virology, 2001. **283**(1): p. 1-6.
145. Jasenosky, L.D., et al., *Ebola virus VP40-induced particle formation and association with the lipid bilayer.* Journal of virology, 2001. **75**(11): p. 5205-5214.
146. Harty, R.N., et al., *A PPxY motif within the VP40 protein of Ebola virus interacts physically and functionally with a ubiquitin ligase: implications for filovirus budding.* Proc Natl Acad Sci U S A, 2000. **97**(25): p. 13871-6.
147. Takada, A., et al., *A system for functional analysis of Ebola virus glycoprotein.* Proc Natl Acad Sci U S A, 1997. **94**(26): p. 14764-9.
148. Wool-Lewis, R.J. and P. Bates, *Characterization of Ebola virus entry by using pseudotyped viruses: identification of receptor-deficient cell lines.* J Virol, 1998. **72**(4): p. 3155-60.
149. Chandran, K., et al., *Endosomal proteolysis of the Ebola virus glycoprotein is necessary for infection.* Science, 2005. **308**(5728): p. 1643-5.
150. Carette, J.E., et al., *Ebola virus entry requires the cholesterol transporter Niemann–Pick C1.* Nature, 2011. **477**(7364): p. 340-343.

151. Dahlke, C., et al., *Comprehensive Characterization of Cellular Immune Responses Following Ebola Virus Infection.* The Journal of Infectious Diseases, 2017. **215**(2): p. 287-292.
152. Becquart, P., et al., *Identification of Continuous Human B-Cell Epitopes in the VP35, VP40, Nucleoprotein and Glycoprotein of Ebola Virus.* PLOS ONE, 2014. **9**(6): p. e96360.
153. Mohan, G.S., et al., *Antigenic subversion: a novel mechanism of host immune evasion by Ebola virus.* PLoS Pathog, 2012. **8**(12): p. e1003065.
154. He, J., et al., *Ebola Virus Delta Peptide Is a Viroporin.* J Virol, 2017. **91**(16).
155. Olukitibi, T.A., et al., *Dendritic Cells/Macrophages-Targeting Feature of Ebola Glycoprotein and its Potential as Immunological Facilitator for Antiviral Vaccine Approach.* Microorganisms, 2019. **7**(10): p. 402.
156. Martinez, O., et al., *Ebola Virus Exploits a Monocyte Differentiation Program To Promote Its Entry.* Journal of Virology, 2013. **87**(7): p. 3801.
157. Martinez, O., L.W. Leung, and C.F. Basler, *The role of antigen-presenting cells in filoviral hemorrhagic fever: gaps in current knowledge.* Antiviral Res, 2012. **93**(3): p. 416-28.
158. Yonezawa, A., M. Cavrois, and W.C. Greene, *Studies of ebola virus glycoprotein-mediated entry and fusion by using pseudotyped human immunodeficiency virus type 1 virions: involvement of cytoskeletal proteins and enhancement by tumor necrosis factor alpha.* J Virol, 2005. **79**(2): p. 918-26.
159. Geisbert, T.W., et al., *Pathogenesis of Ebola hemorrhagic fever in cynomolgus macaques: evidence that dendritic cells are early and sustained targets of infection.* Am J Pathol, 2003. **163**(6): p. 2347-70.
160. Zaki, S.R., et al., *A novel immunohistochemical assay for the detection of Ebola virus in skin: implications for diagnosis, spread, and surveillance of Ebola hemorrhagic fever. Commission de Lutte contre les Epidémies à Kikwit.* J Infect Dis, 1999. **179 Suppl 1**: p. S36-47.
161. Marzi, A., et al., *The signal peptide of the ebolavirus glycoprotein influences interaction with the cellular lectins DC-SIGN and DC-SIGNR.* Journal of virology, 2006. **80**(13): p. 6305-6317.
162. Becker, S., M. Spiess, and H.-D. Klenk, *The asialoglycoprotein receptor is a potential liver-specific receptor for Marburg virus.* Journal of General Virology, 1995. **76**(2): p. 393-399.
163. Gramberg, T., et al., *LSECtin interacts with filovirus glycoproteins and the spike protein of SARS coronavirus.* Virology, 2005. **340**(2): p. 224-236.
164. Lin, G., et al., *Differential N-Linked Glycosylation of Human Immunodeficiency Virus and Ebola Virus Envelope Glycoproteins Modulates Interactions with DC-SIGN and DC-SIGNR.* Journal of Virology, 2003. **77**(2): p. 1337.
165. Takada, A., et al., *Human Macrophage C-Type Lectin Specific for Galactose and N-Acetylgalactosamine Promotes Filovirus Entry.* Journal of Virology, 2004. **78**(6): p. 2943.
166. Aleksandrowicz, P., et al., *Ebola virus enters host cells by macropinocytosis and clathrin-mediated endocytosis.* The Journal of infectious diseases, 2011. **204 Suppl 3**(Suppl 3): p. S957-S967.

167. Côté, M., et al., *Small molecule inhibitors reveal Niemann-Pick C1 is essential for Ebola virus infection.* Nature, 2011. **477**(7364): p. 344-8.
168. Mühlberger, E., *Filovirus replication and transcription.* Future Virol, 2007. **2**(2): p. 205-215.
169. Whelan, S.P.J. and G.W. Wertz, *Transcription and replication initiate at separate sites on the vesicular stomatitis virus genome.* Proceedings of the National Academy of Sciences, 2002. **99**(14): p. 9178.
170. Emerson, S.U., *Reconstitution studies detect a single polymerase entry site on the vesicular stomatitis virus genome.* Cell, 1982. **31**(3 Pt 2): p. 635-42.
171. Shabman, R.S., et al., *Deep Sequencing Identifies Noncanonical Editing of Ebola and Marburg Virus RNAs in Infected Cells.* mBio, 2014. **5**(6): p. e02011-14.
172. Neubauer, J., et al., *Signature motifs of GDP polyribonucleotidyltransferase, a non-segmented negative strand RNA viral mRNA capping enzyme, domain in the L protein are required for covalent enzyme-pRNA intermediate formation.* Nucleic Acids Res, 2016. **44**(1): p. 330-41.
173. Urata, S., et al., *Interaction of Tsg101 with Marburg Virus VP40 Depends on the PPPY Motif, but Not the PT/SAP Motif as in the Case of Ebola Virus, and Tsg101 Plays a Critical Role in the Budding of Marburg Virus-Like Particles Induced by VP40, NP, and GP.* Journal of Virology, 2007. **81**(9): p. 4895.
174. Yasuda, J., et al., *Nedd4 regulates egress of Ebola virus-like particles from host cells.* J Virol, 2003. **77**(18): p. 9987-92.
175. Licata, J.M., et al., *Overlapping motifs (PTAP and PPEY) within the Ebola virus VP40 protein function independently as late budding domains: involvement of host proteins TSG101 and VPS-4.* J Virol, 2003. **77**(3): p. 1812-9.
176. Martin-Serrano, J., T. Zang, and P.D. Bieniasz, *HIV-1 and Ebola virus encode small peptide motifs that recruit Tsg101 to sites of particle assembly to facilitate egress.* Nature Medicine, 2001. **7**(12): p. 1313-1319.
177. Kaletsky, R.L., et al., *Tetherin-mediated restriction of filovirus budding is antagonized by the Ebola glycoprotein.* Proceedings of the National Academy of Sciences, 2009. **106**(8): p. 2886.
178. Radoshitzky, S.R., et al., *Infectious Lassa virus, but not filoviruses, is restricted by BST-2/tetherin.* J Virol, 2010. **84**(20): p. 10569-80.
179. Lopez, L.A., et al., *Ebola Virus Glycoprotein Counteracts BST-2/Tetherin Restriction in a Sequence-Independent Manner That Does Not Require Tetherin Surface Removal.* Journal of Virology, 2010. **84**(14): p. 7243.
180. FDA, *First FDA-approved vaccine for the prevention of Ebola virus disease, marking a critical milestone in public health preparedness and response*. 2019: https://www.fda.gov/news-events/press-announcements/first-fda-approved-vaccine-prevention-ebola-virus-disease-marking-critical-milestone-public-health.
181. Gsell, P.-S., et al., *Ring vaccination with rVSV-ZEBOV under expanded access in response to an outbreak of Ebola virus disease in Guinea, 2016: an operational and vaccine safety report.* The Lancet. Infectious diseases, 2017. **17**(12): p. 1276-1284.
182. Piszczatoski, C.R. and J.G. Gums, *Ervebo (Ebola Zaire Vaccine, Live/rVSVΔG-ZEBOV-GP): The First Licensed Vaccine for the Prevention of Ebola Virus Disease.* Journal of Pharmacy Technology, 2020. **36**(6): p. 243-250.

183. FDA, *FDA Approves First Treatment for Ebola Virus*. 2020: https://www.fda.gov/news-events/press-announcements/fda-approves-first-treatment-ebola-virus.
184. FDA, *FDA Approves Treatment for Ebola Virus*. 2020: https://www.fda.gov/drugs/drug-safety-and-availability/fda-approves-treatment-ebola-virus.
185. Edwards, M.R. and C.F. Basler, *Current status of small molecule drug development for Ebola virus and other filoviruses.* Curr Opin Virol, 2019. **35**: p. 42-56.
186. De Clercq, E., *New Nucleoside Analogues for the Treatment of Hemorrhagic Fever Virus Infections.* Chem Asian J, 2019. **14**(22): p. 3962-3968.
187. Jordan, P.C., S.K. Stevens, and J. Deval, *Nucleosides for the treatment of respiratory RNA virus infections.* Antiviral Chemistry and Chemotherapy, 2018. **26**: p. 2040206618764483.
188. Hoenen, T., A. Groseth, and H. Feldmann, *Therapeutic strategies to target the Ebola virus life cycle.* Nature Reviews Microbiology, 2019. **17**(10): p. 593-606.
189. Seley-Radtke, K.L. and M.K. Yates, *The evolution of nucleoside analogue antivirals: A review for chemists and non-chemists. Part 1: Early structural modifications to the nucleoside scaffold.* Antiviral Res, 2018. **154**: p. 66-86.
190. Dulin, D., et al., *Signatures of Nucleotide Analog Incorporation by an RNA-Dependent RNA Polymerase Revealed Using High-Throughput Magnetic Tweezers.* Cell Rep, 2017. **21**(4): p. 1063-1076.
191. Warren, T.K., et al., *Protection against filovirus diseases by a novel broad-spectrum nucleoside analogue BCX4430.* Nature, 2014. **508**(7496): p. 402-405.
192. Taylor, R., et al., *BCX4430 - A broad-spectrum antiviral adenosine nucleoside analog under development for the treatment of Ebola virus disease.* J Infect Public Health, 2016. **9**(3): p. 220-6.
193. FDA, *FDA's approval of Veklury (remdesivir) for the treatment of COVID-19—The Science of Safety and Effectiveness*. 2020: https://www.fda.gov/drugs/drug-safety-and-availability/fdas-approval-veklury-remdesivir-treatment-covid-19-science-safety-and-effectiveness.
194. Lo, M.K., et al., *GS-5734 and its parent nucleoside analog inhibit Filo-, Pneumo-, and Paramyxoviruses.* Scientific Reports, 2017. **7**(1): p. 43395.
195. Sheahan, T.P., et al., *Broad-spectrum antiviral GS-5734 inhibits both epidemic and zoonotic coronaviruses.* Science Translational Medicine, 2017. **9**(396): p. eaal3653.
196. Brown, A.J., et al., *Broad spectrum antiviral remdesivir inhibits human endemic and zoonotic deltacoronaviruses with a highly divergent RNA dependent RNA polymerase.* Antiviral Research, 2019. **169**: p. 104541.
197. Warren, T.K., et al., *Therapeutic efficacy of the small molecule GS-5734 against Ebola virus in rhesus monkeys.* Nature, 2016. **531**(7594): p. 381-5.
198. Siegel, D., et al., *Discovery and Synthesis of a Phosphoramidate Prodrug of a Pyrrolo[2,1-f][triazin-4-amino] Adenine C-Nucleoside (GS-5734) for the Treatment of Ebola and Emerging Viruses.* Journal of Medicinal Chemistry, 2017. **60**(5): p. 1648-1661.

199. Mulangu, S., et al., *A Randomized, Controlled Trial of Ebola Virus Disease Therapeutics.* N Engl J Med, 2019. **381**(24): p. 2293-2303.
200. Dörnemann, J., et al., *First Newborn Baby to Receive Experimental Therapies Survives Ebola Virus Disease.* The Journal of Infectious Diseases, 2017. **215**(2): p. 171-174.
201. Jacobs, M., et al., *Late Ebola virus relapse causing meningoencephalitis: a case report.* Lancet, 2016. **388**(10043): p. 498-503.
202. Smither, S.J., et al., *Post-exposure efficacy of Oral T-705 (Favipiravir) against inhalational Ebola virus infection in a mouse model.* Antiviral Research, 2014. **104**: p. 153-155.
203. Jin, Z., et al., *The Ambiguous Base-Pairing and High Substrate Efficiency of T-705 (Favipiravir) Ribofuranosyl 5'-Triphosphate towards Influenza A Virus Polymerase.* PLOS ONE, 2013. **8**(7): p. e68347.
204. Furuta, Y., et al., *Favipiravir (T-705), a novel viral RNA polymerase inhibitor.* Antiviral Research, 2013. **100**(2): p. 446-454.
205. Baranovich, T., et al., *T-705 (Favipiravir) Induces Lethal Mutagenesis in Influenza A H1N1 Viruses <em>In Vitro</em&gt.* Journal of Virology, 2013. **87**(7): p. 3741.
206. Furuta, Y., et al., *In vitro and in vivo activities of anti-influenza virus compound T-705.* Antimicrob Agents Chemother, 2002. **46**(4): p. 977-81.
207. Oestereich, L., et al., *Successful treatment of advanced Ebola virus infection with T-705 (favipiravir) in a small animal model.* Antiviral Res, 2014. **105**: p. 17-21.
208. Shiraki, K. and T. Daikoku, *Favipiravir, an anti-influenza drug against life-threatening RNA virus infections.* Pharmacol Ther, 2020. **209**: p. 107512.
209. Bixler, S.L., et al., *Efficacy of favipiravir (T-705) in nonhuman primates infected with Ebola virus or Marburg virus.* Antiviral Res, 2018. **151**: p. 97-104.
210. Kerber, R., et al., *Laboratory Findings, Compassionate Use of Favipiravir, and Outcome in Patients With Ebola Virus Disease, Guinea, 2015—A Retrospective Observational Study.* The Journal of Infectious Diseases, 2019. **220**(2): p. 195-202.
211. Nguyen, T.H., et al., *Favipiravir pharmacokinetics in Ebola-Infected patients of the JIKI trial reveals concentrations lower than targeted.* PLoS Negl Trop Dis, 2017. **11**(2): p. e0005389.
212. Schibler, M., et al., *Clinical features and viral kinetics in a rapidly cured patient with Ebola virus disease: a case report.* Lancet Infect Dis, 2015. **15**(9): p. 1034-1040.
213. Mora-Rillo, M., et al., *Acute respiratory distress syndrome after convalescent plasma use: treatment of a patient with Ebola virus disease contracted in Madrid, Spain.* Lancet Respir Med, 2015. **3**(7): p. 554-62.
214. Sissoko, D., et al., *Experimental Treatment with Favipiravir for Ebola Virus Disease (the JIKI Trial): A Historically Controlled, Single-Arm Proof-of-Concept Trial in Guinea.* PLoS Med, 2016. **13**(3): p. e1001967.
215. Bai, C.Q., et al., *Clinical and Virological Characteristics of Ebola Virus Disease Patients Treated With Favipiravir (T-705)-Sierra Leone, 2014.* Clin Infect Dis, 2016. **63**(10): p. 1288-1294.

216. Bloch, A., M.J. Robins, and J.R. McCarthy, Jr., *The role of the 5'-hydroxyl group of adenosine in determining substrate specificity for adenosine deaminase.* J Med Chem, 1967. **10**(5): p. 908-12.
217. Shealy, Y.F. and J.D. Clayton, *9-[β-DL-2α,3α-Dihydroxy-4β-(hydroxymethyl)-cyclopentyl]adenine, the Carbocyclic Analog of Adenosine1,2.* Journal of the American Chemical Society, 1966. **88**(16): p. 3885-3887.
218. De Clercq, E., *John Montgomery's Legacy: Carbocyclic Adenosine Analogues as Sah Hydrolase Inhibitors with Broad-Spectrum Antiviral Activity.* Nucleosides, Nucleotides & Nucleic Acids, 2005. **24**(10-12): p. 1395-1415.
219. Arita, M., et al., *Enantioselective synthesis of new analogues of neplanocin A.* Nucleic Acids Symp Ser, 1983(12): p. 25-8.
220. Faith, W.C., et al., *An approach to the synthesis of neplanocin A.* The Journal of Organic Chemistry, 1985. **50**(11): p. 1983-1985.
221. Lim, M.-I. and V.E. Marquez, *Total synthesis of (−)-neplanocin A.* Tetrahedron Letters, 1983. **24**(50): p. 5559-5562.
222. Jung, M., G. Offenbächer, and J. Rétey, *Total Synthesis of Neplanocin A.* Helvetica Chimica Acta, 1983. **66**(7): p. 1915-1921.
223. Yaginuma, S., et al., *Studies on neplanocin A, new antitumor antibiotic. I. Producing organism, isolation and characterization.* J Antibiot (Tokyo), 1981. **34**(4): p. 359-66.
224. Hayashi, M., et al., *Studies on neplanocin A, new antitumor antibiotic. II. Structure determination.* The Journal of antibiotics, 1981. **34**(6): p. 675-680.
225. Glazer, R.I., et al., *3-Deazaneplanocin: A new and potent inhibitor of S-adenosylhomocysteine hydrolase and its effects on human promyelocytic leukemia cell line HL-60.* Biochemical and Biophysical Research Communications, 1986. **135**(2): p. 688-694.
226. Huggins, J., Z.-X. Zhang, and M. Bray, *Antiviral Drug Therapy of Filovirus Infections: S-Adenosylhomocysteine Hydrolase Inhibitors Inhibit Ebola Virus In Vitro and in a Lethal Mouse Model.* The Journal of Infectious Diseases, 1999. **179**(Supplement_1): p. S240-S247.
227. Bray, M., et al., *3-Deazaneplanocin A induces massively increased interferon-α production in Ebola virus-infected mice.* Antiviral Research, 2002. **55**(1): p. 151-159.
228. Liu, C., Q. Chen, and S.W. Schneller, *Enantiomeric 3-deaza-1',6'-isoneplanocin and its 3-bromo analogue: Synthesis by the Ullmann reaction and their antiviral properties.* Bioorganic & Medicinal Chemistry Letters, 2016. **26**(3): p. 928-930.
229. Liu, C., Q. Chen, and S.W. Schneller, *3-Bromo-3-deazaneplanocin and 3-bromo-3-deazaaristeromycin: Synthesis and antiviral activity.* Bioorganic & Medicinal Chemistry Letters, 2012. **22**(16): p. 5182-5184.
230. De La Haba, G. and G.L. Cantoni, *The enzymatic synthesis of S-adenosyl-L-homocysteine from adenosine and homocysteine.* J Biol Chem, 1959. **234**(3): p. 603-8.
231. Caudill, M.A., et al., *Intracellular S-adenosylhomocysteine concentrations predict global DNA hypomethylation in tissues of methyl-deficient cystathionine beta-synthase heterozygous mice.* J Nutr, 2001. **131**(11): p. 2811-8.

232. Hoffman, D.R., W.E. Cornatzer, and J.A. Duerre, *Relationship between tissue levels of S-adenosylmethionine, S-adenylhomocysteine, and transmethylation reactions.* Can J Biochem, 1979. **57**(1): p. 56-65.
233. Zheng, S., et al., *Mutational analysis of Encephalitozoon cuniculi mRNA cap (guanine-N7) methyltransferase, structure of the enzyme bound to sinefungin, and evidence that cap methyltransferase is the target of sinefungin's antifungal activity.* J Biol Chem, 2006. **281**(47): p. 35904-13.
234. Zhang, J. and Y.G. Zheng, *SAM/SAH Analogs as Versatile Tools for SAM-Dependent Methyltransferases.* ACS Chem Biol, 2016. **11**(3): p. 583-97.
235. Zappia, V., R. Zydek-Cwick, and F. Schlenk, *The specificity of S-adenosylmethionine derivatives in methyl transfer reactions.* J Biol Chem, 1969. **244**(16): p. 4499-509.
236. Weretilnyk, B.A.M.a.E.A., *Sustaining S-adenosyl-L-methionine-dependent methyltransferase activity in plant cells.* PHYSIOLOGIA PLANTARUM, 2001. **113**: p. 435–442.
237. Richon, V.M., et al., *Chemogenetic analysis of human protein methyltransferases.* Chem Biol Drug Des, 2011. **78**(2): p. 199-210.
238. Poulton, J.E., *22 - Transmethylation and Demethylation Reactions in the Metabolism of Secondary Plant Products*, in *Secondary Plant Products*, E.E. Conn, Editor. 1981, Academic Press: San Diego. p. 667-723.
239. Pegg, A.E., *Studies on inhibitors of mammalian tRNA methylases.* FEBS Letters, 1971. **16**(1): p. 13-16.
240. Kredich, N.M. and M.S. Hershfield, *Perturbations in S-adenosylhomocysteine and S-adenosylmethionine metabolism: effects on transmethylation.* Adv Enzyme Regul, 1980. **18**: p. 181-91.
241. Kerr, S.J., *Competing methyltransferase systems.* J Biol Chem, 1972. **247**(13): p. 4248-52.
242. Hoffman, J.L., *The rate of transmethylation in mouse liver as measured by trapping S-adenosylhomocysteine.* Archives of Biochemistry and Biophysics, 1980. **205**(1): p. 132-135.
243. Hildesheim, J., R. Hildesheim, and E. Lederer, *Nouvelles synthèses d'analogues de la S-adénosyl homocystéine, inhibiteurs potentiels des méthyl-transférases.* Biochimie, 1972. **54**(4): p. 431-437.
244. Hildesheim, J., R. Hildesheim, and E. Lederer, *Synthèses d'inhibiteurs des méthyl-transférases : analogues de la S-adénosyl homocystéine.* Biochimie, 1971. **53**(10): p. 1067-1071.
245. Hildesheim, J., et al., *Studies on synthetic inhibitors of t-RNA methyl transferases: analogs of S-adenosyl homocysteine.* Biochimie, 1973. **55**(5): p. 541-546.
246. Fuller, R.W. and R. Nagarajan, *Inhibition of methyltransferases by some new analogs of S-adenosylhomocysteine.* Biochemical Pharmacology, 1978. **27**(15): p. 1981-1983.
247. Fabianowska-Majewska, K., J.A. Duley, and H.A. Simmonds, *Effects of novel anti-viral adenosine analogues on the activity of S-adenosylhomocysteine hydrolase from human liver.* Biochemical Pharmacology, 1994. **48**(5): p. 897-903.

248. Deguchi, T. and J. Barchas, *Inhibition of transmethylations of biogenic amines by S-adenosylhomocysteine. Enhancement of transmethylation by adenosylhomocysteinase.* J Biol Chem, 1971. **246**(10): p. 3175-81.
249. Crooks, P.A., M.J. Tribé, and R.J. Pinney, *Inhibition of bacterial DNA cytosine-5-methyltransferase by S-adenosyl-l-homocysteine and some related compounds†.* Journal of Pharmacy and Pharmacology, 1984. **36**(2): p. 85-89.
250. Coward, J.K. and E.P. Slisz, *Analogs of S-adenosylhomocysteine as potential inhibitors of biological transmethylation. Specificity of the S-adenosylhomocysteine binding site.* Journal of Medicinal Chemistry, 1973. **16**(5): p. 460-463.
251. Coward, J.K., D.L. Bussolotti, and C.-D. Chang, *Analogs of S-adenosylhomocysteine as potential inhibitors of biological transmethylation. Inhibition of several methylases by S-tubercidinylhomocysteine.* Journal of Medicinal Chemistry, 1974. **17**(12): p. 1286-1289.
252. Chiang, P.K., H.H. Richards, and G.L. Cantoni, *S-Adenosyl-L-homocysteine hydrolase: analogues of S-adenosyl-L-homocysteine as potential inhibitors.* Mol Pharmacol, 1977. **13**(5): p. 939-47.
253. Borchardt, R.T., et al., *Potential inhibitors of S-adenosylmethionine-dependent methyltransferases. 6. Structural modifications of S-adenosylmethionine.* Journal of Medicinal Chemistry, 1976. **19**(9): p. 1104-1110.
254. Borchardt, R.T. and Y.S. Wu, *Potential inhibitors of S-adenosylmethionine-dependent methyltransferases. 3. Modifications of the sugar portion of S-adenosylhomocysteine.* Journal of Medicinal Chemistry, 1975. **18**(3): p. 300-304.
255. Borchardt, R.T. and Y.S. Wu, *Potential inhibitors of S-adenosylmethionine-dependent methyltransferases. 1. Modification of the amino acid portion of S-adenosylhomocysteine.* Journal of Medicinal Chemistry, 1974. **17**(8): p. 862-868.
256. Borchardt, R.T., J.A. Huber, and Y.S. Wu, *Potential inhibitors of S-adenosylmethionine-dependent methyltransferases. 2. Modification of the base portion of S-adenosylhomocysteine.* Journal of Medicinal Chemistry, 1974. **17**(8): p. 868-873.
257. Aouadi, W., et al., *Binding of the Methyl Donor S-Adenosyl-l-Methionine to Middle East Respiratory Syndrome Coronavirus 2'-O-Methyltransferase nsp16 Promotes Recruitment of the Allosteric Activator nsp10.* J Virol, 2017. **91**(5).
258. Bader, J.P., et al., *3-Deazaadenosine, an inhibitor of adenosylhomocysteine hydrolase, inhibits reproduction of rous sarcoma virus and transformation of chick embryo cells.* Virology, 1978. **89**(2): p. 494-505.
259. Baker, R.O., M. Bray, and J.W. Huggins, *Potential antiviral therapeutics for smallpox, monkeypox and other orthopoxvirus infections.* Antiviral Research, 2003. **57**(1): p. 13-23.
260. Baker, R.O., M. Bray, and J.W. Huggins, *Potential antiviral therapeutics for smallpox, monkeypox and other orthopoxvirus infections.* Antiviral Res, 2003. **57**(1-2): p. 13-23.
261. Bodner, A.J., G.L. Cantoni, and P.K. Chiang, *Anti-viral activity of 3-deazaadenosine and 5'-deoxy-5'-isobutylthio-3-deazaadenosine (3-deaza-SIBA).* Biochemical and Biophysical Research Communications, 1981. **98**(2): p. 476-481.

262. Borchardt, R.T., B.T. Keller, and U. Patel-Thombre, *Neplanocin A. A potent inhibitor of S-adenosylhomocysteine hydrolase and of vaccinia virus multiplication in mouse L929 cells.* J Biol Chem, 1984. **259**(7): p. 4353-8.
263. Both, G.W., A.K. Banerjee, and A.J. Shatkin, *Methylation-dependent translation of viral messenger RNAs in vitro.* Proceedings of the National Academy of Sciences, 1975. **72**(3): p. 1189.
264. Bray, M., J. Driscoll, and J.W. Huggins, *Treatment of lethal Ebola virus infection in mice with a single dose of an S-adenosyl-l-homocysteine hydrolase inhibitor.* Antiviral Research, 2000. **45**(2): p. 135-147.
265. de Clercq, E., *Nucleoside analogues as antiviral agents.* Acta Microbiol Acad Sci Hung, 1981. **28**(3): p. 289-306.
266. De Clercq, E., *Specific targets for antiviral drugs.* Biochem J, 1982. **205**(1): p. 1-13.
267. De Clercq, E., *Antiviral and antimetabolic activities of neplanocins.* Antimicrobial Agents and Chemotherapy, 1985. **28**(1): p. 84.
268. De Clercq, E., *Recent trends and development in antiviral chemotherapy.* Antiviral Research, 1985. **5**: p. 11-19.
269. De Clercq, E., *S-adenosylhomocysteine hydrolase inhibitors as broad-spectrum antiviral agents.* Biochemical Pharmacology, 1987. **36**(16): p. 2567-2575.
270. De Clercq, E., *Antivirals and antiviral strategies.* Nature reviews. Microbiology, 2004. **2**(9): p. 704-720.
271. De Clercq, E., *Antiviral drug discovery and development: Where chemistry meets with biomedicine.* Antiviral Research, 2005. **67**(2): p. 56-75.
272. De Clercq, E., *Antivirals: Past, present and future.* Biochemical Pharmacology, 2013. **85**(6): p. 727-744.
273. De Clercq, E., *Ebola virus (EBOV) infection: Therapeutic strategies.* Biochemical Pharmacology, 2015. **93**(1): p. 1-10.
274. De Clercq, E., et al., *Broad-spectrum antiviral activity of adenosine analogues.* Antiviral Research, 1984. **4**(3): p. 119-133.
275. De Clercq, E. and M. Cools, *Antiviral potency of adenosine analogues: Correlation with inhibition of S-adenosylhomocysteine hydrolase.* Biochemical and Biophysical Research Communications, 1985. **129**(1): p. 306-311.
276. De Clercq, E., et al., *Broad-spectrum antiviral activities of neplanocin A, 3-deazaneplanocin A, and their 5'-nor derivatives.* Antimicrobial Agents and Chemotherapy, 1989. **33**(8): p. 1291.
277. De Clercq, E., et al., *(S)-9-(2,3-Dihydroxypropyl)adenine: An Aliphatic Nucleoside Analog with Broad-Spectrum Antiviral Activity.* Science, 1978. **200**(4341): p. 563-565.
278. De Clercq, E. and J.A. Montgomery, *Broad-spectrum antiviral activity of the carbocyclic analog of 3-deazaadenosine.* Antiviral Research, 1983. **3**(1): p. 17-24.
279. de Ferra, F. and C. Baglioni, *Increase in S-adenosylhomocysteine concentration in interferon-treated HeLa cells and inhibition of methylation of vesicular stomatitis virus mRNA.* J Biol Chem, 1983. **258**(4): p. 2118-21.

280. Glazer, R.I. and M.C. Knode, *Neplanocin A. A cyclopentenyl analog of adenosine with specificity for inhibiting RNA methylation.* J Biol Chem, 1984. **259**(21): p. 12964-9.
281. Hasan, A. and P.C. Srivastava, *Synthesis and biological studies of unsaturated acyclonucleoside analogues of S-adenosyl-L-homocysteine hydrolase inhibitors.* J Med Chem, 1992. **35**(8): p. 1435-9.
282. Hasobe, M., et al., *9-(trans-2',trans-3'-Dihydroxycyclopent-4'-enyl)-adenine and -3-deazaadenine: analogs of neplanocin A which retain potent antiviral activity but exhibit reduced cytotoxicity.* Antimicrobial Agents and Chemotherapy, 1987. **31**(11): p. 1849.
283. Jacquemont, B. and J. Huppert, *Inhibition of viral RNA methylation in herpes simplex virus type 1-infected cells by 5' S-isobutyl-adenosine.* Journal of Virology, 1977. **22**(1): p. 160.
284. Keller, B.T. and R.T. Borchardt, *Adenosine dialdehyde: a potent inhibitor of vaccinia virus multiplication in mouse L929 cells.* Molecular Pharmacology, 1987. **31**(5): p. 485.
285. Li, J., J.S. Chorba, and S.P.J. Whelan, *Vesicular Stomatitis Viruses Resistant to the Methylase Inhibitor Sinefungin Upregulate RNA Synthesis and Reveal Mutations That Affect mRNA Cap Methylation.* Journal of Virology, 2007. **81**(8): p. 4104.
286. Pugh, C.S., R.T. Borchardt, and H.O. Stone, *Inhibition of Newcastle disease virion messenger RNA (guanine-7-)-methyltransferase by analogues of S-adenosylhomocysteine.* Biochemistry, 1977. **16**(17): p. 3928-32.
287. Pugh, C.S., R.T. Borchardt, and H.O. Stone, *Sinefungin, a potent inhibitor of virion mRNA(guanine-7-)-methyltransferase, mRNA(nucleoside-2'-)-methyltransferase, and viral multiplication.* J Biol Chem, 1978. **253**(12): p. 4075-7.
288. Raies, A., F. Lawrence, and M. Robert-Gero, *Effect of 5'-deoxy-5'-S-isobutyl adenosine on polyoma virus replication.* FEBS Lett, 1976. **72**(1): p. 48-52.
289. Robert-Géro, M., et al., *Inhibition of virus-induced cell transformation by synthetic analogues of S-adenosyl homocysteine.* Biochemical and Biophysical Research Communications, 1975. **65**(4): p. 1242-1249.
290. Serafinowski, P., et al., *Synthesis and antiviral activity of some new S-adenosyl-L-homocysteine derivatives.* Journal of Medicinal Chemistry, 1992. **35**(24): p. 4576-4583.
291. Shatkin, A.J., *Methylated messenger RNA synthesis in vitro by purified reovirus.* Proc Natl Acad Sci U S A, 1974. **71**(8): p. 3204-7.
292. Shin, Y.S., et al., *Identification of 6'-β-fluoro-homoaristeromycin as a potent inhibitor of chikungunya virus replication.* European Journal of Medicinal Chemistry, 2020. **187**: p. 111956.
293. Siddiqi, S.M., et al., *S-Adenosyl-L-homocysteine Hydrolase Inhibitors as Anti-Viral Agents: 5'-Deoxyaristeromycin.* Nucleosides and Nucleotides, 1993. **12**(2): p. 185-198.
294. Stoltzfus, C.M. and J.A. Montgomery, *Selective inhibition of avian sarcoma virus protein synthesis in 3-deazaadenosine-treated infected chicken embryo fibroblasts.* Journal of Virology, 1981. **38**(1): p. 173.

295. Vedel, M., et al., *The antifungal antibiotic sinefungin as a very active inhibitor of methyltransferases and of the transformation of chick embryo fibroblasts by Rous sarcoma virus.* Biochem Biophys Res Commun, 1978. **85**(1): p. 371-6.
296. Yuan, C.-S., et al., *Design and synthesis of S-adenosylhomocysteine hydrolase inhibitors as broad-spectrum antiviral agents*, in *Advances in Antiviral Drug Design*, E. De Clercq, Editor. 1996, Elsevier. p. 41-88.
297. Yuan, C.-S., et al., *Recent advances in S-adenosyl-L-homocysteine hydrolase inhibitors and their potential clinical applications.* Expert Opinion on Therapeutic Patents, 1999. **9**(9): p. 1197-1206.
298. Secombes, C.J. and J. Zou, *Evolution of Interferons and Interferon Receptors.* Frontiers in immunology, 2017. **8**: p. 209-209.
299. McNab, F., et al., *Type I interferons in infectious disease.* Nature Reviews Immunology, 2015. **15**(2): p. 87-103.
300. Majzoub, K., F. Wrensch, and T.F. Baumert, *The Innate Antiviral Response in Animals: An Evolutionary Perspective from Flagellates to Humans.* Viruses, 2019. **11**(8): p. 758.
301. Pestka, S., C.D. Krause, and M.R. Walter, *Interferons, interferon-like cytokines, and their receptors.* Immunol Rev, 2004. **202**: p. 8-32.
302. Chow, K.T., M. Gale, Jr., and Y.M. Loo, *RIG-I and Other RNA Sensors in Antiviral Immunity.* Annu Rev Immunol, 2018. **36**: p. 667-694.
303. Amarante-Mendes, G.P., et al., *Pattern Recognition Receptors and the Host Cell Death Molecular Machinery.* Frontiers in Immunology, 2018. **9**(2379).
304. Okamoto, M., et al., *Recognition of Viral RNA by Pattern Recognition Receptors in the Induction of Innate Immunity and Excessive Inflammation During Respiratory Viral Infections.* Viral Immunol, 2017. **30**(6): p. 408-420.
305. Kato, H., K. Takahasi, and T. Fujita, *RIG-I-like receptors: cytoplasmic sensors for non-self RNA.* Immunol Rev, 2011. **243**(1): p. 91-8.
306. Takeuchi, O. and S. Akira, *Pattern recognition receptors and inflammation.* Cell, 2010. **140**(6): p. 805-20.
307. Hopfner, K.-P. and V. Hornung, *Molecular mechanisms and cellular functions of cGAS–STING signalling.* Nature Reviews Molecular Cell Biology, 2020. **21**(9): p. 501-521.
308. Honda, K., et al., *Regulation of the type I IFN induction: a current view.* International Immunology, 2005. **17**(11): p. 1367-1378.
309. Panne, D., T. Maniatis, and S.C. Harrison, *An atomic model of the interferon-beta enhanceosome.* Cell, 2007. **129**(6): p. 1111-23.
310. Piehler, J., et al., *Structural and dynamic determinants of type I interferon receptor assembly and their functional interpretation.* Immunological reviews, 2012. **250**(1): p. 317-334.
311. Mogensen, T.H., *IRF and STAT Transcription Factors - From Basic Biology to Roles in Infection, Protective Immunity, and Primary Immunodeficiencies.* Frontiers in Immunology, 2019. **9**(3047).
312. McBride, K.M. and N.C. Reich, *The ins and outs of STAT1 nuclear transport.* Sci STKE, 2003. **2003**(195): p. Re13.

313. Sekimoto, T., et al., *Extracellular signal-dependent nuclear import of Stat1 is mediated by nuclear pore-targeting complex formation with NPI-1, but not Rch1.* EMBO J, 1997. **16**(23): p. 7067-77.
314. Darnell, J.E., I.M. Kerr, and G.R. Stark, *Jak-STAT pathways and transcriptional activation in response to IFNs and other extracellular signaling proteins.* Science, 1994. **264**(5164): p. 1415.
315. Au, W.C., et al., *Identification of a member of the interferon regulatory factor family that binds to the interferon-stimulated response element and activates expression of interferon-induced genes.* Proc Natl Acad Sci U S A, 1995. **92**(25): p. 11657-61.
316. Schoggins, J.W., *Interferon-stimulated genes: roles in viral pathogenesis.* Curr Opin Virol, 2014. **6**: p. 40-6.
317. Schneider, W.M., M.D. Chevillotte, and C.M. Rice, *Interferon-stimulated genes: a complex web of host defenses.* Annual review of immunology, 2014. **32**: p. 513-545.
318. Ren, Z., et al., *Regulation of MAVS Expression and Signaling Function in the Antiviral Innate Immune Response.* Frontiers in Immunology, 2020. **11**(1030).
319. Basler, C.F. and G.K. Amarasinghe, *Evasion of interferon responses by Ebola and Marburg viruses.* J Interferon Cytokine Res, 2009. **29**(9): p. 511-20.
320. Bray, M., *The role of the Type I interferon response in the resistance of mice to filovirus infection.* Journal of General Virology, 2001. **82**(6): p. 1365-1373.
321. Gibb, T.R., et al., *Pathogenesis of experimental Ebola Zaire virus infection in BALB/c mice.* J Comp Pathol, 2001. **125**(4): p. 233-42.
322. Lofts, L.L., et al., *Key Genomic Changes Necessary for an In Vivo Lethal Mouse Marburgvirus Variant Selection Process.* Journal of Virology, 2011. **85**(8): p. 3905.
323. Warfield, K.L., et al., *Development and Characterization of a Mouse Model for Marburg Hemorrhagic Fever.* Journal of Virology, 2009. **83**(13): p. 6404.
324. Valmas, C. and C.F. Basler, *Marburg virus VP40 antagonizes interferon signaling in a species-specific manner.* Journal of virology, 2011. **85**(9): p. 4309-4317.
325. Harcourt, B.H., A. Sanchez, and M.K. Offermann, *Ebola virus selectively inhibits responses to interferons, but not to interleukin-1beta, in endothelial cells.* J Virol, 1999. **73**(4): p. 3491-6.
326. Basler, C.F., et al., *The Ebola virus VP35 protein functions as a type I IFN antagonist.* Proceedings of the National Academy of Sciences, 2000. **97**(22): p. 12289.
327. Edwards, M.R., et al., *Differential Regulation of Interferon Responses by Ebola and Marburg Virus VP35 Proteins.* Cell reports, 2016. **14**(7): p. 1632-1640.
328. Albariño, C.G., et al., *Recombinant Marburg viruses containing mutations in the IID region of VP35 prevent inhibition of Host immune responses.* Virology, 2015. **476**: p. 85-91.
329. Bale, S., et al., *Ebolavirus VP35 Coats the Backbone of Double-Stranded RNA for Interferon Antagonism.* Journal of Virology, 2013. **87**(18): p. 10385.
330. Ramanan, P., et al., *Structural basis for Marburg virus VP35-mediated immune evasion mechanisms.* Proc Natl Acad Sci U S A, 2012. **109**(50): p. 20661-6.

331. Bale, S., et al., *Marburg virus VP35 can both fully coat the backbone and cap the ends of dsRNA for interferon antagonism.* PLoS Pathog, 2012. **8**(9): p. e1002916.
332. Prins, K.C., et al., *Mutations Abrogating VP35 Interaction with Double-Stranded RNA Render Ebola Virus Avirulent in Guinea Pigs.* Journal of Virology, 2010. **84**(6): p. 3004.
333. Prins, K.C., et al., *Basic residues within the ebolavirus VP35 protein are required for its viral polymerase cofactor function.* J Virol, 2010. **84**(20): p. 10581-91.
334. Leung, D.W., et al., *Structural and functional characterization of Reston Ebola virus VP35 interferon inhibitory domain.* J Mol Biol, 2010. **399**(3): p. 347-57.
335. Leung, D.W., et al., *Structural basis for dsRNA recognition and interferon antagonism by Ebola VP35.* Nat Struct Mol Biol, 2010. **17**(2): p. 165-72.
336. Kimberlin, C.R., et al., *Ebolavirus VP35 uses a bimodal strategy to bind dsRNA for innate immune suppression.* Proc Natl Acad Sci U S A, 2010. **107**(1): p. 314-9.
337. Hartman, A.L., et al., *Reverse Genetic Generation of Recombinant Zaire Ebola Viruses Containing Disrupted IRF-3 Inhibitory Domains Results in Attenuated Virus Growth In Vitro and Higher Levels of IRF-3 Activation without Inhibiting Viral Transcription or Replication.* Journal of Virology, 2006. **80**(13): p. 6430.
338. Cárdenas, W.B., et al., *Ebola virus VP35 protein binds double-stranded RNA and inhibits alpha/beta interferon production induced by RIG-I signaling.* J Virol, 2006. **80**(11): p. 5168-78.
339. Williams, C.G., et al., *Impact of Mengla Virus Proteins on Human and Bat Innate Immune Pathways.* J Virol, 2020. **94**(13).
340. Hume, A. and E. Muhlberger, *Marburg Virus Viral Protein 35 Inhibits Protein Kinase R Activation in a Cell Type-Specific Manner.* J Infect Dis, 2018. **218**(suppl_5): p. S403-S408.
341. Leung, D.W., et al., *Structure of the Ebola VP35 interferon inhibitory domain.* Proceedings of the National Academy of Sciences, 2009. **106**(2): p. 411.
342. Hartman, A.L., J.S. Towner, and S.T. Nichol, *A C-terminal basic amino acid motif of Zaire ebolavirus VP35 is essential for type I interferon antagonism and displays high identity with the RNA-binding domain of another interferon antagonist, the NS1 protein of influenza A virus.* Virology, 2004. **328**(2): p. 177-84.
343. Luthra, P., et al., *Mutual antagonism between the Ebola virus VP35 protein and the RIG-I activator PACT determines infection outcome.* Cell Host Microbe, 2013. **14**(1): p. 74-84.
344. Kok, K.-H., et al., *The Double-Stranded RNA-Binding Protein PACT Functions as a Cellular Activator of RIG-I to Facilitate Innate Antiviral Response.* Cell Host & Microbe, 2011. **9**(4): p. 299-309.
345. Prins, K.C., W.B. Cardenas, and C.F. Basler, *Ebola virus protein VP35 impairs the function of interferon regulatory factor-activating kinases IKKepsilon and TBK-1.* J Virol, 2009. **83**(7): p. 3069-77.
346. Basler, C.F., et al., *The Ebola virus VP35 protein inhibits activation of interferon regulatory factor 3.* J Virol, 2003. **77**(14): p. 7945-56.

347. Feng, Z., et al., *The VP35 Protein of Ebola Virus Inhibits the Antiviral Effect Mediated by Double-Stranded RNA-Dependent Protein Kinase PKR.* Journal of Virology, 2007. **81**(1): p. 182.
348. Xu, W., et al., *Ebola virus VP24 targets a unique NLS binding site on karyopherin alpha 5 to selectively compete with nuclear import of phosphorylated STAT1.* Cell Host Microbe, 2014. **16**(2): p. 187-200.
349. Reid, S.P., et al., *Ebola virus VP24 proteins inhibit the interaction of NPI-1 subfamily karyopherin alpha proteins with activated STAT1.* J Virol, 2007. **81**(24): p. 13469-77.
350. Reid, S.P., et al., *Ebola virus VP24 binds karyopherin alpha1 and blocks STAT1 nuclear accumulation.* J Virol, 2006. **80**(11): p. 5156-67.
351. Feagins, A.R. and C.F. Basler, *Lloviu virus VP24 and VP35 proteins function as innate immune antagonists in human and bat cells.* Virology, 2015. **485**: p. 145-52.
352. Valmas, C., et al., *Marburg Virus Evades Interferon Responses by a Mechanism Distinct from Ebola Virus.* PLOS Pathogens, 2010. **6**(1): p. e1000721.
353. Guito, J.C., et al., *Novel activities by ebolavirus and marburgvirus interferon antagonists revealed using a standardized in vitro reporter system.* Virology, 2017. **501**: p. 147-165.
354. Page, A., et al., *Marburgvirus hijacks nrf2-dependent pathway by targeting nrf2-negative regulator keap1.* Cell Rep, 2014. **6**(6): p. 1026-1036.
355. Edwards, M.R., et al., *The Marburg virus VP24 protein interacts with Keap1 to activate the cytoprotective antioxidant response pathway.* Cell Rep, 2014. **6**(6): p. 1017-1025.
356. Jain, A.K., D.A. Bloom, and A.K. Jaiswal, *Nuclear Import and Export Signals in Control of Nrf2 *.* Journal of Biological Chemistry, 2005. **280**(32): p. 29158-29168.
357. Baird, L. and A.T. Dinkova-Kostova, *The cytoprotective role of the Keap1-Nrf2 pathway.* Arch Toxicol, 2011. **85**(4): p. 241-72.
358. Stenvinkel, P., et al., *Understanding the role of the cytoprotective transcription factor nuclear factor erythroid 2-related factor 2—lessons from evolution, the animal kingdom and rare progeroid syndromes.* Nephrology Dialysis Transplantation, 2020. **35**(12): p. 2036-2045.
359. Banerjee, A.K., *Transcription and replication of rhabdoviruses.* Microbiol Rev, 1987. **51**(1): p. 66-87.
360. Thomas, D., et al., *Mass and molecular composition of vesicular stomatitis virus: a scanning transmission electron microscopy analysis.* Journal of Virology, 1985. **54**(2): p. 598.
361. Emerson, S.U. and R.R. Wagner, *Dissociation and reconstitution of the transcriptase and template activities of vesicular stomatitis B and T virions.* J Virol, 1972. **10**(2): p. 297-309.
362. Emerson, S.U. and M. Schubert, *Location of the binding domains for the RNA polymerase L and the ribonucleocapsid template within different halves of the NS phosphoprotein of vesicular stomatitis virus.* Proc Natl Acad Sci U S A, 1987. **84**(16): p. 5655-9.

363. Banerjee, A.K. and S. Barik, *Gene expression of vesicular stomatitis virus genome RNA.* Virology, 1992. **188**(2): p. 417-428.
364. Canter, D.M. and J. Perrault, *Stabilization of vesicular stomatitis virus L polymerase protein by P protein binding: a small deletion in the C-terminal domain of L abrogates binding.* Virology, 1996. **219**(2): p. 376-86.
365. Chattopadhyay, D. and A.K. Banerjee, *Phosphorylation within a specific domain of the phosphoprotein of vesicular stomatitis virus regulates transcription in vitro.* Cell, 1987. **49**(3): p. 407-14.
366. Rahmeh, A.A., et al., *Critical phosphoprotein elements that regulate polymerase architecture and function in vesicular stomatitis virus.* Proceedings of the National Academy of Sciences, 2012. **109**(36): p. 14628.
367. Grdzelishvili, V.Z., et al., *A single amino acid change in the L-polymerase protein of vesicular stomatitis virus completely abolishes viral mRNA cap methylation.* Journal of virology, 2005. **79**(12): p. 7327-7337.
368. Li, J., J.T. Wang, and S.P.J. Whelan, *A unique strategy for mRNA cap methylation used by vesicular stomatitis virus.* Proceedings of the National Academy of Sciences, 2006. **103**(22): p. 8493.
369. Abraham, G., D.P. Rhodes, and A.K. Banerjee, *The 5' terminal structure of the methylated mRNA synthesized in vitro by vesicular stomatitis virus.* Cell, 1975. **5**(1): p. 51-8.
370. Banerjee, A.K., S.A. Moyer, and D.P. Rhodes, *Studies on the in vitro adenylation of RNA by vesicular stomatitis virus.* Virology, 1974. **61**(2): p. 547-558.
371. Li, J., E.C. Fontaine-Rodriguez, and S.P. Whelan, *Amino acid residues within conserved domain VI of the vesicular stomatitis virus large polymerase protein essential for mRNA cap methyltransferase activity.* J Virol, 2005. **79**(21): p. 13373-84.
372. Grdzelishvili, V.Z., et al., *Identification of a new region in the vesicular stomatitis virus L polymerase protein which is essential for mRNA cap methylation.* Virology, 2006. **350**(2): p. 394-405.
373. Ogino, T. and A.K. Banerjee, *Unconventional Mechanism of mRNA Capping by the RNA-Dependent RNA Polymerase of Vesicular Stomatitis Virus.* Molecular Cell, 2007. **25**(1): p. 85-97.
374. Li, J., et al., *A Conserved Motif in Region V of the Large Polymerase Proteins of Nonsegmented Negative-Sense RNA Viruses That Is Essential for mRNA Capping.* Journal of Virology, 2008. **82**(2): p. 775.
375. Jenni, S., et al., *Structure of the Vesicular Stomatitis Virus L Protein in Complex with Its Phosphoprotein Cofactor.* Cell Reports, 2020. **30**(1): p. 53-60.e5.
376. Rougeron, V., et al., *Ebola and Marburg haemorrhagic fever.* J Clin Virol, 2015. **64**: p. 111-9.
377. Team, W.H.O.E.R., et al., *After Ebola in West Africa--Unpredictable Risks, Preventable Epidemics.* N Engl J Med, 2016. **375**(6): p. 587-96.
378. Organization, W.H. *Ebola situation reports: Democratic Republic of the Congo*. 2019; Available from: https://www.who.int/ebola/situation-reports/drc-2018/en/.
379. Basler, C.F., et al., *The Ebola virus VP35 protein functions as a type I IFN antagonist.* Proc Natl Acad Sci U S A, 2000. **97**(22): p. 12289-94.

380. Cardenas, W.B., et al., *Ebola virus VP35 protein binds double-stranded RNA and inhibits alpha/beta interferon production induced by RIG-I signaling.* J Virol, 2006. **80**(11): p. 5168-78.
381. Edwards, M.R., et al., *Differential Regulation of Interferon Responses by Ebola and Marburg Virus VP35 Proteins.* Cell Rep, 2016. **14**(7): p. 1632-1640.
382. Leung, D.W., et al., *Structure of the Ebola VP35 interferon inhibitory domain.* Proc Natl Acad Sci U S A, 2009. **106**(2): p. 411-6.
383. Prins, K.C., et al., *Mutations abrogating VP35 interaction with double-stranded RNA render Ebola virus avirulent in guinea pigs.* J Virol, 2010. **84**(6): p. 3004-15.
384. Yen, B., et al., *Molecular basis for ebolavirus VP35 suppression of human dendritic cell maturation.* J Virol, 2014. **88**(21): p. 12500-10.
385. Bale, S., et al., *Ebolavirus VP35 coats the backbone of double-stranded RNA for interferon antagonism.* J Virol, 2013. **87**(18): p. 10385-8.
386. Dilley, K.A., et al., *The Ebola virus VP35 protein binds viral immunostimulatory and host RNAs identified through deep sequencing.* PLoS One, 2017. **12**(6): p. e0178717.
387. Feng, Z., et al., *The VP35 protein of Ebola virus inhibits the antiviral effect mediated by double-stranded RNA-dependent protein kinase PKR.* J Virol, 2007. **81**(1): p. 182-92.
388. Schumann, M., T. Gantke, and E. Muhlberger, *Ebola virus VP35 antagonizes PKR activity through its C-terminal interferon inhibitory domain.* J Virol, 2009. **83**(17): p. 8993-7.
389. Edwards, M.R., et al., *Conservation of Structure and Immune Antagonist Functions of Filoviral VP35 Homologs Present in Microbat Genomes.* Cell Rep, 2018. **24**(4): p. 861-872 e6.
390. McBride, K.M., et al., *Regulated nuclear import of the STAT1 transcription factor by direct binding of importin-alpha.* EMBO J, 2002. **21**(7): p. 1754-63.
391. Mateo, M., et al., *Ebolavirus VP24 binding to karyopherins is required for inhibition of interferon signaling.* J Virol, 2010. **84**(2): p. 1169-75.
392. Valmas, C., et al., *Marburg virus evades interferon responses by a mechanism distinct from ebola virus.* PLoS Pathog, 2010. **6**(1): p. e1000721.
393. Valmas, C. and C.F. Basler, *Marburg virus VP40 antagonizes interferon signaling in a species-specific manner.* J Virol, 2011. **85**(9): p. 4309-17.
394. Feagins, A.R. and C.F. Basler, *Amino Acid Residue at Position 79 of Marburg Virus VP40 Confers Interferon Antagonism in Mouse Cells.* J Infect Dis, 2015. **212 Suppl 2**: p. S219-25.
395. He, F., et al., *Ebolavirus protein VP24 interferes with innate immune responses by inhibiting interferon-lambda1 gene expression.* Virology, 2017. **509**: p. 23-34.
396. Johnson, B., et al., *Dimerization Controls Marburg Virus VP24-dependent Modulation of Host Antioxidative Stress Responses.* J Mol Biol, 2016. **428**(17): p. 3483-94.
397. Edwards, M.R. and C.F. Basler, *Marburg Virus VP24 Protein Relieves Suppression of the NF-kappaB Pathway Through Interaction With Kelch-like ECH-Associated Protein 1.* J Infect Dis, 2015. **212 Suppl 2**: p. S154-9.

398. Quintas-Cardama, A., et al., *Preclinical characterization of the selective JAK1/2 inhibitor INCB018424: therapeutic implications for the treatment of myeloproliferative neoplasms.* Blood, 2010. **115**(15): p. 3109-17.
399. Baum, A., R. Sachidanandam, and A. Garcia-Sastre, *Preference of RIG-I for short viral RNA molecules in infected cells revealed by next-generation sequencing.* Proc Natl Acad Sci U S A, 2010. **107**(37): p. 16303-8.
400. Hartman, A.L., et al., *Reverse genetic generation of recombinant Zaire Ebola viruses containing disrupted IRF-3 inhibitory domains results in attenuated virus growth in vitro and higher levels of IRF-3 activation without inhibiting viral transcription or replication.* J Virol, 2006. **80**(13): p. 6430-40.
401. Jasenosky, L.D., et al., *Ebola virus VP40-induced particle formation and association with the lipid bilayer.* J Virol, 2001. **75**(11): p. 5205-14.
402. Kolesnikova, L., et al., *The matrix protein of Marburg virus is transported to the plasma membrane along cellular membranes: exploiting the retrograde late endosomal pathway.* J Virol, 2004. **78**(5): p. 2382-93.
403. Michalska, A., et al., *A Positive Feedback Amplifier Circuit That Regulates Interferon (IFN)-Stimulated Gene Expression and Controls Type I and Type II IFN Responses.* Front Immunol, 2018. **9**: p. 1135.
404. Noda, T., et al., *Mapping of the VP40-binding regions of the nucleoprotein of Ebola virus.* J Virol, 2007. **81**(7): p. 3554-62.
405. Olejnik, J., et al., *Filovirus Strategies to Escape Antiviral Responses.* Curr Top Microbiol Immunol, 2017. **411**: p. 293-322.
406. Rehwinkel, J., et al., *RIG-I detects viral genomic RNA during negative-strand RNA virus infection.* Cell, 2010. **140**(3): p. 397-408.
407. Kok, K.H., et al., *The double-stranded RNA-binding protein PACT functions as a cellular activator of RIG-I to facilitate innate antiviral response.* Cell Host Microbe, 2011. **9**(4): p. 299-309.
408. Yen, B.C. and C.F. Basler, *Effects of Filovirus Interferon Antagonists on Responses of Human Monocyte-Derived Dendritic Cells to RNA Virus Infection.* J Virol, 2016. **90**(10): p. 5108-5118.
409. Lubaki, N.M., et al., *The lack of maturation of Ebola virus-infected dendritic cells results from the cooperative effect of at least two viral domains.* J Virol, 2013. **87**(13): p. 7471-85.
410. Lubaki, N.M., et al., *The Ebola Interferon Inhibiting Domains Attenuate and Dysregulate Cell-Mediated Immune Responses.* PLoS Pathog, 2016. **12**(12): p. e1006031.
411. Ilinykh, P.A., et al., *Different Temporal Effects of Ebola Virus VP35 and VP24 Proteins on Global Gene Expression in Human Dendritic Cells.* J Virol, 2015. **89**(15): p. 7567-83.
412. Hartman, A.L., et al., *Inhibition of IRF-3 activation by VP35 is critical for the high level of virulence of ebola virus.* J Virol, 2008. **82**(6): p. 2699-704.
413. Woolsey, C., et al., *A VP35 Mutant Ebola Virus Lacks Virulence but Can Elicit Protective Immunity to Wild-Type Virus Challenge.* Cell Rep, 2019. **28**(12): p. 3032-3046 e6.

414. Paweska, J.T., et al., *Virological and serological findings in Rousettus aegyptiacus experimentally inoculated with vero cells-adapted hogan strain of Marburg virus.* PLoS One, 2012. **7**(9): p. e45479.
415. Jones, M.E., et al., *Experimental Inoculation of Egyptian Rousette Bats (Rousettus aegyptiacus) with Viruses of the Ebolavirus and Marburgvirus Genera.* Viruses, 2015. **7**(7): p. 3420-42.
416. Amman, B.R., et al., *Oral shedding of Marburg virus in experimentally infected Egyptian fruit bats (Rousettus aegyptiacus).* J Wildl Dis, 2015. **51**(1): p. 113-24.
417. Zhang, A.P., et al., *Crystal structure of Marburg virus VP24.* J Virol, 2014. **88**(10): p. 5859-63.
418. Copple, I.M., *The Keap1-Nrf2 cell defense pathway--a promising therapeutic target?* Adv Pharmacol, 2012. **63**: p. 43-79.
419. Glazer, R.I., et al., *3-Deazaneplanocin A: a new inhibitor of S-adenosylhomocysteine synthesis and its effects in human colon carcinoma cells.* Biochem Pharmacol, 1986. **35**(24): p. 4523-7.
420. Zhang, J. and Y.G. Zheng, *SAM/SAH Analogs as Versatile Tools for SAM-Dependent Methyltransferases.* ACS Chemical Biology, 2016. **11**(3): p. 583-597.
421. Salata, C., et al., *Ebola Virus Entry: From Molecular Characterization to Drug Discovery.* Viruses, 2019. **11**(3): p. 274.
422. Whelan, S.P.J., *Vesicular Stomatitis Virus.* Encyclopedia of Virology, 2008. **Third Edition**: p. 291-299.
423. De Clercq, E., et al., *Broad-spectrum antiviral activities of neplanocin A, 3-deazaneplanocin A, and their 5'-nor derivatives.* Antimicrobial Agents and Chemotherapy, 1989. **33**(8): p. 1291.
424. Li, W., et al., *Complementary Mutations in the N and L Proteins for Restoration of Viral RNA Synthesis.* Journal of Virology, 2018. **92**(22): p. e01417-18.
425. Garijo, R., et al., *Constrained evolvability of interferon suppression in an RNA virus.* Scientific Reports, 2016. **6**(1): p. 24722.
426. He, S.L. and R. Green, *Chapter Ten - Polysome Analysis of Mammalian Cells*, in *Methods in Enzymology*, J. Lorsch, Editor. 2013, Academic Press. p. 183-192.
427. Abraham, G. and A.K. Banerjee, *Sequential transcription of the genes of vesicular stomatitis virus.* Proceedings of the National Academy of Sciences, 1976. **73**(5): p. 1504.
428. Ball, L.A. and C.N. White, *Order of transcription of genes of vesicular stomatitis virus.* Proceedings of the National Academy of Sciences, 1976. **73**(2): p. 442.
429. Iverson, L.E. and J.K. Rose, *Localized attenuation and discontinuous synthesis during vesicular stomatitis virus transcription.* Cell, 1981. **23**(2): p. 477-484.
430. Liu, C., et al., *6'-Fluoro-3-deazaneplanocin: Synthesis and antiviral properties, including Ebola.* Bioorganic & Medicinal Chemistry Letters, 2018. **28**(23): p. 3674-3675.
431. Ye, W. and S.W. Schneller, *The enantiomers of the 1',6'-isomer of neplanocin A: synthesis and antiviral properties.* Bioorganic & medicinal chemistry, 2014. **22**(19): p. 5315-5319.
432. Li, J., et al., *Opposing Effects of Inhibiting Cap Addition and Cap Methylation on Polyadenylation during Vesicular Stomatitis Virus mRNA Synthesis.* Journal of Virology, 2009. **83**(4): p. 1930.

433. Galloway, S.E. and G.W. Wertz, *S-Adenosyl Homocysteine-Induced Hyperpolyadenylation of Vesicular Stomatitis Virus mRNA Requires the Methyltransferase Activity of L Protein.* Journal of Virology, 2008. **82**(24): p. 12280.
434. Rose, J.K., H.F. Lodish, and M.L. Brock, *Giant heterogeneous polyadenylic acid on vesicular stomatitis virus mRNA synthesized in vitro in the presence of S-adenosylhomocysteine.* Journal of Virology, 1977. **21**(2): p. 683.
435. Beilharz, T.H. and T. Preiss, *Widespread use of poly(A) tail length control to accentuate expression of the yeast transcriptome.* RNA, 2007. **13**(7): p. 982-97.
436. Read, R.L. and C.J. Norbury, *Roles for cytoplasmic polyadenylation in cell cycle regulation.* Journal of Cellular Biochemistry, 2002. **87**(3): p. 258-265.
437. Read, R.L., et al., *Cytoplasmic poly(A) polymerases mediate cellular responses to S phase arrest.* Proceedings of the National Academy of Sciences, 2002. **99**(19): p. 12079.
438. Nicholson, A.L. and A.E. Pasquinelli, *Tales of Detailed Poly(A) Tails.* Trends in cell biology, 2019. **29**(3): p. 191-200.
439. Dratewka-Kos, E., et al., *Catalytic utilization of eIF-2 and mRNA binding proteins are limiting in lysates from vesicular stomatitis virus infected L cells.* Biochemistry, 1984. **23**(25): p. 6184-6190.
440. Lodish, H.F. and M. Porter, *Translational control of protein synthesis after infection by vesicular stomatitis virus.* Journal of Virology, 1980. **36**(3): p. 719.
441. Mudd, J.A. and D.F. Summers, *Protein synthesis in vesicular stomatitis virus-infected HeLa cells.* Virology, 1970. **42**(2): p. 328-340.
442. Ma, Y., et al., *mRNA cap methylation influences pathogenesis of vesicular stomatitis virus in vivo.* Journal of virology, 2014. **88**(5): p. 2913-2926.
443. Galloway, S.E., P.E. Richardson, and G.W. Wertz, *Analysis of a structural homology model of the 2'-O-ribose methyltransferase domain within the vesicular stomatitis virus L protein.* Virology, 2008. **382**(1): p. 69-82.
444. Li, J., E.C. Fontaine-Rodriguez, and S.P.J. Whelan, *Amino Acid Residues within Conserved Domain VI of the Vesicular Stomatitis Virus Large Polymerase Protein Essential for mRNA Cap Methyltransferase Activity.* Journal of Virology, 2005. **79**(21): p. 13373.
445. Valle, C., et al., *The C-Terminal Domain of the Sudan Ebolavirus L Protein Is Essential for RNA Binding and Methylation.* Journal of Virology, 2020. **94**(12): p. e00520-20.
446. Ruedas, J.B. and J. Perrault, *Putative Domain-Domain Interactions in the Vesicular Stomatitis Virus L Polymerase Protein Appendage Region.* Journal of Virology, 2014. **88**(24): p. 14458.
447. Ali Zafar, C.T., Errol Graham, John Panzer *2014-2015 West Africa Ebola Crisis: Impact Update*. 2016.
448. Letko, M., et al., *Bat-borne virus diversity, spillover and emergence.* Nature Reviews Microbiology, 2020. **18**(8): p. 461-471.
449. Plowright, R.K., et al., *Pathways to zoonotic spillover.* Nat Rev Microbiol, 2017. **15**(8): p. 502-510.

450. Woolsey, C., et al., *A VP35 Mutant Ebola Virus Lacks Virulence but Can Elicit Protective Immunity to Wild-Type Virus Challenge.* Cell Reports, 2019. **28**(12): p. 3032-3046.e6.
451. Siragam, V., G. Wong, and X.-G. Qiu, *Animal models for filovirus infections.* Zoological research, 2018. **39**(1): p. 15-24.
452. Banadyga, L., M.A. Dolan, and H. Ebihara, *Rodent-Adapted Filoviruses and the Molecular Basis of Pathogenesis.* J Mol Biol, 2016. **428**(17): p. 3449-66.
453. Volchkov, V.E., et al., *Molecular characterization of guinea pig-adapted variants of Ebola virus.* Virology, 2000. **277**(1): p. 147-55.
454. Lofts, L.L., et al., *Genomic Differences between Guinea Pig Lethal and Nonlethal Marburg Virus Variants.* The Journal of Infectious Diseases, 2007. **196**(Supplement_2): p. S305-S312.
455. Ebihara, H., et al., *Molecular Determinants of Ebola Virus Virulence in Mice.* PLOS Pathogens, 2006. **2**(7): p. e73.
456. Leung, D.W., et al., *Structural basis for dsRNA recognition and interferon antagonism by Ebola VP35.* Nature Structural & Molecular Biology, 2010. **17**(2): p. 165-172.
457. Bale, S., et al., *Marburg Virus VP35 Can Both Fully Coat the Backbone and Cap the Ends of dsRNA for Interferon Antagonism.* PLOS Pathogens, 2012. **8**(9): p. e1002916.
458. Ramanan, P., et al., *Structural basis for Marburg virus VP35–mediated immune evasion mechanisms.* Proceedings of the National Academy of Sciences, 2012. **109**(50): p. 20661.
459. Guito, J.C., et al., *Novel activities by ebolavirus and marburgvirus interferon antagonists revealed using a standardized in vitro reporter system.* Virology, 2017. **501**: p. 147-165.
460. Han, Z., et al., *Modular mimicry and engagement of the Hippo pathway by Marburg virus VP40: Implications for filovirus biology and budding.* PLOS Pathogens, 2020. **16**(1): p. e1008231.
461. Ringel, M., et al., *Replication of a Nipah Virus Encoding a Nuclear-Retained Matrix Protein.* J Infect Dis, 2020. **221**(Suppl 4): p. S389-s394.
462. Wang, Y.E., et al., *Ubiquitin-regulated nuclear-cytoplasmic trafficking of the Nipah virus matrix protein is important for viral budding.* PLoS Pathog, 2010. **6**(11): p. e1001186.
463. Ghildyal, R., et al., *The Respiratory Syncytial Virus Matrix Protein Possesses a Crm1-Mediated Nuclear Export Mechanism.* Journal of Virology, 2009. **83**(11): p. 5353.
464. Ciancanelli, M.J. and C.F. Basler, *Mutation of YMYL in the Nipah Virus Matrix Protein Abrogates Budding and Alters Subcellular Localization.* Journal of Virology, 2006. **80**(24): p. 12070.
465. Ghildyal, R., et al., *Nuclear import of the respiratory syncytial virus matrix protein is mediated by importin beta1 independent of importin alpha.* Biochemistry, 2005. **44**(38): p. 12887-95.
466. Ghildyal, R., et al., *The matrix protein of Human respiratory syncytial virus localises to the nucleus of infected cells and inhibits transcription.* Arch Virol, 2003. **148**(7): p. 1419-29.

467. Glodowski, D.R., J.M. Petersen, and J.E. Dahlberg, *Complex nuclear localization signals in the matrix protein of vesicular stomatitis virus.* J Biol Chem, 2002. **277**(49): p. 46864-70.
468. von Kobbe, C., et al., *Vesicular Stomatitis Virus Matrix Protein Inhibits Host Cell Gene Expression by Targeting the Nucleoporin Nup98.* Molecular Cell, 2000. **6**(5): p. 1243-1252.
469. Petersen, J.M., et al., *The Matrix Protein of Vesicular Stomatitis Virus Inhibits Nucleocytoplasmic Transport When It Is in the Nucleus and Associated with Nuclear Pore Complexes.* Molecular and Cellular Biology, 2000. **20**(22): p. 8590.
470. Her, L.-S., E. Lund, and J.E. Dahlberg, *Inhibition of Ran Guanosine Triphosphatase-Dependent Nuclear Transport by the Matrix Protein of Vesicular Stomatitis Virus.* Science, 1997. **276**(5320): p. 1845.
471. Coleman, N.A. and M.E. Peeples, *The matrix protein of Newcastle disease virus localizes to the nucleus via a bipartite nuclear localization signal.* Virology, 1993. **195**(2): p. 596-607.
472. Peeples, M.E., et al., *Nuclear entry and nucleolar localization of the Newcastle disease virus (NDV) matrix protein occur early in infection and do not require other NDV proteins.* J Virol, 1992. **66**(5): p. 3263-9.
473. Peeples, M.E., *Differential detergent treatment allows immunofluorescent localization of the Newcastle disease virus matrix protein within the nucleus of infected cells.* Virology, 1988. **162**(1): p. 255-9.
474. Lyles, D.S., L. Puddington, and B.J. McCreedy, *Vesicular stomatitis virus M protein in the nuclei of infected cells.* Journal of Virology, 1988. **62**(11): p. 4387.
475. Yoshida, T., et al., *Membrane (M) protein of HVJ (Sendai virus): its role in virus assembly.* Virology, 1976. **71**(1): p. 143-61.
476. Ghildyal, R., A. Ho, and D.A. Jans, *Central role of the respiratory syncytial virus matrix protein in infection.* FEMS Microbiology Reviews, 2006. **30**(5): p. 692-705.
477. Donnelly, C.M., et al., *The Structural Features of Henipavirus Matrix Protein Driving Intracellular Trafficking.* Viral Immunol, 2021. **34**(1): p. 27-40.
478. McLinton, E.C., et al., *Nuclear localization and secretion competence are conserved among henipavirus matrix proteins.* J Gen Virol, 2017. **98**(4): p. 563-576.
479. Bharaj, P., et al., *The Matrix Protein of Nipah Virus Targets the E3-Ubiquitin Ligase TRIM6 to Inhibit the IKKε Kinase-Mediated Type-I IFN Antiviral Response.* PLOS Pathogens, 2016. **12**(9): p. e1005880.
480. Oka, M. and Y. Yoneda, *Importin α: functions as a nuclear transport factor and beyond.* Proc Jpn Acad Ser B Phys Biol Sci, 2018. **94**(7): p. 259-274.
481. Goldfarb, D.S., et al., *Importin alpha: a multipurpose nuclear-transport receptor.* Trends Cell Biol, 2004. **14**(9): p. 505-14.
482. Bourgeois, B., et al., *Nonclassical nuclear localization signals mediate nuclear import of CIRBP.* Proceedings of the National Academy of Sciences, 2020. **117**(15): p. 8503.
483. Kosugi, S., et al., *Six Classes of Nuclear Localization Signals Specific to Different Binding Grooves of Importin α*.* Journal of Biological Chemistry, 2009. **284**(1): p. 478-485.

484. Shin, H.Y. and N.C. Reich, *Dynamic trafficking of STAT5 depends on an unconventional nuclear localization signal.* Journal of Cell Science, 2013. **126**(15): p. 3333.
485. Li, G., et al., *Mechanisms Mediating Nuclear Trafficking Involved in Viral Propagation by DNA Viruses.* Viruses, 2019. **11**(11): p. 1035.
486. Nishi, K., et al., *Leptomycin B targets a regulatory cascade of crm1, a fission yeast nuclear protein, involved in control of higher order chromosome structure and gene expression.* Journal of Biological Chemistry, 1994. **269**(9): p. 6320-6324.
487. García-Dorival, I., et al., *Elucidation of the Ebola Virus VP24 Cellular Interactome and Disruption of Virus Biology through Targeted Inhibition of Host-Cell Protein Function.* Journal of Proteome Research, 2014. **13**(11): p. 5120-5135.
488. Pichlmair, A., et al., *Viral immune modulators perturb the human molecular network by common and unique strategies.* Nature, 2012. **487**(7408): p. 486-490.
489. (NIAID), N.I.o.A.a.I.D. *GS-5734 to Assess the Antiviral Activity, Longer-Term Clearance of Ebola Virus, and Safety in Male Ebola Survivors With Evidence of Ebola Virus Persistence in Semen*. 2021 [cited 2021.
490. Haverkamp, C., C. Liu, and S.W. Schneller, *Enantiomeric 4'-Truncated 6'-Fluoro-3-deazaneplanocin and its 3-Bromo Derivative: Synthesis and Antiviral Properties, including Ebola and Marburg.* Bioorganic & Medicinal Chemistry Letters, 2021: p. 127985.
491. Uchiyama, N., et al., *Identification of AHCY inhibitors using novel high-throughput mass spectrometry.* Biochemical and Biophysical Research Communications, 2017. **491**(1): p. 1-7.
492. Nakao, A., et al., *Discovery and structural analyses of S-adenosyl-L-homocysteine hydrolase inhibitors based on non-adenosine analogs.* Bioorg Med Chem, 2015. **23**(15): p. 4952-4969.
493. Kusakabe, Y., et al., *Structural insights into the reaction mechanism of S-adenosyl-L-homocysteine hydrolase.* Scientific Reports, 2015. **5**(1): p. 16641.
494. Lee, K.M., et al., *X-ray Crystal Structure and Binding Mode Analysis of Human S-Adenosylhomocysteine Hydrolase Complexed with Novel Mechanism-Based Inhibitors, Haloneplanocin A Analogues.* Journal of Medicinal Chemistry, 2011. **54**(4): p. 930-938.
495. Yamada, T., et al., *Structure and function of eritadenine and its 3-deaza analogues: potent inhibitors of S-adenosylhomocysteine hydrolase and hypocholesterolemic agents.* Biochem Pharmacol, 2007. **73**(7): p. 981-9.
496. Wang, M., et al., *Effects of Ligand Binding and Oxidation on Hinge-Bending Motions in S-Adenosyl-l-homocysteine Hydrolase.* Biochemistry, 2006. **45**(25): p. 7778-7786.
497. Yamada, T., et al., *Catalytic mechanism of S-adenosylhomocysteine hydrolase: roles of His 54, Asp130, Glu155, Lys185, and Aspl89.* Int J Biochem Cell Biol, 2005. **37**(11): p. 2417-35.
498. Wang, M., et al., *Domain Motions and the Open-to-Closed Conformational Transition of an Enzyme: A Normal Mode Analysis of S-Adenosyl-l-homocysteine Hydrolase.* Biochemistry, 2005. **44**(19): p. 7228-7239.

499. Yang, X., et al., *Catalytic strategy of S-adenosyl-L-homocysteine hydrolase: transition-state stabilization and the avoidance of abortive reactions.* Biochemistry, 2003. **42**(7): p. 1900-9.
500. Huang, Y., et al., *Inhibition of S-Adenosylhomocysteine Hydrolase by Acyclic Sugar Adenosine Analogue d-Eritadenine: CRYSTAL STRUCTURE OF S-ADENOSYLHOMOCYSTEINE HYDROLASE COMPLEXED WITH d-ERITADENINE*.* Journal of Biological Chemistry, 2002. **277**(9): p. 7477-7482.
501. Turner, M.A., et al., *Structure determination of selenomethionyl S-adenosylhomocysteine hydrolase using data at a single wavelength.* Nat Struct Biol, 1998. **5**(5): p. 369-76.
502. Whelan, S.P., et al., *Efficient recovery of infectious vesicular stomatitis virus entirely from cDNA clones.* Proceedings of the National Academy of Sciences of the United States of America, 1995. **92**(18): p. 8388-8392.
503. Pattnaik, A.K., et al., *Infectious defective interfering particles of VSV from transcripts of a cDNA clone.* Cell, 1992. **69**(6): p. 1011-20.
504. Ogino, T., *In vitro capping and transcription of rhabdoviruses.* Methods (San Diego, Calif.), 2013. **59**(2): p. 188-198.